Halofuginone: A Story of How Target Identification of an Ancient Chinese Medicine and Multi-Step Evolution Informs Malaria Drug Discovery

Halofuginone: A Story of How Target Identification of an Ancient Chinese Medicine and Multi-Step Evolution Informs Malaria Drug Discovery

A dissertation presented

by

Jonathan David Herman

to

The Division of Medical Sciences

in partial fulfillment of the requirements

for the degree of

Doctor of Philosophy

in the subject of

Biological and Biomedical Sciences

Harvard University

Cambridge, Massachusetts

April 2014

Thesis Advisor: Professor Dyann F. Wirth Jonathan David Herman

HALOFUGINONE: A STORY OF HOW TARGET IDENTIFICATION OF AN ANCIENT CHINESE MEDICINE AND MULTI-STEP EVOLUTION INFORMS MALARIA DRUG DISCOVERY

Abstract

Malaria is a treatable communicable disease yet remains a common cause of death and disease especially among pregnant women and children. Most of malaria's worldwide burden disproportionately lies in Southeast Asia and Sub-Saharan Africa. Western medicine's 100+ year history of combating *Plasmodium falciparum* has taught us that the global population of malaria parasites has a unique and dangerous ability to rapidly evolve and spread drug resistance. Recently it was documented that resistance to the first-line antimalarial artemisinin may be developing in Southeast Asia.

The goal of this work is to develop new targets for antimalarial drug development and use these new tools to better understand the evolutionary process of adaptation to antimalarial drugs. We focused on derivatives of the natural product antimalarial febrifugine. We first identified that febrifugine derivative halofuginone targets the *P. falciparum* cytoplasmic prolyl tRNA synthetase (cPRS). We then found another febrifugine derivative, halofuginol, which shared halofuginone's mechanism of action but lacked its toxicity in an *in vivo* murine model of malaria.

By studying the multiple mechanisms that *P. falciparum* utilizes to evolve resistance to halofuginone, we present a three-step sequential model of the evolution of drug resistance in malaria. In the case of halofuginone, we found non-genetic regulation of the

clag family of genes achieved specific increase of proline pools in addition to genetic modification of the cPRS were fundamental in the evolution of resistance.

By focusing on cPRS drug resistance mutations with a reverse genetic approach, we further found evidence that drug resistance mutations can be the second of a two-step evolutionary process. We found that both cPRS mutations L482F (HFGRI) and L482H (HFGRII) required a cellular environment with the overexpression of clag gene family members to confer resistance to halofuginone.

Taken together, these data identify the cPRS as a new and promising target for malaria drug development, halofuginol as a promising chemical scaffold for the development of future cPRS-based antimalarials, and a new model of the evolution of drug resistance involving sequential non-genetic and genetic adaptations.

Contents

1. Introduction

    1.1 Malaria 2

    1.2 Parasite biology 4

    1.3 History of Control and Eradication 6

    1.4 Drug resistance 8

    1.5 Evolution of Drug Resistance – Fitness Maximization 10

    1.6 Current Regimen for Treatment and Control of Malaria and the Need for New Antimalarials 11

    1.7 Febrifugine Derivatives and Halofuginone 12

    1.8 tRNA Synthetases – A New Antimalarial target 13

    1.9 Amino Acid homeostasis, New Permeability Pathway, and the Clag Gene Family 13

    1.10 Summary of chapters and aims 14

2. CHAPTER 2: Plasmodium Prolyl-tRNA Synthetase: A Druggable Next Generation Dual-Stage Target for Malaria Elimination

    2.1. Attribution 17

    2.2. Introduction 18

    2.3. Materials and Methods 19

    2.4. Results 26

    2.5. Discussion 36

3. Chapter 3: Sequential Evolution of Resistance to Halofuginone: Evidence for Genetic and Epigenetic Regulation

    3.1. Attribution 40

    3.2. Introduction 40

3.3. Materials and Methods 41

3.4. Results 46

3.5. Discussion 57

4. Chapter 4: Analysis of Allelic Replacements of Halofuginone Resistance Mutations at the cPRS Locus

4.1. Attribution 65

4.2. Introduction 65

4.3. Materials and Methods 66

4.4. Results 72

4.5. Discussion 83

5. Conclusions and Future Directions 90

Appendix 98

References 113

Listing of Figures

1.1.1	Clinical burden of *Plasmodium falciparum in 2007*	2
1.2.1	The life cycle human-infecting *Plasmodia*	5
1.4.1	Common drug resistance mechanisms of Intra-erythrocytic *Plasmodium falciparum* parasites	9
2.4.1	Halofuginol is active against the erythrocytic and liver stages of malaria	28
2.4.2	Identification and Validation of cPRS as target of Halofuginone in *P. falciparum*	31
2.4.3	Models of the ternary complex of PfcPRS with ATP and halofuginone	34
2.4.4	Halofuginol and Halofuginone Induce eIF2α Phosphorylation	35
3.4.1	cPRS copy number and mutational variation of in vitro evolution experiments	49
3.4.2	The acquisition of halofuginone resistance in vitro evolved line HFGRII precedes genetic adaption that first appears at cycle 32	50
3.4.3	Short-term treatment of wild-type parasites results in immediate induction of halofuginone resistance	50
3.4.4	Induced Parasites Specifically Upregulate Intracellular Proline Concentration	51
3.4.5	Stronger Correlation of Other Amino Acids with Proline in iRBC Led us to *Clag* Gene Overexpression	53
3.4.6	Induced Dd2 parasites have no evidence of genetic modifications at cPRS locus	54
3.4.7	HFGRII and HFGRIII in vitro Evolved Halofuginone Resistant Lines Have Increased Proline Concentration	55
3.4.8	Copy number variation frequency spectrum at cPRS locus in HFGRIII 2-200x cloned parasites	56
3.4.9	Amplification of cPRS confers resistance to halofuginone	56

3.5.1 A Model of Step-wise Acquisition of Halofuginone Drug Resistance 63

4.4.1 cPRS HFGRII transgenic parasites are more resistant to halofuginone 73

4.4.2 cPRS HFGRI transgenic parasites are hypersensitive to halofuginone 74

4.4.3 Expression analysis reveals co-allelic expression and amplification in AR-HFGRI not present in other transfectants 75

4.4.4 Mapping the Recombined cPRS Loci in transfected parasites with qPCR 77

4.4.5 HFGRI and HFGRII cPRS alleles confer advantage only in the presence of halofuginone 79

4.4.6 Pre-Exposure of AR-HFGRI transfectants to halofuginone induces resistance but does not in AR-HFGRII 81

4.4.7 Overexpression of *Clag* 2 and *Clag* 3.2 associated with halofuginone pre-treatment of AR-HFGRI #25 parasites but not in AR-HFGRII #71 82

Appendix:

2.5.1 Halofuginone is not cross-resistant with common anti-antimalarials 98

2.5.1 Enantiomer-Specific Potency of Halofuginone and Halofuginol 98

2.5.3 *In vivo* potency of halofuginone in liver stage *P. berghei* infection model 99

2.5.4 High resolution melt assay of PfcPRS identifies mutant loci 99

2.5.5 Dose dependent inhibition of P. falciparum growth is dependent on the concentration of free proline 99

2.5.6 Transgenic *S. cerevisiae* expressing wild type PfcPRS is sensitivity to halofuginone 100

2.5.7 Dose dependent inhibition of PfcPRS-expressing yeast growth by halofuginone is abolished by addition of proline 100

2.5.8 Dose dependent inhibition of *S. cerevisiae* expressing wild type PfcPRS by halofuginol 100

2.5.9 Molecular models of Leu482 resistant mutations 101

2.5.10 Amino Acid Response Pathway 101

2.5.11 Quantification of peIF2α protein levels in the western blots from Figure 2.3.4a 102

2.5.12 Multiple protein sequence alignment of the Class II Core Domains of Proline tRNA Synthetases from diverse species 102

Listing of Tables

1.4.1	Time to resistant parasites in clinical use of Antimalarial drugs	8
3.3.1	qPCR Control Primers	43
3.3.2	qPCR Primers for cPRS Target	43
3.3.3	qPCR primers for clag gene family expression analysis	46
3.4.1	Sequenced time points from the HFGRII in vitro evolution experiment	47
3.4.2	Sequenced time points from the HFGRIII in vitro evolution experiment	47
3.4.3	Correlation between cPRS copy number and drug resistance	57
4.3.1	qPCR Control Primers	66
4.3.2	qPCR Primers for cPRS Target	67
4.3.3	PCR Primers for Analysis of 3' Allelic Replacement Transgenic Parasites	68
4.3.4	cPRS allelic discrimination assay primers and probes	70
4.3.5	qPCR primers for expression analysis of the *clag* gene family	72
4.4.1	Summary of cPRS mutations in drug resistance selected lines HFGRII and HFGRIII	72
4.4.2	Fold-increase in HFG EC50 after pre-exposure with 2.8nM HFG in transfectants	81

Acknowledgements

The work I have had the honor to perform and summarize here may only have my name on the title page, but it represents the love and labor of a community. My wife Liliana Ornelas is my rock and inspiration. She understands my passion for global health and has supported me even after the hundredth conversation about halofuginone, or parasites, or qPCR.

I'd like to thank my parents and brother for their support, love, sometimes tough-love, and life long education over these twenty-eight years. My parents' love and dedication allowed me to find my passion for medical science and equipped me to follow this passion. I first came to know the importance of resilience and dedication from watching my mom work 12-hour days and still take care of my brother and I at home. I first came to understand the scientific process from eavesdropping on conversations between my father and his graduate students on days I would visit his lab at Columbia. And I first came to understand the genomic revolution of biology from discussions with my brother about his work on the genetics of human cardiomyopathies.

The community that has enabled this research would not be possible without my mentor Professor Dyann Wirth. Dyann gave me the opportunity to work in her lab and take the reins of the halofuginone project early on in my career as a graduate student. I will forever be grateful for her tolerance of my roving imagination and her steadfast ability to refocus my efforts to the goal at hand. I have learned many a life lesson from Dyann and have made more quarter bets than either she or I recall. But with Dyann's guidance I have started to understand how to understand scientific happenstance. The last eight months of work

have been intellectually challenging but also invigorating. I would not have been able to make the progress presented in Chapters 3 and 4 without Dyann's incisive knack for science and questioning of my working model of epigenetic drug resistance.

Two key scientific mentors I must also thank are Professors Ulf Ribacke and Ralph Mazitschek. Ulf taught me first-hand the art, science, and sweat of molecular parasitology. He taught me how to be a productive laboratory scientist, troubleshoot disappointing results, and design experiments pertinent to the question in mind all while we cracked infantile jokes back and forth. Ralph Mazitschek has co-directed the halofuginone research program and provided me with constant feedback and instruction furthering my development as a scientist.

My colleagues in the Wirth lab have helped through the highs and lows of working on this project on febrifugine derivatives. I'd like to thank Selina Bopp, Rachel Daniels, Allison Demas, Tomoyo Kato, Amanda Lukens, Pamela Magistrado, Angana Mukherjee, Clarissa Valim, Sarah Volkman, and Leila Ross for your conversations, advice, and friendship in the 1st and 7th floors of Building I.

I would also like to thank my Dissertation Advisory Committee, Professors Nathanael Gray, Daniel Hartl, and Sarah Fortune. Their constructive advice helped to push my work forward and deepened my understanding of the scientific method. The PhD Program in Biological and Biomedical Sciences, MD-PhD Program, and Harvard-MIT Health Sciences and Technology Program have supported me through my training as PhD student and in my larger journey as a dual-degree at Harvard Medical School and the Harvard School of Public Health.

Chapter 1: Introduction

1.1 MALARIA

Malaria is an infectious disease caused by mosquito-transmission of eukaryotic protozoan parasites of the genus *Plasmodium* with quite possibly the largest global health impact of any disease. Young children, ages 6-36 months, and pregnant women are the most at risk for severe disease. That being said, symptoms of malaria vary greatly depending on the age-group and previous exposure to the disease [1,2].

Clinical definitions of malaria divide cases into two broad categories: uncomplicated and complicated malaria. A case of uncomplicated malaria is defined as a malaria-infected person with fewer than 5000 parasites/microL of blood, usually experiencing a constellation of symptoms including fever, chills, malaise, fatigue, and diaphoresis. Complicated malaria is defined by hyperparasitemia (≥100,000 parasites/microL) [3]. Much of the clinical symptomotology of complicated malaria is due to cytoadherance of infected and non-infected red blood cells in small blood vessels. These capillary-blocking rosettes cause small infarctions, capillary leakage, and end organ dysfunction that can include the spleen, kidneys, lungs, brain, and liver [2]. Though five Plasmodium species can infect humans, most cases of severe malaria are caused by *P. falciparum* infections [1].

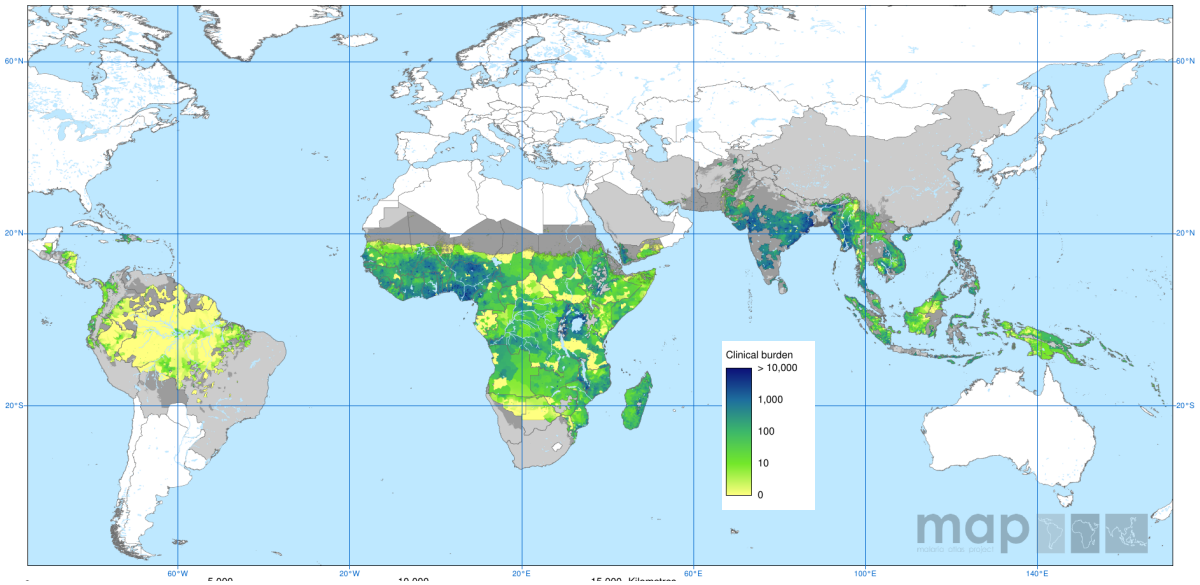

Figure 1.1.1: Clinical burden of *Plasmodium falciparum* in 2007

This map shows the mean predicted clinical burden of *Plasmodium falciparum* malaria in terms of the number of clinical cases in people of all ages per year per 5x5km. [4,5].

Putting on the hat of social epidemiology, malaria is also a disease of climate and a disease of poverty. The worldwide burden of malarial disease is estimated at 1,238,000 deaths in 2010. The clear majority (1,133,000) of those deaths occurred in Sub-Saharan Africa in 2010,[6] where the greatest burden of clinical disease also predominates (Figure 1.1.1). Despite the shocking number of world-wide mortalities, this represents steady progress. From 2004 to 2010, malaria mortality has decreased most likely due to scaling-up of malaria control measures especially in Sub-Saharan Africa [6].

The epidemiological distribution of malaria described above is shaped by climate and its effect on Plasmodium-transmitting vectors. Much of the burden of malaria is restricted to tropical and sub-tropical climates. The *Anopheline* mosquitoes present in tropical climates, especially in Sub-Saharan Africa, are far more competent vectors for malaria than those found elsewhere. Thus malaria control and eradication faces far greater challenges in the tropics than those that were faced by formerly endemic nations in more temperate climes (eg. The United States of America) [7].

From a critical anthropological lens, malaria is also a disease of poverty. On the basis of country-level data, Gwatkin and Guillot estimated that 57.9% of all deaths from malaria in the world in 1990 occurred among the poorest 20% of the world's population. [8]. The relationship between malaria and poverty is a tautological circle: in some respects it is both caused by poverty and the cause of poverty itself. Malaria, among other infectious diseases, has been suggested as part of the reason for impoverished living conditions in less developed countries. More specifically, Sachs et al. estimate that malaria has inflicted an annual cost of $12 billion through death and disability in the continent of Africa [9]. Part of that cost is also due to the cost of malaria treatment itself, which falls disproportionately on low-income households in sub-Saharan Africa. A 1994 survey in Malawi demonstrated that malaria-related costs accounted for 32% of annual household income of families in the low income bracket, compared to 4% for wealthier Malawian households [10].

On the other side, poverty itself perpetuates malarial disease and maintains the conditions that perpetuate endemic malarial disease. Poverty prevents access to prevention and treatment. Poverty forces people to

live in swampy mosquito-infested environments. There is also some evidence that malarial disease is more common and severe in undernourished children for yet unappreciated physiological reasons [11,12].

1.2 PARASITE BIOLOGY

Human malaria infections are caused by four species – *P. falciparum, P. vivax, P. malariae, P. ovale,* and *P. knowlesi*. *Plasmodia* are classified in the unicellular protist phylum *Apicomplexa*, named for the *apical complex* of organelles (rhoptries, micronemes, and dense granules) present in the sporozoite – the infectious stage of each member of *Apicomplexa;* the apical organelles are also present in the merozoite and ookinete forms of *Plasmodia*. Most members also contain a chloroplast-like organelle, the apicoplast, required for isoprenoid biosynthesis *Plasmodia* [13]. *Apicomplexa* also includes related species: *Babesia*, *Cryptosporidiosis*, and *Toxoplasma*.

The genus *Plasmodium* includes hundreds of species. Each species is largely defined by its secondary host; in the case of *P. falciparum, P. vivax, P. malariae, P. ovale,* and *P. knowlesi,* humans are the secondary host and Anopheline mosquitos, the primary. *P. relictum* and *P. elongatum* are two avian malarias that often rise to world-wide attention when they infect the penguins living in captivity [14].

Any parasitic organism with two hosts must have a complex life cycle and developmental program to allow it to survive in multiple environments and travel from one host to another. The parasite *P. falciparum* accomplishes this with a haploid genome of approximately 23 million base-pairs of DNA (Mb) and just over 5,000 genes [15]. To put this in context, the average size of a bacteria genome such as E. coli is 4-5 million bases while the human genome is 3.2 billion bases [16-18].

A human malaria infection begins with the bite of a female Anopheline mosquito carrying sporozoites waiting in its salivary glands (Figure 1.2.1). *Plasmodium* sporozoites travel from superficial capillaries to infect liver hepatocytes within 2 hours [2] (Figure 1.2.1 #1). Within hepatocytes, the haploid hepatic parasites undergo the first cycle of asexual replication – exoerythrocytic schizogony.

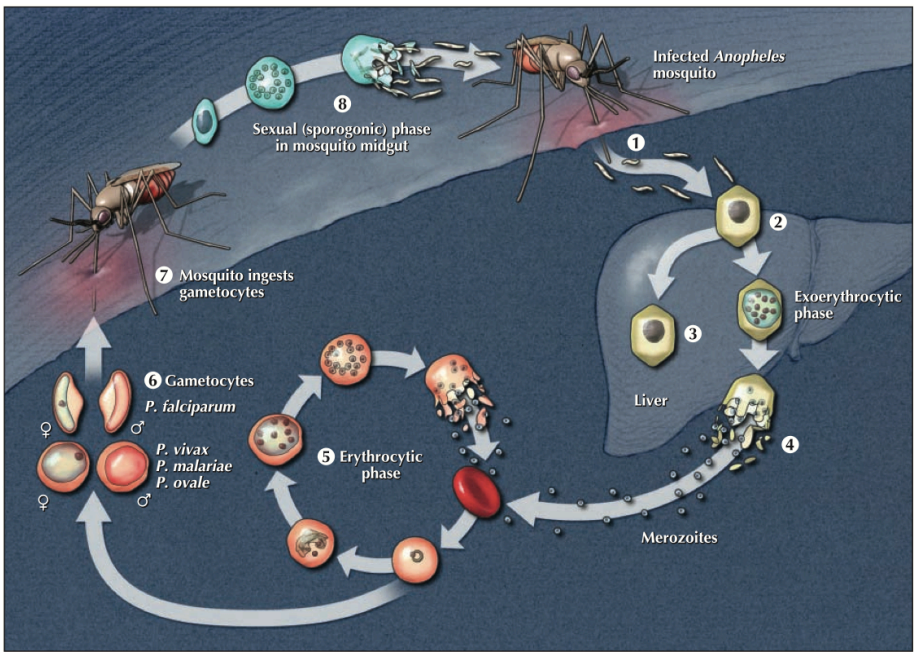

Figure 1.2.1: The life cycle human-infecting *Plasmodia*.

Life-cycle stages of human malaria are enumerated 1-8 beginning with the bite of a malaria-infected mosquito [1].

In this replicative stage one merozoite gives rise to thousands of merozoites [19] (Figure 1.2.1 #2). These merozoites enter the blood stream and begin the hematogenous stage of infection responsible for malaria's clinical symptoms and morbidity (Figure 1.2.1 #4). However in *P. vivax and P. ovale* infections, a subset of merozoites become inactive and form the latent hypnozoite form of malaria responsible for recrudescent infections (Figure 1.2.1 #3).

The erythrocytic stage of malaria infection usually manifests itself 12 to 14 days after the initial mosquito bite. Once in the blood stream, daughter merozoites attach and infect red blood cells to commence the second phase of asexual replication. Within the erythrocyte, malaria parasites surround themselves with the parasitophorous vacuole – a membrane that the parasite invaginates from the erythrocyte cell membrane. The parasite remodels the host erythrocyte in many ways including reprogramming nutrient import via the new permeability pathway/PSAC transport [20]. The parasite undergoes replication, passing through the hallmarked asexual life-cycle stages: ring, trophozoite, and schizont. Asymmetric cell division produces 16-32 maturing merozoites within the infected erythrocyte. Upon full maturation of the daughter merozoites,

the late stage schizonts initiate a calcium-dependent lysis program [21] and release the daughter merozoites that will perpetuate the un-ending erythrocytic cycle (Figure 1.2.1 #5). The bursting of infected red blood cells triggers the release of a storm of host cytokines resulting in the classic symptoms of uncomplicated malaria – fever, tachycardia, tachypnea, chills, malaise, fatigue, diaphoresis, and headache [2].

During a clinical case of malaria, only ring-stage parasites are present in the peripheral blood. Late-stages – trophozoites and schizonts – are either sequestered in small capillaries and post-capillary venules of specific organs or filtered out of circulation by macrophage-mediated splenic clearance. Much of the burden of parasite sequestration occurs in the brain and lungs leading to the end-organ dysfunction associated with severe malaria [22].

A small subset of ring-stage erythrocytic cycle parasites leave the asexual stage and become committed to form male and female gametocytes – the sexual forms of Plasmodium [23] (Figure 1.2.1 #6). Mature gametocytes sequester to small vessels awaiting ingestion by a feeding female mosquito (Figure 1.2.1 #7). Plasmodium parasites only undergo meiosis, i.e. sexual reproduction, within the mid-gut of the mosquito vector (Figure 1.2.1 #8). After recombination of genetic material from male and female gametocytes, sporogenesis in the mosquito midgut reproduces the transmissible sporozoites that migrate to the salivary glands to restart the cycle.

1.3 History of Control and eradication

Eradication of any infectious disease relies on four major conditions: biologic feasibility, adequate public health infrastructure, sufficient funding, and sustained political/societal will [24]. This thesis will focus mostly on the biological feasibility, which must be achievable before the three other conditions can come onboard for the eradication of any human disease. Within the field of public health, small pox eradication is held up as an example of a well-organized and successful eradication campaign. It is also illustrative of the three disease characteristics that facilitate eradication [25], many of which remain challenges for any malaria eradication effort. First, the main intervention of the small pox eradication campaign was a highly effective vaccine that eliminated the possibility of future infection. Second, disease state – whether a person is

infected or not infected with the smallpox virus – is apparent by visual diagnosis; there is no latent or sub-clinical yet contagious carrier state. Third, transmission is person to person and thus does not involve a separate vector population or animal reservoir, i.e. mosquitos or sandflies.

All three of these factors explain the serious challenges that remain for malaria control and eradication. There is no effective vaccine as of yet [26,27]; the most studied malaria vaccine, RTS,S/AS01, remains poorly efficacious only preventing 47% and 26% of severe disease in 5-17month olds and newborns respectively [26]. Malaria disease state is more complicated than smallpox. Sub-clinical infections persist especially in areas of endemic or hypo-endemic transmission [28-31] and reactivation of latent disease is possible, especially in areas where *P.* vivax and *P. ovale* are active [32,33]. Both sub-clinical and reactivated infections can continue to transmit disease leading to resurgence of malaria in regions previously free of clinical disease and transmission. And third, malaria is a vector born disease transmitted by a multitude of mosquito species. Thus, the lack of a vaccine, the ability to have continued transmission without clinical disease, and the transmission of the disease by mosquitos have flouted many heroic attempts at malaria disease eradication.

The discovery of "rods" in the salivary glands of mosquito fed on malarias birds by Ronald Ross in 1898 established mosquito transmission of malaria and commenced a new approach in malaria control [34]. The era of malariology was born as a discipline focused around malaria as a mosquito vector-born infectious disease. Encouraged by the effectiveness and endurance of the newly discovered insecticide dichloro-diphenyl-trichloroethane (DDT), The World Health Organization (WHO) spearheaded the Global Malaria Eradication Programme (GMEP) in1955. The control and eradication efforts of GMEP relied on indoor residual spraying with DDT. From the outset of the programme, it followed a strict timeline for progression from endemic disease to eradication [35]. Fourteen years later, the GMEP was plagued by malaria resurgence in many countries that had previously interrupted transmission and it was recognized that eradication of malaria was infeasible in a short-term campaign. The WHO abandoned the goal of worldwide malaria eradication and refocused on disease control.

1.4 DRUG RESISTANCE

A major cause of the failure of the Global Malaria Eradication Program was acquired resistance of the mosquito vector and the Plasmodium parasite itself. For the sake of this work, we will focus largely on acquired drug resistance of Plasmodium parasites. First line drugs for malaria have changed over time due to clinical drug resistance. First in the form of Cinchona Bark and later reformulated as a tablet, quinine was the first and only effective therapy. Quinine was then replaced with the synthetic derivative chlororquine. More recently, the combination folate pathway inhibitor sulfadoxine-pyrimethamine replaced chlororquine, only now to be shelved for artemisinin-combination therapies. The constant evolution of drug resistance necessitated switching chemotherapies (Table 1.4.1).

Table 1.4.1: Time to resistant parasites in clinical use of Antimalarial drugs

Antimalarial drug	Introduced	First reported resistance	Difference (years)
Quinine	1632	1910	278
Chloroquine	1945	1957	12
Proguanil	1948	1949	1
Sulfadoxine-pyrimethamine	1967	1967	0
Mefloquine	1977	1982	5
Atovaquone	1996	1996	0
Artemisinin	1994	2008*	

Based upon data from [36] *Delayed clearance, but not flagrant, resistance has been witnessed [37]

Two predominant resistance mechanisms have been witnessed in malaria research. The first is pump-based efflux of a drug away from its subcellular location of activity. In the case of *Plasmodium falciparum* Chloroquine Resistance Transporter (*Pf*CRT), the gene product sits in the membrane of the digestive vacuole (Figure 1.4.1). Chloroquine is hypothesized to inhibit detoxification of the heme functional group released during hemoglobin degradation [38]. Thus, certain 'resistant' alleles of *Pf*CRT displace chloroquine from its site of action and allow for phenotypic drug resistance. Another example of pump-mediated resistance is the *Plasmodium falciparum* multi drug resistance gene 1(*PfMDR1*) also know as P-glycoprotein (Pgph1). The

product of *Pf*MDR1 also sits in the digestive vacuolar membrane and is hypothesized to pump cytosolic-acting drugs into the digestive vacuole [39] (Figure 1.4.1).

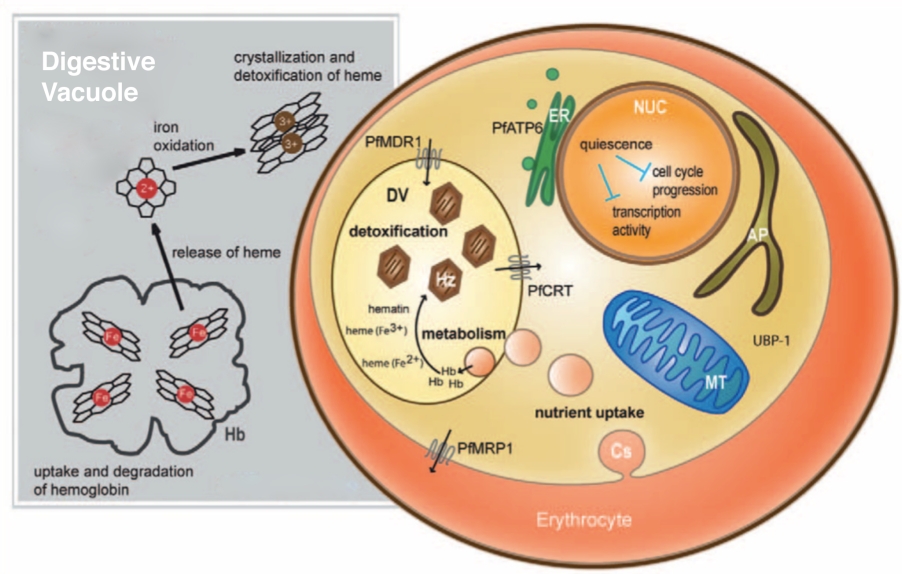

Figure 1.4.1: Common drug resistance mechanisms of Intra-erythrocytic *Plasmodium falciparum* parasites[39]

The second class of drug-resistance mechanisms in *Plasmodium* species are target site mutations. Both folate pathway and mitochondria-targeting drugs have selected for single nucleotide polymorphisms (SNPs) in their biochemical target. In response to sulfadoxine-pyrimethamine pressure in vitro and clinically, mutations in dihydrofolate reductase (DHFR) and dihydropteroate synthetase (DHPS) evolved as resistance adaptations. In the mitochondria, bc1 complex inhibitors, such as atovaquone, rapidly select for resistant parasites in vitro with SNPs in cytochrome bc1. During clinical trials of atovaquone of malaria cases in the United Kingdom, 6 out of 8 patients treated with 500mg dose had recrudescent malaria with in vitro resistance to the drug [40].

The above-discussed mechanisms of drug resistance have only been described as single genetic markers and single event molecular mechanisms. There is significant evidence that evolution of drug resistance is not a single event. The evolution of chloroquine resistance, when dissected, makes a convincing case that drug

resistance in *P. falciparum* occurs in discrete and sequential steps. Unlike target-site driven resistance mechanism that have taken days to months to evolve and fix in patient populations, chloroquine resistance was first observed after 12 years of clinical use and has evolved independently in more than four distinct geographic locations worldwide. In Sub-Saharan Africa, resistance was first observed after almost 30 years of use and involves multiple mutations in linkage disequilibrium between *Pf*MDR1 and *Pf*CRT [41]. All of these observations argue for multiple genetic steps to achieve chloroquine resistance.

1.5 Evolution of Drug Resistance – Fitness Maximization

Many lines of evidence indicate drug resistance mutations impart selective advantages to parasites under drug pressure, but are also detrimental in absence of that drug [41]. Much work has been done in bacterial and viral biology to understand the fitness costs of drug resistance. A common model employed to understand the evolution of drug resistance and its fitness costs is that of compensatory mutation: evolution of drug resistance results in decreased fitness in the absence of drug pressure. Over time, later mutations accumulate in the drug-resistant lines that rescue the fitness defects; these mutations are termed compensatory mutations [42,43].

One complication of investigating selective fitness in *P. falciparum* is the multi-host multi-stage lifecycle. Each environment will have a different fitness landscape and favor different alleles and variants. Therefore, a drug resistance allele with superior fitness in the presence of the drug in the intraerythrocytic stage, may not have increased fitness within the mosquito midgut or within human hepatocytes during the liver stage of human infection. From a cross-sectional study in Zambia, Mharakurwa et al. found that pyrimethamine-resistant *P. falciparum* parasites were underrepresented in the midguts of *Anopheles arabiensis* vector mosquitoes when compared to their prevalence in human infections. In contrast, cycloguanil-resistant parasites were more highly enriched in the midguts of *A. arabiensis* than in the human populations. These observations built a convincing case that the pyrimethamine-resistant parasites were less fit and cycloguanil-resistant parasites were more fit in the mosquito vector [44].

There is a great deal of evidence that drug-resistance mutations in *P. falciparum* do have significant fitness costs. A great example of such a mutation is the chloroquine resistance haplotype at PfCRT. After Kenya and Malawi discontinued use of chloroquine as their first-line antimalarial therapy, the prevalence of PfCRT resistance mutations in each country dropped significantly [45]. Another strongly studied pair of drug and drug resistance mechanisms leading to decreased fitness is atovaquone and cytochrome bc1. The 1000-fold atovaquone resistant strain with mutations M133I and G280D also had a 5-9% fitness cost and in competitive growth in the absence of atovaquone was out-competed by its parent line, [46]. Additionally, the cytochrome b Y268S mutation observed in an atovaquone-resistant isolate from Thailand led to decreased enzymatic function of the bc1 complex [47,48].

The evidence that compensatory mutations can rescue malaria drug-resistance strains is much weaker. Most epidemiological evidence demonstrating the decline in prevalence of drug-resistance alleles after the withdrawal of clinical use of the corresponding drug suggests that on a population basis compensatory mutations do not predominate and rescue the fitness costs of deleterious resistance mutations before they are removed. However, laboratory-based experiments have suggested that compensatory mutations can rescue the fitness cost of drug resistance. Experimentation with pyrimethamine-resistant *P. chabaudi* parasites supports the notion that compensatory mutations [49] can rescue an otherwise growth deficient strain.

1.6 Current Regimen for Treatment and Control of Malaria and the Need for New Antimalarials

In response to the continued evolution of drug resistance to mono-therapies, malaria pharmaceutical development has shifted focus to developing 2 drug combinations. Drug combinations for malaria have been devised based on pharmacokinetic compatibilities. Artemisinin, a drug with a half-life of 2 to 5 hours [50], has been combined with previously clinically used monotherapies with significantly longer half-lives in order to decrease parasite recrudescence. Based on the success of these artemisinin-based combination therapies (ACTs), the WHO has updated its guidelines to recommend ACTs for treatment of uncomplicated *P. falciparum* malaria [3]. The recommended treatment for severe malaria is intravenous artesunate. Unfortunately, all second line therapies for uncomplicated malaria are other ACTs. Currently no

drugs with novel mechanisms of action will be coming through the development pipeline in the next 5 years [51]. When malaria evolves flagrant resistance to artemisinins, will we be left with any treatments?

The foreboding loss of effective therapies for malaria motivates us to find drugs that work through novel targets in the parasite. Ethnobotany is a great source of potential leads for drugs to treat human disease. It has been an especially great source of antimalarials; most antimalarials, in fact, are natural products. The first effective treatment for malaria was Jesuit bark, an herbal remedy from the quinine-rich bark of the cinchona tree in the Peruvian Amazon [52]. Western medical science isolated the active pharmacophore, quinine, and through rational-based drug design created a series of chemical derivatives including chloroquine. Artemisinin itself, our last efficacious monotherapy, is a product of traditional Chinese medicine. Chinese physician Ge Hong identified the antipyretic effects of *Artemisia annua in 340 AD in Si Ku Quan Shu (*A Handbook of Prescriptions for Emergencies). Though modern Chinese medical science rediscovered this traditional cure for malaria in 1971, the specter of the Cultural Revolution and the Cold war halted investigation and use of artemisinin outside of the People's Republic of China [53]. The antimalarial properties and promise of artemisinin first received worldwide attention in the 1980s.

1.7 Febrifugine Derivatives and Halofuginone

The promise of natural products for antimalarial drug development drew our attention to febrifugine derivatives – a family of small molecules derived from the active principle component of *Dichroa febrifuga*. Used as an antipyretic in traditional Chinese medical practice, extracts of *D. febrifuga* were shown to have antimalarial properties in 1945 [54]. In the 1960s, the Walter Reed Army Institute of Research (WRAIR) developed halofuginone and other febrifugine analogues as part of a large antimalarial drug development program [52].

In parallel with our work on halofuginone in *P.* falciparum, our collaborators have investigated the anti-inflammatory properties of halofuginone in human physiology. Our collaborators demonstrated that halofuginone potently inhibits the differentiation of proinflammatory Th17 cells through activation of the

nutrient-sensing amino acid response pathway[72]. Furthermore, they have recently identified the glutamyl-prolyl-tRNA synthetase (EPRS) as the molecular targets of halofuginone in humans[55,56].

1.8 tRNA Synthetases and Amino Acid Sensing

Translation of the genetic code occurs with the two subunits of the ribosome. RNA enters the assembly line of protein synthesis and the charged tRNA molecules translate the triplets of RNA bases into single amino acids. tRNA synthetase are the grammarians of the central dogma. They charge the tRNA with the correct amino acids and then edit those that are mischarged to ensure fidelity of the translated protein. On top of their function in protein synthesis, cells use tRNA synthetases as measurements of overall amino acid homeostasis. Cells directly sense the amount of uncharged tRNAs and reprogram their behavior via a signal transduction pathway called the Amino Acid Starvation Response (AAR).

Amino Acid Starvation Response (AAR) is a stress response pathway well appreciated in yeast and mammalian biology as part of the larger Integrated Stress Response (ISR). The AAR reprograms cellular behavior in response to deprivation of available amino acids [57]. The aggregate affect of the AAR is to inhibit cell-wide protein synthesis and selective translation of stress-response proteins. Despite redundant amino acid supplies, recent work in the Wirth lab has confirmed that the parasite remains vulnerable to amino acid starvation. In fact, in vitro experimentation has demonstrated that growing parasites in media lacking isoleucine activates the AAR [58,59].

1.9 Amino Acid homeostasis, New Permeability Pathway, and the *Clag* Gene Family

The malaria parasite has a dual amino acid supply in the erythrocytic stage. Within the red blood cell, *P. falciparum* parasites digest human hemoglobin. Theoretically, *P. falciparum* could receive all of its amino acid for protein synthesis from hemoglobin degradation except for isoleucine. However, *P. falciparum* also imports amino acid from the extracellular milieu, at least in *in vitro* culture. Proline is one of seven amino acids that are essential ingredients in media used for *in vitro* cultivation of *P. falciparum* [60]. Very little is

known about how amino acid homeostasis is achieved and maintained in *Plasmodium* species. Because of the unique sources of amino acids and unique challenges of intracellular parasitism, much of the molecular machinery is likely to be the genus-specific.

The malaria field has known for many years that the new permeability pathway (NPP), an increased permeability to various solutes that plasmodium parasites induce during erythrocytic parasitism. The NPP, also know as the Plasmodium-specific anion current, increased influx of many amino acids [61] including proline [62]. *Clag* 3 has been identified as a genetic determinant of the PSAC channel [20]. Two groups recently found clag3 expression was suppressed by treatment with toxic substrates of the PSAC channel; both found that *P. falciparum* parasites downregulated *clag* 3 expression in response to blasticidin S treatment [63,64].

1.10 SUMMARY OF CHAPTERS AND AIMS

The focus of this thesis is to further the development of antimalarials and better understand the evolution machinery that empowers *P. falciparum* to develop resistance to the drugs used to treat it. We chose to focus on derivatives of febrifugine, a plant derived antimalarial identified from the traditional Chinese pharmacopoeia, because it represented a probe for a novel mechanism of anti-parasitic activity. Much of the work was carried out with the febrifugine chemical derivative halofuginone.

In Chapter 2, we used forward genetic approaches to identify the cytoplasmic prolyl tRNA synthetase (cPRS) as the *Plasmodial* target of halofuginone. To validate the clinical relevance of cPRS as a pharmacological target we devised halofuginol, an *in vivo* active antimalarial that retains the potency and target of halofuginone without the host-toxicity.

In Chapter 3, we look deeper into the evolution of drug resistance to halofuginone with metagenomic sequencing of two *in vitro* evolution experiments. We identify epigenetic-driven resistance to halofuginone that involved *clag* gene-overexpression and increased cytosolic proline. This is the first of a three step evolutionary trajectory on the acquisition of halofuginone resistance.

In Chapter 4, we used a reverse genetic approach to confirm the halofuginone resistance phenotype we associated with the two cPRS mutations we found in Chapter 2. Rather, we found that both cPRS mutations are epistatic with clag gene expression and can only confer halofuginone resistance in a background of *clag* gene overexpression. Taken together, this reverse genetic approach demonstrated that cPRS drug resistance mutations could only take place as a second evolutionary step.

Chapter 2: Plasmodium Prolyl-tRNA synthetase: A Druggable Next Generation Dual-Stage Target for Malaria Elimination

2.1 ATTRIBUTION

Authors: Jonathan Herman[†1,2], Lauren R. Pepper[†3], Joseph F. Cortese[1], Guillermina Estiu[4,5], Kevin Galinsky[1], Vanessa Zuzarte-Luis[6], Emily R. Derbyshire[7], Ulf Ribacke[2], Amanda K Lukens[2], Vishal Patel[7], Clary B. Clish[1], William J. Sullivan Jr. [8], Huihao Zhou[9], Paul Schimmel[9], Susan Lindquist[3,10], Jon Clardy[1,7], Maria M. Mota[6], Tracy L. Keller[11], Malcolm Whitman[11], Olaf Wiest[4,5,12], Dyann F. Wirth*[1,2], Ralph Mazitschek*[1,2,13]

[1] The Broad Institute, Infectious Diseases Initiative, Cambridge, MA 02142, USA
[2] Harvard School of Public Health, Department of Immunology and Infectious Disease, Boston, MA 02115, USA
[3] Whitehead Institute for Biomedical Research, Cambridge, MA 02142, USA
[4] Department of Chemistry and Biochemistry, University of Notre Dame, Notre Dame, IN 46556, USA
[5] Center for Rare and Neglected Diseases, University of Notre Dame, Notre Dame, IN 46556, USA
[6] Instituto de Medicina Molecular, Faculdade de Medicina Universidade de Lisboa,1649-028 Lisbon, Portugal
[7] Harvard Medical School, Department of Biological Chemistry and Molecular Pharmacology, Boston, MA 02115, USA
[8] Department of Pharmacology and Toxicology and Microbiology and Immunology, Indiana University School of Medicine, Indianapolis, IN 46202, USA.
[9] The Skaggs Institute for Chemical Biology, Department of Molecular Biology, The Scripps Research Institute, 10550 North Torrey Pines Road, La Jolla, California 92037, USA.
[10] Howard Hughes Medical Institute, Department of Biology, Massachusetts Institute of Technology, Cambridge, MA 02139, USA
[11] Department of Developmental Biology, Harvard School of Dental Medicine, Boston, MA 02115, USA.
[12] School of Chemical Biology and Biotechnology, Peking University, Shenzhen Graduate School, Shenzhen 518055, China
[13] Massachusetts General Hospital, Center for Systems Biology, Boston, MA 02142, USA
*To whom correspondence should be addressed:
† Contributed equally

J.D.H and A.K.L. performed the cross-resistance. J.D.H. analyzed the cross-resistance studies. In vitro profiling of febrifugine analogues against *P. falciparum* was performed and analyzed by J.D.H. In vivo profiling of febrifugine analogues against liver and eryrocytic stages of malaria was performed by V.Z.L. and M.M.M. Drug resistance selections were performed by J.D.H. and J.F.C. Characterization of selections was performed by J.D.H.. Genomic analysis of HFGRI strain was performed by K.G. Yeast heterologous modeling was performed by L.R.P.. Modeling of *Pf*cPRS was performed by G.E. and O.W. Amino acid starvation studies in *P. falciparum* were performed by J.D.H. and in yeast by L.R.P. Proline growth supplementation assays, high-resolution melt assay development and experimentation, and phylogenetic analysis of ProRS genes was performed by J.D.H..

We gratefully acknowledge financial support this work by Gates Foundation (DFW and RM), the National Institute of Health (DFW) AI084031 (WSJ), AI077502 (WSJ), 5F32AI084440-02 (LRP), The Center for Rare and Neglected Diseases at the University of Notre Dame (OW), generous allocation of computing resources by the National Science Foundation through TeraGrid grant TG-CHE090124 (OW), PTDC/SAU-MIC/113697/2009 (VZL) and EXCL/IMI-MIC/0056/2012 (MMM) (Fundação para a Ciência e Tecnologia, Portugal), and start-up funding provided by the Center for Systems Biology/Mass. General Hospital (RM).

2.2 INTRODUCTION

Almost one-third of the world's population is susceptible to malaria, with the highest burden of disease focused on poverty stricken nations in Asia, South America, and Africa. The World Health Organization estimates that malaria parasites infect over 200 million people each year, killing approximately 600,000 people – mostly young children and pregnant women in sub-Saharan Africa - while many more suffer from permanent disabilities[65]. Independent evaluations paint an even grimmer picture, estimating the death toll at 1.2 million[6,66]. In addition to the human costs of severe morbidity and mortality, malaria imposes an enormous burden on the economic growth of developing countries as a result of lost productivity. In Africa alone, the WHO TDR estimates that malaria is responsible for 10% of the continent's disease burden and an annual cost of $12 billion through death and disability [9].

The causative agents of malaria are protozoan parasites of the genus *Plasmodium* that are transmitted between human hosts by mosquitoes. In humans, parasite evolve through a liver stage, a symptomatic intra-erythrocytic (asexual) stage and a sexual blood stage (gametocytes), which is responsible for malaria transmission.

Current approved antimalarial drugs are limited to a few parasite targets and most drugs are only efficacious against the blood stage, which is sufficient for the treatment of acute malaria, however, of limited use for prophylaxis, transmission blocking, and eradication efforts[67-69]. In addition, the emergence and spread of clinical resistance to mainstay drugs, including artemisinis, is the major limitation for the use of current antimalarials[70-72]. Thus the discovery not only of novel chemical classes, but also novel druggable targets and pathways is essential[73,74]. Developing therapies that act on unexploited vulnerabilities in the *Plasmodium* parasite is necessary to maintain the effectiveness of malarial therapy for the renewed worldwide efforts to eradicate malaria.

Aminoacyl tRNA synthetases (aaRSs) and associated pathways have been proposed as attractive targets for chemotherapeutic intervention in malaria[75]. However, the exploration of tRNA synthetase inhibitors in malaria has been scarce. While some tRNA synthetase inhibitors that were identified in other

organisms display antimalarial activity, validation of actual on target mechanism has been elusive[58,76,77]. The repertoire of aaRSs in Plasmodium diverges from other organisms because of the need to carry out protein synthesis in multiple subcellular compartments[77].

Following our previous work demonstrating that halofuginone potently inhibits the differentiation of proinflammatory Th17 cells through activation of the nutrient-sensing amino acid response pathway we have recently identified the glutamyl-prolyl-tRNA synthetase (GPRS) as the molecular targets of halofuginone in humans[55,56]. Halofuginone is a synthetic derivative of the natural product febrifugine, which constitutes the curative ingredient of an ancient Chinese herbal remedy that has been used for over 2000 years for the treatment of fevers and malaria[54].

Halofuginone had originally been developed in an unsuccessful effort to identify derivatives with improved pharmacological properties to overcome the severe side effects observed with febrifugine that preclude the compound from safe clinical use as an antimalarial [78]. Subsequent identification of the broad-spectrum antiprotozoal activity of halofuginone led to the approval in veterinary medicine. This in turn resulted in the recognition of the potent anti-fibrotic and immunomodulatory activity of halofuginone in metazoans and investigation as a therapeutic for cancer and fibrotic diseases [79,80].

The exceptional antimalarial potency and unique activity profile of halofuginone has prompted our interest to better understand the molecular basis of halofuginone's anti-parasitic activity with the aim to provide a well-defined and practical path forward to next-generation antimalarials. To accomplish this goal it was critical to develop small molecule inhibitors lacking the dose-limiting toxicity of previously reported febrifugine derivatives, and to identify and validate the therapeutic potential of halofuginone's target in *P. falciparum*.

2.3 METHODS

P. FALCIPARUM CULTURE

Dd2 is a chloroquine resistant *in vitro* cultured parasite cloned from the Laos derived W2-MEF parasite. Malaria culture was performed as described by Trager *et al*. [81].

P. falciparum Erythrocytic Stage in vitro Dose-Response and Analysis

A SYBR green method was performed as described in Johnson et al. [82]. EC50 values were calculated in Graphpad Prism using a four-parameter nonlinear regression curve fit from three assays, each with 12-point drug dilution curves.

Drug-Resistance Correlation Analysis

We used a set of 31 culture adapted *P. falciparum isolates* from Senegal previously published in Park et al.(*45*) *In vitro* EC50 values were determined, as described above, for 12 standard antimalarials and halofuginone. Included standard antimalarials represent a diverse set of targets including the mitochondria, the folate pathway, and the heme detoxification pathway. Pearson correlation between the EC50 values was determined with Graphpad. A heatmap matrix of correlation coefficients (R^2) was generated in GENE-E (http://www.broadinstitute.org/cancer/software/GENE-E/). Absolute correlation of drug resistance between two antimalarials (R^2=1) is colored red. Lack of correlation of drug resistance between two drugs (R^2=0) is colored blue.

Step-Wise Artificial Selection for Drug Resistance

Resistance selection under intermittent drug pressure was performed over six months time as reported earlier [83].

Dilutional Cloning

We performed limited dilution of ring stage parasites at concentrations of 0.8 and 0.2 parasites per well to isolate individual parasite clones as reported by Rosario [84].

Whole Genome Sequencing

DNA was isolated from cultures with QIAamp DNA Blood Kit (Qiagen). Whole genome sequencing of Dd2 and halofuginone resistant cloned parasites was performed by Illumina 75bp sequence read technology on GAIIx machines to at least 80x coverage on Illuminia HiSeq machines. Single nucleotide polymorphisms between each halofuginone resistant strain and its Dd2 parent were called using GATK and Samtools [85,86]. We compiled the intersection of both sets of nonsynonomous SNPs into a final set of hits. The SNPs called between resistant and parental strains are deposited in dbSNP (http://www.ncbi.nlm.nih.gov/projects/SNP/) and their respective sequences will be deposited at NCBI's Sequence Read Archive http://www.ncbi.nlm.nih.gov/sra. Sanger sequencing was performed by Genewiz (South Plainview, NY).

High Resolution Melt

We developed a highly-sensitive high-throughput assay for the region containing the SNP found at nucleotide 1445 of PFL0670c in HFGR I. To genotype the halofuginone selection timepoints, we used a 29-mer probe identical to the WT PFL0670c sequence, 5'CATCTCATTATCTTGGAACAAATTTTGC'3-block and with forward primer 5'TGGAAGAGCCATACAAGCAG3' and reverse primer 5'GTTTAACTTCATTTTCATCTTCAAATTCAA3'. Amplification was undertaken with a forward to reverse primer ratio of 0.5 mM to 2.5 mM with LightScanner Master Mix (HRLS-ASY-0003, Idaho Technology. Inc., Salt Lake City UT). We ran forty-five cycles of amplification with an annealing temperature of 60 °C. The HRM genotyping was performed with the LightScanner® System (Idaho Technology. Inc., Salt Lake City UT).

PCR Sequencing

Primers were designed to amplify the PFL0670c gene and validate the SNPs identified in whole-genome sequencing. PCR products were purified by ExoSAP-IT treatment per the manufacturer's directions (USB Scientific, USA) and sequenced using big dye termination chemistry (ABI prism automated sequencer) from both the forward and reverse strands (Genewiz, USA). Raw sequence data was evaluated and aligned to the wt reference sequence. SNPs were identified using SeqMan Pro and the Clustal algorithm in MegAlign (DNAStar).

P. falciparum Whole Cell Lysate Western Blot

Dd2 parasites were allowed to grow to asynchrony for 7 replicative generations. 800 mLs of 8% asynchronous, asexual Dd2 parasites were pooled, washed twice with PBS, and 100 mL aliquots were exposed to the experimental treatments for 90 minutes. Drug treated cells were incubated in the presence of small molecule inhibitors in standard RPMI media (GIBCO). Control samples were incubated with a corresponding amount of DMSO with either complete RPMI media or RPMI media lacking amino acids (RPMI-AA, US Biological). The RPMI-AA culture served as a positive control for AAR [59]. Protein lysates from each of the 100 mL cultures were prepared by first lysing infected erythrocytes with 0.1% saponin (Sigma) and the resultant parasite pellets were lysed in 1x Laemmli Sample Buffer (Bio-Rad) supplemented with 5% beta-mercaptoethanol and 2% NP40 (G-Biosciences). All lysis buffers contained 1x Complete protease inhibitor cocktail (Roche) and 1x phosphatase inhibitor cocktail PhosStop (Roche). Western blots were probed with a phospho-specific eIF2a pAb raised to a *Toxoplasma gondii* peptide antigen MSDERLpSKRRFRS, an eIf2a pAb raised to *T. gondii* peptide KGYIDLSKRRVS which recognizes total eIF2a protein (*47*), and a histone-H3 rabbit pAb (Abcam ab1791).

Yeast Strains and Media

The PfProRS gene PFL0670c was optimized for yeast codon preference (see below) and cloned into the Gateway entry plasmid pDONR221 by GenScript. Yeast gene YHR020w was selected from the Flexgene library in pBY011 and cloned into pDONR221 using the Gateway BP reaction (Invitrogen) [87]. Point mutations found in *P. falciparum* halofuginone resistance selections were introduced to the pDONR221-PFL0670c plasmid following manufacturer's directions using the QuikChange Site Directed Mutagenesis Kit (Stratagene). All destination vectors were taken from the pAG vector collection and destination constructs were made using the Gateway LR reaction (Invitrogen) [88].

The yeast strain BY4743 (his3Δ1/his3Δ1 leu2Δ0/leu2Δ0 met15Δ0/+ lys2Δ0/+ ura3Δ0/ura3Δ0) heterozygous for the deletion of essential gene YHR020w from a yeast heterozygous deletion library (OpenBioSystems) was transformed with pAG416-YHR020w using a standard lithium acetate method [89]. This strain was

sporulated for five days at 23°C and tetrads were dissected as described [90]. Tetrads were replica-plated onto YPD (1% yeast extract, 2% peptone, 2% glucose, 2% agar (yeast media reagents were from BD unless otherwise noted) + 200 µg/mL G418 (Invitrogen) to identify those spores that had the chromosomal deletion of YHR020w marked by the KanMX cassette. For deletion of *PDR1*, the *LEU2* cassette was amplified from pUG73 with primers in the genomic region flanking the gene (yeastdeletion.stanford.edu/) [91]. Yeast were transformed and selected on SD-Leu plates (0.67% yeast nitrogen base, 2% glucose, 2% agar, supplemented with complete amino acid mix minus leucine (Sunrise Science Products)). Colonies able to grow on Leu^- media were tested for the pdr1 deletion using PCR and primers as described on the Saccharomyces Genome Deletion Project webpage. The pdr1Δ::LEU2 mutants were subsequently deleted for *pdr3* using the same methods with the hygromycin B cassette amplified from pAG32 [92].

The resulting strain (wildtype or -pdr1Δ::LEU2, pdr3Δ::Hyg) was transformed with pAG413-YHR020w, pAG413GPD-PFL0670c, or point mutants of pAG413GPD-PFL0670c. Strains were selected on 5-FOA for loss of the pAG416-YHR020w plasmid and loss of the plasmid was confirmed by lack of growth on Ura^- media [87].

Yeast Growth Assays

Yeast strains were grown overnight in assay media (0.17% yeast nitrogen base without amino acids, without ammonium sulfate (Bio101), 0.1% glutamic acid, 2% glucose supplemented with complete amino acid mix minus histidine (Sunrise Bioproducts)) at 23 °C to maintain log growth phase. The OD_{600} of cultures was measured and yeast strains were diluted to 0.01 OD_{600} in assay media with indicated concentrations of drugs or a corresponding volume of DMSO (Sigma). In indicated experiments, media was supplemented with 1 mg/mL proline (Sigma). Cells were grown in 100 µL of media in covered 96-well Nunc Edge assay plates at 30°C with interval shaking every 15 minutes in a ThermoScientific Multiskan GO instrument that read OD_{600} every 15 minutes.

Yeast Western Blots

Pump-deleted yeast strains were grown overnight in assay media at 23°C, after which either 25 mM halofuginone or a corresponding volume of DMSO was added to cultures, which were then grown at 30°C for six hours. Yeast pellets were washed with water and resuspended in lysis buffer (100 mM Tris, pH 8.0, 20 mM NaCl, 2 mM $MgCl_2$, 50 mM b-mercaptoethanol, 0.025 U/ml benzonase, 1% Triton X-100, 2 x Halt protease inhibitor (Sigma-Aldrich), 1x Halt Phosphotase Inhibitor (Thermo-Fisher) and acid-washed beads and bead beaten for five minutes at 4°C. Supernatants were collected and normalized for protein content using a BCA assay (Pierce). Proteins were resolved and transferred using standard techniques, and membranes were blotted for p-eIF2a mAb (Ser51) #3398 or total eIF2a pAb #9722 (Cell Signaling Technology).

IN VIVO P. BERGHEI ASSAY

Liver stage: Male C57BL/6 mice, aged 6–8 wk and weighing 20–22 g were purchased from Charles River and housed in the pathogen-free facilities of the Instituto de Medicina Molecular, Lisbon.

Liver infection was initiated by intravenous injection of 10^4 *P. berghei* ANKA sporozoites. Parasite liver load was measured 42–44 h after infection by qRT-PCR of *P. berghei* 18S rRNA.

Blood stage: For blood infection, mice were inoculated with 10^6 red blood cells infected with GFP-expressing *P. berghei* ANKA- (iRBCs). Blood parasitaemia was accessed by FACS analysis and thin blood smear count.

Halofuginol was administered 1 hour or 1 day after infection with sporozoites or iRBCs, respectively. Halofuginol was diluted to the final concentration in drinking water for oral administration or saline solution for intra-peritonal injection. Mice received 200 µL of compound solution and control groups received an equivalent amount of vehicle.

All *in vivo* protocols were approved by the Animal Care Committee of the Instituto de Medicina Molecular and were performed according to the regulations of the European guidelines 86/609/EEG.

MODELING STUDIES

Homology models of prolyl tRNA synthetase for *S. cerevisiae*, *P. falciparum* and *H. sapiens* (prolyl tRNA synthetase domain of GPRS) were constructed using Prime (*54*), the protein prediction structure software of Schroedinger Suite2010, using the available structure of *T. thermophilus* (pdb code 1H4S) and *H. sapiens* (pdb code 4HVC) as the templates. Halofuginone was docked in the resulting structures using Glide, version 4.5. [93,94]. The protein structures were previously prepared using the Protein Preparation Module, whereas the Ligprep module was used to obtain energy minimized 3D halofuginone structures, which were then docked in the respective grids using the extra precision scoring algorithm (XP mode).

The resulting structures served as starting point for the molecular dynamics (MD) simulations, which were carried out in analogy to our previously validated protocol using the PMEMD version included in the AMBER10 suite of programs, [95] after careful relaxation of the system using minimization and equilibration procedures. The ionizable residues were set to their normal ionization states at pH 7. The protein atoms, as well as all the water molecules of the crystal structure, were surrounded by a periodic box of TIP3P [96] water molecules that extended 10 Å from the protein. Na^+ counterions were placed by LEaP [97] to neutralize the system.

The ff03 version of the all-atom AMBER force field was used to model the protein, and the GAFF force field for ATP and the organic ligand[98,99]. Atom-centered partial charges were derived by using the AMBER antechamber program (RESP methodology) [100], after geometry optimization at the B3LYP/6-31G* level [101]. In the molecular dynamics simulation protocol, the time step was chosen to be 2 fs, and the SHAKE algorithm [102] was used to constrain all bonds involving hydrogen atoms. A non bonded cutoff of 10.0 Å was used, and the non bonded pair list was updated every 25 time steps. Langevin dynamics was used to control the temperature (300 K) using a collision frequency of 1.0 ps^{-1}, with isotropic position scaling to maintain the pressure (1 atm)[103]. Periodic boundary conditions were applied to simulate a continuous system. Long-range interactions were treated by the Particle-Mesh-Ewald (PME)[104,105] method was used with a grid spacing of ~1

Å combined with a fourth-order B-spline interpolation to compute the potential and forces in between grid points. The trajectories were analyzed using the PTRAJ module of AMBER10.

Multiple Sequence Alignment

The Prolyl-tRNA synthetase (ProRS) class II core catalytic domain of PfcPRS was identified with NCBI's Conserved Domain Database search v3.1, a position-specific scoring matrix based approach [106]. This methodology identified the CDD domain cd00778. All prolyl-tRNA synthetase sequences were aligned by ClustalW. Using Macvector, we built a neighbor joining tree of the class II core domain based upon bootstrapping through 1000 replicates.

Synthetic Procedures Halofuginol

207mg (0.5mmol) MAZ1310 were suspended in 10mL methanol and 3 mL THF. Following cooling to 0°C 10mg (0.3mmol) $NaBH_4$ were added and the clear reaction mixture was stirred for additional 60min. Upon stirring at 0C the desired product precipitated from solution as white solid. The solid was isolated by filtration and recrystallized from methanol to afford racemic Boc-protected halofuginol (142mg, 68%).

200uL HCl (4M in dioxane) were added to a solution of 10mg Boc-protected halofuginol in 2ml methanol/THF (1:1). The reaction mixture was stirred over night at room temperature. The desired product was obtained following removal of the solvent under reduced pressure in quantitative yield without the need for further purification as white powder as the hydrochloride salt.

Individual halofuginol and halofuginol enantiomers were synthesized from enantiomerically pure MAZ1310, which was obtained following the procedure reported previously by Linder *et al*. [107]. Epi-halofuginol was synthesized adapting the procedure for febrifugine reported by Kikuchi *et al*. [108].

2.4 Results

Febrifugine Derivatives are not Cross-resistant to Traditional Antimalarials.

Lack of cross-resistance to clinically used antimalarials is a critical prerequisite for new antimalarial drug candidates. Thus, we tested a panel of 31 *P. falciparum* clinical isolates with diverse drug resistance profiles for their dose-response to halofuginone and a representative set of 12 antimalarials that cover the major classes of malaria chemotherapies. Halofuginone did not show significant cross-resistance with any of the tested antimalarials (see SFigure 2.5.1), consistent with the profile of a drug with a distinct mechanism.

HALOFUGINOL IS ACTIVE AGAINST THE ERYTHROCYTIC STAGE OF MALARIA IN VITRO AND IN VIVO.

We speculated that the observed side effects of halofuginone and febrifugine could be independent from inhibition of the host EPRS and caused by off-target effects originating from the compounds' reported ability to epimerize in solution through formation of a reactive intermediate [109]. This undesired feature, which is also likely the reason for poor stability in aqueous buffer at physiological pH, can be attributed the central ketone common to febrifugine and halofuginone. Previously reported efforts to remove this functionality have resulted in loss of activity. We reasoned that formal reduction of the ketone to yield a secondary alcohol would retain the potential to form critical hydrogen bonds within the target complex while eliminating the ability to form a reactive Michael-acceptor. Introduction of the alcohol also introduces an additional stereocenter and consequently results in two possible diastereomers, one of which has already been reported for febrifugine to result in significant loss of activity. (*24*) We therefore established a synthetic approach to access both epimers (Figure 2.4.1a) derived from halofuginone as racemates for *in vitro* and *in vivo* profiling.

We next tested both epimers for *in vitro* activity against the asexual *P. falciparum* 3D7 parasite. As expected, the epimer matching the relative stereochemistry of the previously reported febrifugine analog was approximately 1000-fold less active than halofuginone [108]. However, the other stereoisomer, which we termed halofuginol, demonstrated low nanomolar potency (EC50 = 5.8 nM) comparable to febrifugine (4.0nM) (SFig 2.5.1b). Importantly, the principle activity is attributed to one enantiomer with the same absolute configuration of the piperidyl substituent as febrifugine and the active enantiomer of halofuginone (see SFigure 2.5.2).

Encouraged by these findings, we next evaluated halofuginol's tolerability and activity against the erythrocytic stage of malaria in a *P. berghei* mouse model. Using an adapted version of Peters' suppressive test [110,111], we found that halofuginol dosed at 10mg/kg intraperitoneally over 4 days inhibits *P. berghei in vivo* with an efficacy of >99% (Fig 2.4.1C) without observation of any adverse effects that have been reported for febrifugine and halofuginone at efficacious doses [110,111].

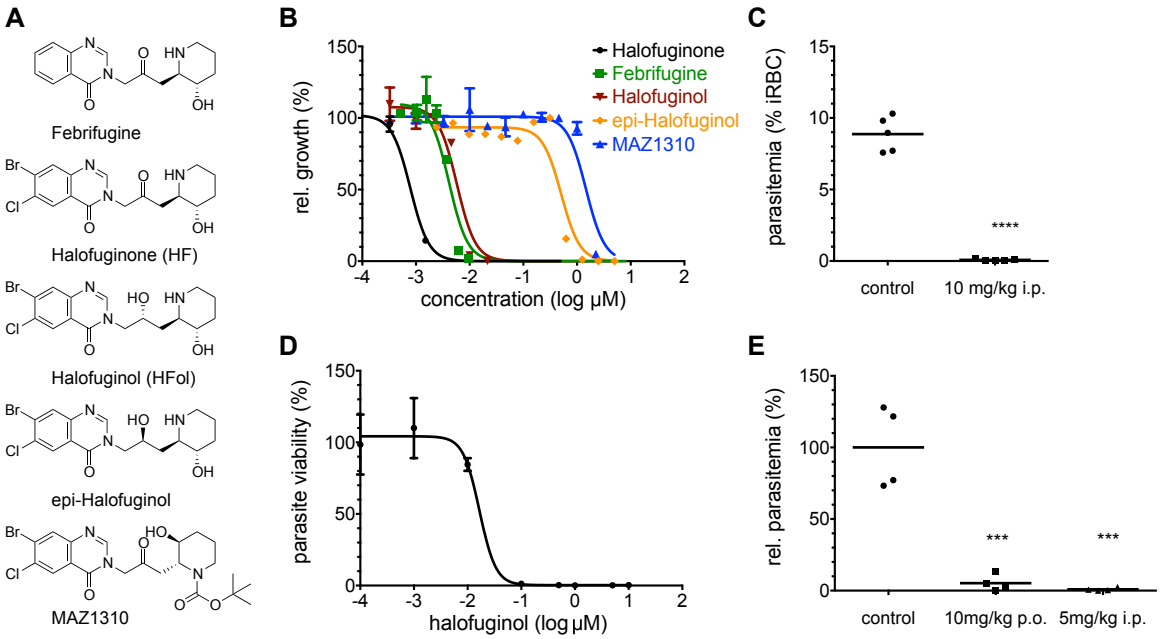

Figure 2.4.1: Halofuginol is active against the erythrocytic and liver stages of malaria

(A) Chemical structures of febrifugine, halofuginone (relative stereochemistry), halofuginol (relative stereochemistry), epi-halofuginol (relative stereochemistry) and MAZ1310 (relative stereochemistry). **(B)** In vitro activity of halofuginone, febrifugine, MAZ1310, halofuginol, and epi-halofuginol against *P. falciparum* strain 3D7 erythrocytic stage parasites. Growth inhibition was quantified after 72 hours by SYBR green staining. **(C)** Blood parasitemia at day 5 after infection. Mice were treated 24hr post inoculation with 10^6 red blood cells infected with GFP-expressing *P. berghei* ANKA with 10mg/kg/day halofuginol (i.p.) or vehicle alone for 4 days. Blood parasite levels were analyzed by FACS. **(D)** In vitro dose-response of luciferase-expressing *P. berghei* ANKA liver stage parasites to halofuginol infecting HepG2 cells. **(E)** In vivo potency of halofuginol in *P. berghei* infection model. Relative parasitemia in mouse livers 44 h after infection with *P. berghei* sporozoites. Mice were treated 1hr post infection with halofuginol (5mg/kg i.p. and 10mg/kg p.o.) and vehicle, respectively. Parasite load was quantified relative to vehicle control by qRT-PCR of *P. berghei* 18S rRNA. Data are displayed as mean relative to vehicle treated control, with the mean of the control group set to 100%. p values (***$p < 0.001$, ****$p < 0.0001$) were calculated from multiple animals by ordinary one-way ANOVA (Graphpad PRISM).

HALOFUGINOL IS ACTIVE AGAINST THE LIVER STAGES OF MALARIA IN VITRO AND IN VIVO

Activity against liver stages of malarial is critical for the next generation of antimalarials for use in global efforts to eliminate and eradicate malarial disease. Following our recent work identifying halofuginone as potent inhibitor of the *P. berghei* liver stage *in vitro*, we investigated the activity of halofuginol [112]. Halofuginol demonstrated potent inhibition (EC_{50} = 14 nM) of *P. berghei* ANKA liver stage parasites *in vitro* (Figure 2.4.1d). Supported by the good tolerability, activity against blood stage parasites and the confirmation of *in vitro* liver stage activity, we next investigated the *in vivo* activity of halofuginol in a *P. berghei* sporozoite challenge model [111]. As shown in Figure 2.4.1e, halofuginol reduced the growth of liver stage parasites by >99% following a single 5 mg/kg i.p. dose. Importantly, similar efficacy was observed with a single oral bolus of 10 mg/kg that resulted in 95% reduced parasite load, indicative of oral bioavailability of halofuginol (Figure 2.4.1e) [113].

Halofuginol Maintains the Antimalarial Potency but Lacks the Toxicity of Halofuginone in Mice.

Gastrointestinal toxicity observed in mice has prevented halofuginone's development as an antimalarial. Further clinical trials exploring halofuginone for cancer treatment have established nausea and fatigue as dose limiting [114], which is consistent with the well-documented emetic effects of febrifugine. Previous studies have reported significant toxicity in mice with an oral dose > 1mg/kg [113]. Thus, we set out to compare halofuginone and halofuginol at therapeutically relevant doses. Consistent with previous findings, poor tolerability of halofuginone was evident at the efficacious doses of 0.5mg/kg p.o., and 1 mg/kg resulted in pronounced gastrointestinal toxicities (4/5) and lethality (1/5) (SFigure 2.5.3). In contrast, treatment with halofuginol at the efficacious dose of 10 mg/kg p.o. reduced infection by >95% without evidence for gastrointestinal or other side effects from gross pathological assessment (Figure 2.4.1e).

FORWARD GENETIC APPROACH CONFIRMS CYTOSOLIC PROLYL-TRNA SYNTHETASE (PFL0670C) AS MOLECULAR TARGET OF HALOFUGINOL IN P. FALCIPARUM

The identification of the molecular mechanism of febrifugine derivatives in *Plasmodium* is of paramount interest for a comprehensive understanding of the antiprotozoal activity of this compound class and critical for the rational development of next generation antimalarials. We previously identified the bifunctional

glutamyl-prolyl-tRNA synthetase (EPRS) as the target of febrifugine analogs in metazoans [56]. However, the tRNA synthetase machinery differs greatly between humans and *P. falciparum*. In humans the EPRS is the only enzyme with prolyl tRNA synthetase activity. EPRS forms the central framework of the multi-subunit complex (MSC) that is involved in a diverse number of biological processes [115]. In contrast, *P. falciparum* expresses two prolyl tRNA synthetases, one targeted to the apicoplast and one targeted to the cytoplasm. Due to the difference in tRNA synthetase machinery and large evolutionary distance between alveolates and metazoans, we selected an unbiased approach to identify the target of febrifugine derivatives in plasmodium.

We chose a select-seq experimental design based on multiple independent drug resistance selection followed by whole genome sequencing to identify the acquired genetic mutations. We carried out independent stepwise resistance selections under intermittent drug pressure with halofuginone (IC_{50} = 0.5 nM) (Fig 2.4.1b) [83]. *P. falciparum* strains with decreased sensitivity to halofuginone were subjected to increased drug pressure until stable resistance was achieved (Figure 2.4.2A, B).

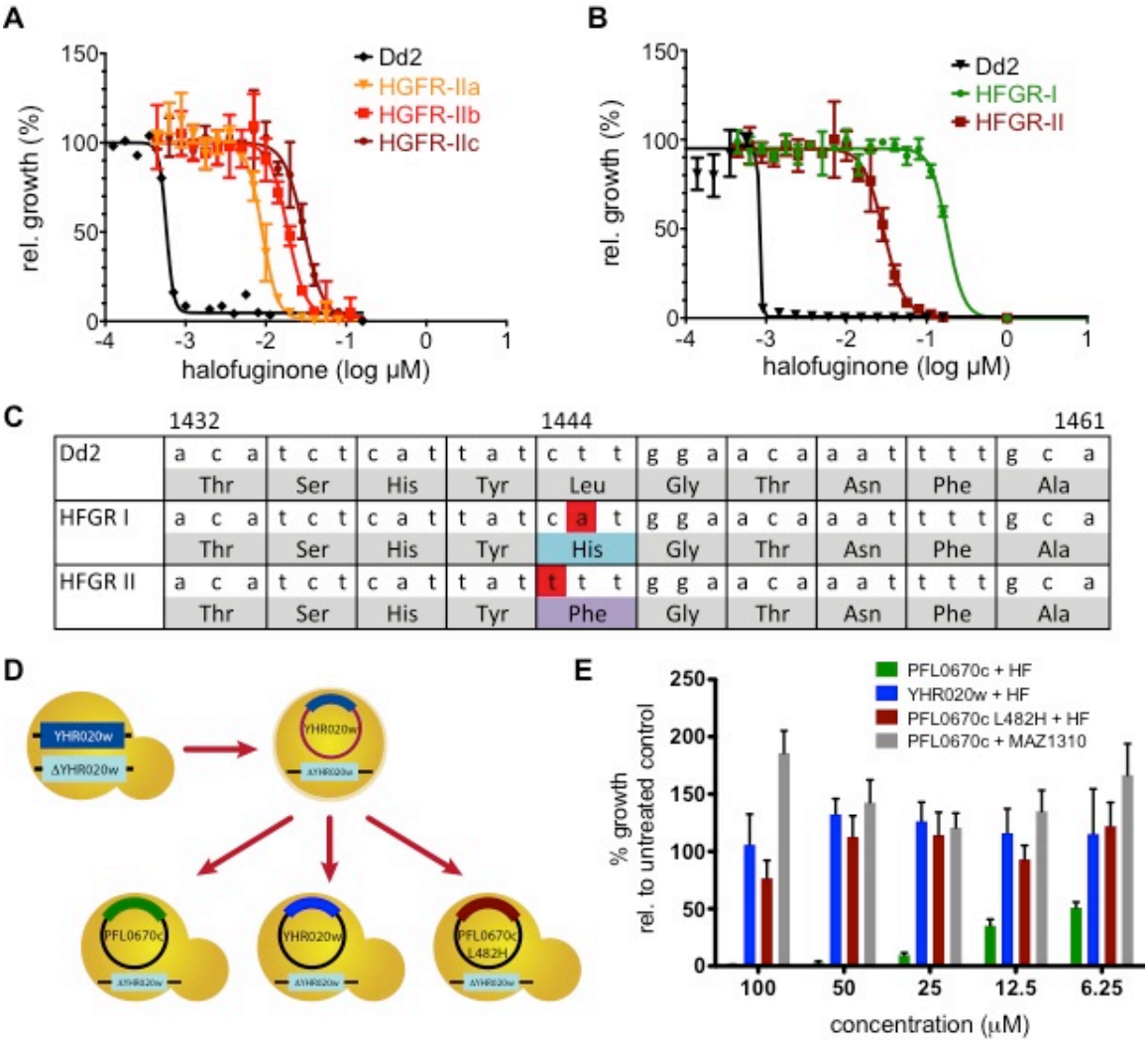

Figure 2.4.2: Identification and Validation of cPRS as target of Halofuginone in *P. falciparum*

(A) Resistance selection under intermittent and dose-adjusted drug pressure allowed for generation of parasite strains with stepwise increased resistance to halofuginone. **(B)** Independent selection experiments starting from the Dd2 lab strain yielded two highly resistant clones. **(C)** Whole genome sequencing identified nonsynonomous mutations in HGFRI and HGFRII that map to the same amino acid codon (L482) in PfcPRS (PFL0670c). **(D)** Target Confirmations using a heterologous yeast model. +/-YHR020w heterozygous *S. cerevisiae* was transformed with a YHR020w-containing plasmid and haploid spores were selected for genomic deletion of YHR020w. The intermediate strain was transformed with a second plasmid with an orthogonal selection marker and YHR020w, codon optimized PFL0670c and mutant PFL0670c, respectively, and further selected for loss of the first plasmid. **(E)** Only transgenic *S. cerevisiae* expressing wild type PfcPRS (green) displayed dose-dependent sensitivity to halofuginone, while strains expressing ScPRS (blue) or the L482H PfcPRS mutant (red) were insensitive to halofuginone treatment up to 100uM (all strains are pdr1,3 deleted). In addition, MAZ1310 does not affect growth of PFL0670c expressing yeast (gray).

We sequenced the full genome of two highly resistant parasite strains that were independently selected

(HFGR-I (IC_{50} = 180 nM), HFGR-II (IC_{50} = 30 nM)) along with the parental Dd2 strain to identify the genetic

loci that contribute to halofuginone resistance [85,86]. The only gene with nonsynonymous SNPs identified in multiple independently selected resistant strains was PFL0670c, which has been assigned as putative cytoplasmic proline amino acyl tRNA synthetase (PfcPRS) [116]. Importantly, both transversion mutations occurred in the same codon of PfcPRS (Figure 2.4.2C) translating in a L482H (HFGR-I) and L482F (HFGR-II) amino acid change, respectively. The missense mutations were independently confirmed with a High Resolution Melting genotyping assay (SFigure 2.5.4) and verified by Sanger sequencing.

Of the two prolyl tRNA synthetases in the *P. falciparum* genome, our forward genetic approach identified the ProRS that shares a high level of similarity with the human orthologue. The class II tRNA synthetase domains of EPRS and PfcProRS share 78% similarity. These results suggest that the primary target of halofuginone and febrifugine is the P. falciparum cytoplasmic prolyl tRNA synthetase. This hypothesis is further supported by the observation that addition of exogenous proline to the in vitro culture media reversed the growth inhibition in a dose-dependent manner (SFigure 2.5.5).

Furthermore, we found that the HFGR-I line was also resistant to febrifugine and halofuginol (SFigure 2.5.2), confirming that the molecular target identified for halofuginone, PfcPRS, is shared by all of our febrifugine derivatives.

Replacement of S. cerevisiae PRS by PfcPRS confers sensitivity to halofuginone and halofuginol in yeast

Saccharomyces cerevisiae PRS (ScPRS, YHR020w) is very similar to the *P. falciparum* cPRS and *H. sapiens* EPRS. Within the core Class II catalytic domains, the yeast PRS shares 77% and 70% similarity with human and plasmodium enzymes, respectively. Despite the high similarity we discovered that *S. cerevisiae* was not sensitive to halofuginone. This allowed us to use a yeast model for both target confirmation of halofuginone and validation of the resistance phenotype of the mutant alleles identified in our drug resistance selections.

First, we performed a complementation test of PfcPRS in *S. cerevisiae*. We deleted the chromosomal copy of ScPRS, an essential gene and the only locus that codes for a prolyl tRNA synthetase in *S. cerevisiae*. We found that episomal expression of PfcPRS could complement the ScPRS knock-out strain. Next, we

generated transgenic yeast strains that would express only ScPRS or PfcPRS , respectively (Figure 2.4.2d). While both strains exhibit comparable growth characteristics, only the PfcPRS-expressing strain displayed a dose-dependent sensitivity to halofuginone treatment (Figure 2.4.2e, SFigure 2.5.6). The sensitivity of the PfcPRS strain was attenuated by addition of free L-proline (SFigure 2.5.7).

To validate the resistant allele L482H, we generated a yeast strain expressing L482H PfcPRS. This strain was viable both in the presence and absence of halofuginone consistent with the L482H mutation conferring resistance to halofuginone (Figure 2.4.2e). Similar activity was observed for the L482F mutant. None of the tested yeast strains were susceptible to inhibition by the control compound MAZ1310 [55]. Halofuginol displayed an equivalent activity profile when tested against the wild-type and mutant yeast strains (SFigure 2.5.8).

Molecular Characterization of the Ligand-Target Interaction

To provide a molecular rational for the experimental results, we modeled the binding dynamics of the *Plasmodium falciparum* PRS to ATP and halofuginone based on the recently published structure of ternary human PRS complex (PDB: 4HVC) [117]. Our model shows that the N- protonated hydroxypiperidine moiety of halofuginone is strongly stabilized by a network of hydrogen bonding interactions (Figure 2.4.3a), which cannot be formed by MAZ1310. As is to be expected from the high similarity (77%) of the *Plasmodium falciparum* PRS core catalytic domains including the complete identity of the active site residues, the interactions between halofuginone, ATP and PRS are essentially identical to the one discussed for the case of human PRS [117].

Next, we investigated the L482H PfcPRS mutant to understand the experimentally observed insensitivity of this mutant; the Molecular Dynamics simulations revealed that the position of E361 changes from coordination to halofuginone (shown in white in Figure 2.4.3b) to a position where it is coordinated to S508 and Y365. We hypothesize this structural change is due to the hydrogen bond that the mutant H482 residue establishes with S508, thus re-orienting S508 to hydrogen bond with E361. The experimental observation that the L482H mutant is less strongly inhibited by halofuginone thus underscores again the critical

importance of this interaction. The L482F mutation, on the other hand, induces steric repulsion with residues nearby, again disrupting the interactions in the binding pocket (SFigure 2.5.9).

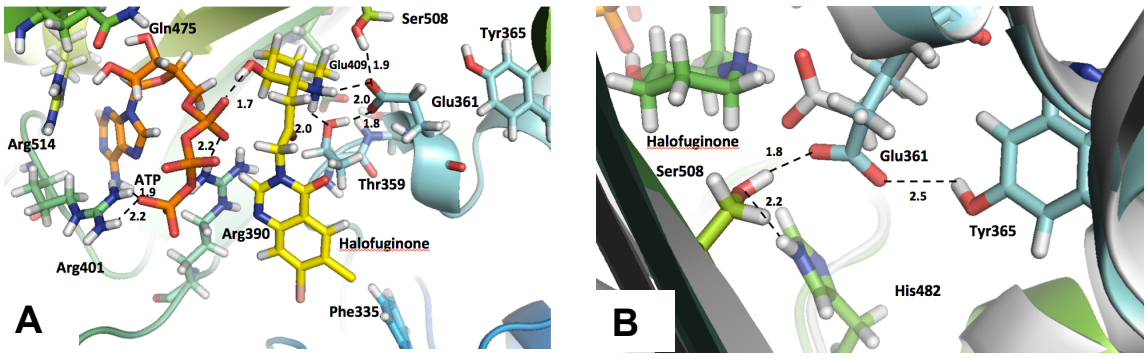

Figure 2.4.3: Models of the ternary complex of PfcPRS with ATP and halofuginone
Comparison of wild-type (**A**) and L482H mutant (**B**)

Halofuginol, Febrifugine and Halofuginone Induce the Amino Acid Starvation Response in P. falciparum

Following validation of PfcPRS as the molecular target of febrifugine and analogs, we turned our interest to understanding how the parasite senses amino acids and how halofuginol dysregulates these mechanisms. Like direct amino acid deprivation, inhibition of AARSs results in the accumulation of uncharged tRNA, which in turn binds and activates the eIF2α kinase GCN2 as the central control element of the conserved Amino Acid Starvation Response (AAR) pathway (SFigure 2.5.10) [118]. Recent research has confirmed the existence of a functional AAR in P. falciparum's intraerythrocytic stage and demonstrated the phosphorylation of eIF2α in response to isoleucine starvation (the sole amino acid that can be fully depleted as it is the only amino acid that is absent from hemoglobin) [58,59]. However, treatment with isoleucine tRNA synthetase inhibitors unexpectedly did not induce eIF2α phosphorylation[58].

To probe for the induction of the AAR, we have treated asynchronous Dd2 cultures with halofuginol, halofuginone, febrifugine, or MAZ1310 and quantified the amount of eIF2α and p-eIF2α by Western blot analysis relative to amino acid deprivation. (*2'R,2R,3S*)-halofuginol (*RRS*-HFol), the active halofuginol enantiomer (see SFigure 2.5.2), halofuginone, and febrifugine treatment significantly increased eIF2α

phosphorylation in a dose dependent manner comparable to amino acid starvation (Figure 2.4.4a,b, SFigure 2.5.11). DMSO and MAZ1310-control treatments failed to increase levels of eIF2α phosphorylation.

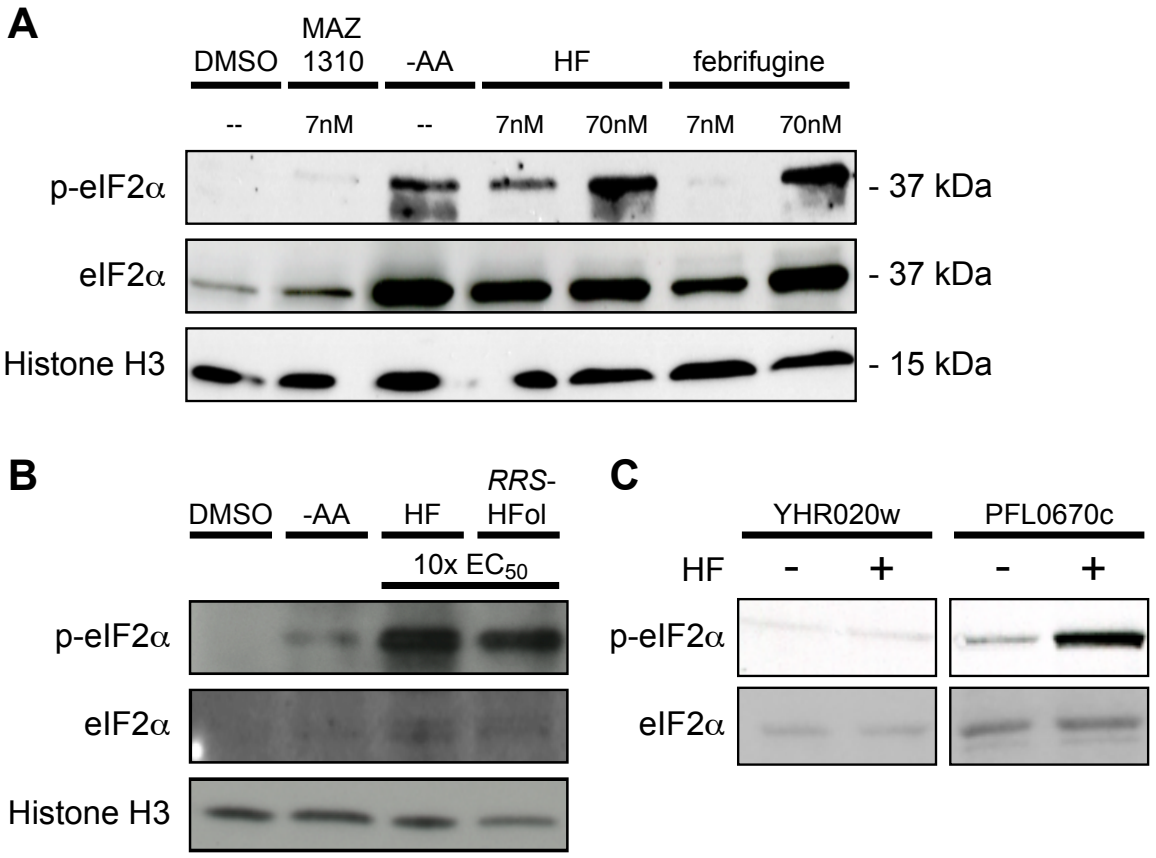

Figure 2.4.4: Halofuginol and Halofuginone Induce eIF2α Phosphorylation

Western blot analysis of p-eIF2α and total eIF2α protein in drug-treated asynchronous Dd2 **(A)** cultures and 3D7 **(B)** cultures relative to an amino acid starved reference (histone H3 serves as a loading control). Each blot is representative of two independent replicates. Halofuginone and febrifugine **(A)** and (*2'R,2R,3S*)-halofuginol (active enantiomer) **(B)** induce phosphorylation of eIF2α after 90 minutes treatment. **(C)** Halofuginone treatment induces pronounced eIF2a phosphorylation in PFL0670c but not in YHR020w-expressing *S. cerevisiae*.

The amino acid starvation response pathway is well characterized in yeast and, as in the P. falciparum pathway, eIF2α is phosphorylated in response to amino acid starvation [59]. To further probe the underlying mechanism of growth inhibition by halofuginone we investigated the effect of drug treatment on eIF2α Ser51-phosphorylation levels in both PfcPRS and ScPRS expressing yeast strains. Only the halofuginone-sensitive PfcPRS expressing strain exhibited robust induction of p-eIF2α in response to compound exposure

(Figure 2.4.4c), while no differential levels of eIF2α-phosphorylation were observed in the ScPRS expressing strain.

2.5 DISCUSSION

The need for new targets for anti-malarial drug development is universally recognized, and many have been proposed. However, well-defined, pharmacologically practical paths forward to new classes of drugs remain scarce. Many traditional druggable targets such as kinases proved challenging to yield promising candidate targets [119]. Febrifugine has been identified over 60 years ago as the active principle of one of the oldest known antimalarial herbal remedies. However, despite extensive efforts the underlying mechanism of febrifugine's antiparasitic activity remained a mystery. Furthermore, poor tolerability has prevented the clinical use of the natural product as a mainstay antimalarial and medicinal chemistry efforts, which were hampered by the unknown mode of action, have failed to identify viable alternatives.

We here report halofuginol, a novel halofuginone analog developed by our group, retains excellent *in vivo* activity against both human relevant malaria stages. Dual-stage activity is essential for antimalarial drugs that will be used to eliminate and eradicate human malaria. Importantly, halofuginol, unlike febrifugine and halofuginone, was very well tolerated *in vivo* when dosed orally or intraperitoneally at pharmaceutically relevant concentrations and did not induce any signs of toxicity even after 4 days of treatment. This attractive pharmacological profile makes halofuginol a promising candidate for further preclinical development.

Furthermore, we identify *P. falciparum* cytoplasmic Prolyl-tRNA-Synthetase (cPRS), one of two Prolyl-tRNA-Synthetases encoded in the *Plasmodium* genome, in an unbiased target-ID approach as the functionally relevant target of halofuginone, halofuginol and febrifugine (Reviewed in [120]). We support our findings by target validation in an orthogonal transgenic yeast model and provide a mechanistic rational for drug action on a molecular level.

Previous reports have suggested that tRNA synthetases represent attractive targets for the treatment of malaria. However, there has been little exploration of tRNA synthetase inhibitors in malaria and the

validation of on-target mechanism has been elusive. Past efforts have primarily focused on isoleucine utilization, as it represents the sole amino acid that the parasite cannot obtain from hemoglobin digestion. Recently the isoleucyl tRNA synthetase inhibitors mupirocin and the isoleucine analog thiaisoleucine have been shown to kill blood stage parasites at mid-nanomolar and low micromolar concentrations, respectively. However, neither compound was capable of inducing the phosphorylation of eIF2α, which is a sensitive indicator of the starvation response and a hallmark of isoleucine withdrawal. Deepening the puzzle, isoleucine starvation, which would also be expected to act through limitation of isoleucyl tRNA synthetase activity, is not acutely toxic to the parasite but induces in a hibernatory state. Our work demonstrates that *P. falciparum* also senses restriction of proline with great sensitivity, which possibly further expands the field to study utilization of other amino acids.

Our findings not only identify the first small molecule tRNA synthetase inhibitor that induce the amino acid starvation response in viable Plasmodium parasites, validating valuable chemical tools for chemogenomic approaches to study this pathway in *P. falciparum* and *S. cerevisiae*, but also establishes amino acyl tRNA synthetases as attractive targets for the development of new classes of antimalarials active against both the red blood cell and liver stages of malaria. The transgenic yeast strain in combination with halofuginone will further prove invaluable to mechanistically dissect nutrient deprivation signaling pathways. These tools enable studies in *S. cerevisiae* to understand the independence/interrelatedness of the nutrient sensing of the AAR and the TOR pathways [121].

The potent *in vivo* activity of halofuginol against both human relevant life-cycle stages is very encouraging and demonstrates that well tolerated and efficacious halofuginone analogs can be developed. Our findings that halofuginol also binds to the human EPRS suggests that the side effects observed with halofuginone and febrifugine are indeed caused by off-target effects. However, more detailed studies that are beyond the scope of this work will be required to rule out that the excellent tolerability is not only the result of a favorable pharmacokinetic profile.

We speculate that the broad-spectrum antiprotozoal activity of halofuginone could be due to conservation of the prolyl tRNA synthetase. Halofuginone is currently approved in veterinary medicine to treat coccidiosis in poultry (caused by *Eimeria tenella*) and cryptosporidiosis in cattle (caused by *Cryptosporidium parvum)* [122-124]. Molecular phylogenetics of the catalytic domain of the ProRS confirmes that the ProRS of both veterinary parasites, *E. tenella* and *C. parvum*, displays 81 and 86 % similarity respectively to that of *P. falciparum* (SFigure 2.5.12). Furthermore, these agents may be effective against other human malarias such as *P. vivax,* which shares 95% conservation of the active site of the cPRS, and a wide swath of infectious diseases caused by protozoan parasites including toxoplasmosis and cryptosporidiosis.

Combined with our recent identification of the human EPRS as the host target, the computational mechanistic study here provides a detailed understanding of the ligand-protein interaction with atomic resolution in both the human and parasite enzyme, establishing a clear path forward to the design of new inhibitors with dual-stage activity in humans that selectively target the malaria parasite. Given the excellent efficacy and excellent tolerability, halofuginol represents an attractive lead candidate for preclinical development.

Chapter 3:

Sequential Evolution of Resistance to Halofuginone: Evidence for Genetic and Epigenetic Regulation

3.1 Attribution

Authors: Jonathan D. Herman[1,2], Daniel P. Rice[3,4], Ulf Ribacke[2], Amy Deik[1], Eli Moss[1], Michael Desai[3,4], Clary B. Clish[1], Ralph Mazitschek[1,2,7], Dyann F. Wirth[1,2]

Affiliations:

[1] The Broad Institute, Infectious Diseases Initiative, Cambridge, MA 02142, USA

[2] Harvard School of Public Health, Department of Immunology and Infectious Disease, Boston, MA 02115, USA

[3] Department of Organismic and Evolutionary Biology, Harvard University, Cambridge MA 02138

[4] FAS Center for Systems Biology, Harvard University, Cambridge MA 02138

[5] Department of Cell and Molecular Biology, Microbiology, Uppsala University, 751 24 Uppsala, Sweden

[7] Massachusetts General Hospital, Center for Systems Biology, Boston, MA 02142, USA

We gratefully acknowledge financial support for this work by the Gates Foundation (DFW and RM) and the National Institute of Health (DFW) (AI084031).

J.D.H. designed and performed HFGRII and HFGRIII *in vitro* selections. J.D.H. characterized selections and clones. E.M. aligned WGS data to a reference genome. D.P.R called SNPs and performed the trajectory-based sequencing analysis. J.D.H performed additional sequencing analysis of CNVs. J.D.H. designed and prepared samples for metabolite profiling experiments. A.D. ran and quality-controlled the mass-spec analysis of metabolites. C.C. and J.D.H. analyzed metabolite experimental data. J.D.H. designed and performed the HFG-induced resistance and *clag* expression experiments.

3.2 Introduction

We have previously described two mutations in the cytoplasmic prolyl tRNA synthetase (cPRS) that confer resistance to halofuginone. We describe here the evolutionary trajectory of resistance of two independent drug resistance selections. We show that non-genetic adaptation to halofuginone precedes mutation or amplification of the cPRS gene. *P. falciparum* first rewires its proline homeostasis in response to halofuginone pressure through overexpression of the PSAC determinants cytoadherence-linked asexual gene (*clag*) 2 and *clag* 3.2. By tracking the evolution of two drug resistance selections with by whole genome sequencing, we demonstrate that the cPRS locus accounts for the majority of genetic adaptation to halofuginone in *P. falciparum*. We further validate that, in addition to mutations in the cPRS locus, copy-

number variations also contribute to halofuginone resistance. Finally, we provide a three-step model for multi-locus evolution of drug resistance via genetic and non-genetic adaptations in *P. falciparum*.

3.3 MATERIALS AND METHODS

METAGENOMIC WHOLE GENOME SEQUENCING OF HFG POPULATIONS SELECTED *IN VITRO*

Genomic DNA extracted from bulk population cultures of the two independent lines selected for halofuginone resistance was extracted and sheared with a Covaris S220 Focused-ultrasonicator (Covaris Woburn, MA). Illumina-compatible libraries were prepared on the Apollo 324 (WaferGen Biosystems Fremont, CA) and sequenced on an Illumina HiSeq 2000 (Illumina San Diego, CA). *P. falciparum* populations were sequenced with the goal of reaching over 60x average fold-coverage across the genome.

Metagenomic Time Series Analysis to Identify Segregating Sites

We used a two-stage process to distinguish real mutations from sequencing and alignment errors in the metapopulation time-series sequence data. First, we used the GATK (Broad Institute Cambridge, MA) to obtain a permissive list of candidate loci and the number of supporting reads for each allele in each time-point. We used the haploid mode of GATK's UnifiedGenotyper with a minimum confidence threshold phred score of 4 to obtain a permissive set of SNPs and small INDELs. We further filtered this set of candidates based on two fundamental assumptions: first the two independent replicate populations should not share the exactly the same mutations. Second, the frequencies of a real mutation should be correlated through time (positive autocorrelation), while sequencing errors should be uncorrelated at different time points (negative or zero autocorrelation).

Thus we 1) discarded all sites with an average coverage depth less than 10x across the time points, 2) discarded all sites with an average frequency above 1% in the non-focal population 3) I discarded all sites with a negative or zero autocorrelation. 4) Further, we noticed that the frequencies of alternate alleles at HFGRII time point 2-30x were aberrant despite deep coverage and we discarded this time point from the analysis due to potential contamination.

METAGENOMIC TIME SERIES ANALYSIS TO IDENTIFY SELECTIVE SWEEPS

We took the unfiltered list of candidate loci called by the Unified Genotyper (GATK) and looked for mutations that began at a frequency near zero at the first time point and ended at a frequency near one at the last time point.

METAGENOMIC TIME SERIES ANALYSIS TO IDENTIFY HITCHHIKING MUTATIONS ALONG WITH CPRS MUTATION IN HFGRII

We searched for mutations that hitchhiked with the known mutation at the C1444T cPRS in HFGRII. To find hitchhiking mutations, we sorted the unfiltered list of candidate loci called by the Unified Genotyper (GATK) by the Euclidean distance between their allele frequencies trajectories and the frequency trajectory of the focal mutation.

QPCR – COPY NUMBER ANALYSIS

Genomic DNA was prepared from saponin-lysed *P. falciparum* parasites using the Qiagen Blood Mini- or Midi Kits (Qiagen Venlo, Limburg). qPCR analysis was performed on an Agilent 7900HT Fast Real-Time System (Agilent Technologies Santa Clara, CA). System using unlabeled primers and Power SYBR Green master mix and. Primers used for copy-number analysis are in Table 3.3.1 (target locus primers) and Table 3.3.2 (control locus primers). Copy number was calculated using the ΔΔCt method included in the SDS version 2.3.2 as described in the Applied Biosystems User Bulletin 2.

Table 3.3.1: qPCR Control Primers

Gene Name	Direction	PlasmoDB ID	Sequence (5′ to 3′)
fructose-bisphosphate aldolase	Forward	PF3D7_1444800	TGTACCACCAGCCTTACCAG
fructose-bisphosphate aldolase	Reverse	PF3D7_1444800	TTCCTTGCCATGTGTTCAAT
B-tubulin	Forward	PF3D7_1008700	CGTGCTGGCCCCTTTG
B-tubulin	Reverse	PF3D7_1008700	TCCTGCACCTGTTTGACCAA
Seryl tRNA Synthetase	Forward	PF3D7_0717700	TATCATCTCAACAGGTATCTACATC TCCTA
Seryl tRNA Synthetase	Reverse	PF3D7_0717700	TTTGAGAGTTACATGTGGTATCAT CTTTT

Table 3.3.2: qPCR Primers for cPRS Target

Gene Name	Region of Gene	Direction	PlasmoDB ID	Sequence (5′ to 3′)
Prolyl tRNA synthetase (cPRS)	5'	Forward	PF3D7_1213800	TGCTATAAGACCAACAA GTGAAACA
Prolyl tRNA synthetase (cPRS)	5'	Reverse	PF3D7_1213800	ACGTACCACAGTATTCC ATTGATTT
Prolyl tRNA synthetase (cPRS)	3'	Forward	PF3D7_1213800	CCAAACAAACAGTGAAA CGACAT
Prolyl tRNA synthetase (cPRS)	3'	Reverse	PF3D7_1213800	TAGGTGGTTGATCTAAC GGGATAC

IN VITRO DRUG SENSITIVITY AND DOSE-RESPONSE ANALYSIS BY SYBR GREEN STAINING

The SYBR Green I method was used as previously described[82]. In brief, we grew *P. falciparum* parasites for 72 hours in 384-well plates at 1% hematocrit and 1% starting parasitemia. Growth was assessed by SYBR Green staining of parasite DNA. All dose-response assays were carried out with twelve-point curves in

technical triplicate. DMSO stocks of drugs used were dispensed by HP D300 Digital Dispenser (Hewlet Packard Palo Alto, CA). Fluorescence measurements were collected on a SpectraMax M5 (Molecular Devices Sunnyvale, CA) and analyzed on GraphPad Prism version 5 (GraphPad Software La Jolla, CA) and EC_{50} values were determined with the curve-fitting algorithm log(inhibitor) vs. response – Variable slope.

In Vitro Drug Sensitivity and Dose-Response Analysis by Tritiated Hypoxanthine Assay

Halofuginone dose-response assays were performed as described by Desjardins et al. using the initial drug-resistance selected HFGRII parasites[125].

Parasite Culture

Malaria culture was performed as described by Trager *et al*. [81]. Dd2 is a chloroquine resistant *in vitro* cultured parasite cloned from the Laos derived W2-MEF parasite obtained from MR4 (ATCC Manassas, Virginia).

Flow Cytometry

Flow cytometry of *P. falciparum* infected erythrocytes was carried out based on SYBR Green I staining of parasite nuclei as previously described [126]. Modifications to the Bei et al. protocol include staining of iRBC with SYBR Green I at a 1:2000 concentration, acquisitions of non-single cells were pre-filtered for cells that fell on the y=x line in a plot of forward scatter area vs. height. All Flow Cytometry was collected on a MACSQuant Flow Cytometer (Miltneyi Biotec Inc. San Diego, CA) and analyzed with MacQuantify and FlowJo 8.8.6 software (Tree Star Ashland, OR).

LC-MS analysis of amino acids and polar metabolites

Highly synchronous (within 4 hours) early schizonts were magnetically purified with MACS CS columns (Miltenyi Biotec). A small aliquot was also made for flow cytometry. The rest of the purified samples were divided into two equal volumes: one for saponin lysis (0.025%) and one for whole iRBC extraction. Each sample was washed 2x in PBS, and then suspended in 10 uL PBS. Polar metabolites were extracted using

nine volumes of 74.9:24.9:0.2 (v/v/v) acetonitrile/methanol/formic acid containing stable isotope-labeled internal standards (0.2 ng/µL valine-d8 (Isotec); and 0.2 ng/µL phenylalanine-d8 (Cambridge Isotope Laboratories)). Profiles of amino acids were measured using LC-MS as described previously[127]. Briefly, positive ionization, multiple reaction mode (MRM) data were acquired using a 4000 QTRAP triple quadrupole mass spectrometer (AB SCIEX) coupled to an 1100 Series pump (Agilent) and an HTS PAL autosampler (Leap Technologies). Cell extracts (10µL) were injected onto a 150 x 2.1 mm Atlantis HILIC column (Waters). The column was eluted isocratically at a flow rate of 250 µL/min with 5% mobile phase A (10 mM ammonium formate and 0.1% formic acid in water) for 1 minute followed by a linear gradient to 40% mobile phase B (acetonitrile with 0.1% formic acid) over 10 minutes. The ion spray voltage was 4.5 kV and the source temperature was 450°C. MultiQuant 1.2 software (AB SCIEX) was used for automated peak integration and metabolite peaks were manually reviewed for quality of integration and compared against a known standard to confirm identity. Stable isotope-labeled internal standards were used to eliminate samples with poor data quality. Metabolite peaks signals were normalized by flow cytometry-determined cell counts and compared to PBS and uninfected red blood cell control measurements. Pearson correlation analysis was performed in prism and heat maps were generated with Gene-e (Broad Institute).

qPCR – Gene Expression Analysis

Total RNA was extracted using Trizol (Life Technologies Carlsbad, CA) according to manufacturer instructions, DNAse-treated, and re-purified with Qiagen RNeasy mini columns ((Qiagen Venlo, Limburg)). First strand cDNA synthesis was performed using SuperScript III (Life Technologies) following manufacturer instructions. The absence of contaminating DNA and the success of the reverse transcriptase reaction were confirmed by comparing qPCR of Rt+ and Rt- with the control Seryl tRNA synthetase primer set in quadruplicate; samples were run on and ABI 7900 HT and fold-expression calculated using the ABI software suite SDS 2.3.2. cDNA concentrations were normalized to SerRS Ct values to minimize biases in PCR efficiency. Samples were run in quadruplicate with two control primer sets for validation of expression analysis. PCR amplification was performed as follows: 15 minutes at 95 °C followed by 40 cycles of two-

step amplification of 94 °C for 30 s and 52 °C for 30 s. All primers used for expression analysis (Table 3.3.3 and 3.3.4) were validated for specificity and efficiency under the same PCR conditions.

Table 3.3.3: qPCR primers for clag gene family expression analysis

Gene Name	Direction	PlasmoDB ID	Sequence (5′ to 3′)
Clag 2	Forward	PF3D7_0220800	CTCTTACTACTTATTATCTATCTCTCA
Clag 2	Reverse	PF3D7_0220800	CCAGGCGTAGGTCCTTTAC
Clag 3.1	Forward	PF3D7_0302500	ACCCATAACTACATATTTTCTAGTAATG
Clag 3.1	Reverse	PF3D7_0302500	TCTGAACTAGGAGGCCAACC
Clag 3.2	Forward	PF3D7_0302200	ACCCATAACTACATATTTTCTAGTAATG
Clag 3.2	Reverse	PF3D7_0302200	TTCAGCAGCAAGTCCGTGA
Clag 8	Forward	PF3D7_0831600	GTTACTACAACATTCCTGATTCAG
Clag 8	Reverse	PF3D7_0831600	AATGAAAATATAAAAATGCTGGGGGAT
Clag 9	Forward	PF3D7_0935800	TACCATTAGTGTTTTATACACTTAAGG
Clag 9	Reverse	PF3D7_0935800	CCAAAATATGGCCAAGTACTTGC

3.4 Results

TRACKING *IN VITRO* EVOLUTION OVER TIME BY WHOLE GENOME SEQUENCING

From our previous work to identify the target of halofuginone, we performed end-point whole genome sequencing on three *in vitro* evolution experiments: HFGRI, HFGRII, and HFGRIII. For two of these selections, HFGRII and HFGRIII, we collected phenotypic data and genetic material from multiple time-points . At cycle 40, we performed whole genome sequencing of HFGRII and HFGRIII though we continued our selection for another 15 generations. In Chapter 2 we identified a L482F mutation in the cytoplasmic Proline tRNA Synthetase (cPRS) in HFGRI selection and an L482H mutation in the cPRS of HFGRII selection.

In this paper, we present a genomic look at the step-wise evolution of halofuginone resistance in HFGRII and HFGRIII. We independently selected two populations with increasing intermittent drug pressure that till

we obtained parasites capable of growing in 140 nM halofuginone, which is 200-times the EC50 of the parental Dd2 line. We performed whole genome sequencing of the entire evolving population to track the rise and fall of mutant alleles over 50 generations (HFGRII) and 58.5 generations (HFGRIII) as displayed in Tables 3.4.1 and 3.4.2.

Table 3.4.1: Sequenced time points from the HFGRII *in vitro* evolution experiment

HFGRII Population Time Points Sequence	Generations	Drug Pressure (EC50)	Drug Pressure (nM)	Fold Coverage
HFGRII 2-10x	18	2-10x	7	185
HFGRII 1-30x	23	1-30x	21	263
HFGRII 2-30x	27	2-30x	21	141
HFGRII 2-60x	34	2-60x	42	232
HFGRII 1-200x	41	1-200x	140	235
HFGRII 2-200x	50	2-200x	140	181

Table 3.4.2: Sequenced time points from the HFGRIII *in vitro* evolution experiment

HFGRIII Population Time Points Sequence	**Generations**	**Drug Pressure (EC50)**	**Drug Pressure (nM)**	**Fold Coverage**
HFGRIII 2-10x	18	2-10x	7	12
HFGRIII 1-30x	23	1-30x	21	263
HFGRIII 1-60x	32	1-60x	42	241
HFGRIII 2-60x	36	2-60x	42	246
HFGRIII 1-200x	45	1-200x	140	240
HFGRIII 2-200x	55	2-200x	140	92
HFGRIII 3-200x	58.5	3-200x	140	92

A View of a genome evolving with few mutations Fixing In the Population

We used our time-course data from HFGRII and HFGRIII to distinguish true mutations from sequencing or alignment-introduced error. From this analysis framework, we found a paucity of genomic mutations over time. To our surprise, most of the genetic adaptation during our evolution experiments occurred at the cPRS locus. With this method, we confirmed the evolution of the L482F cPRS mutation in HFGRII. The L482F mutation first appeared at 27 generations at a 0.6% allele frequency; we manually verified that the 2 out of 332 reads supporting this call were high quality and ruled out sequencing artifact. However, the cPRS mutation in HFGRII did not proceed to fixation as we would have assumed. It reached a maximum allele frequency of 57%. After 20 additional generations, the L482F mutation was competed out and disappeared from the population (Figure 3.4.1a). In contrast, we found that no SNPs proceeded to fixation in HFGRIII over the course of the experiment.

Outside of the cPRS, we found one other mutation that passed through our filters in HFGRII: Pf3D7_1402700, a pre-mRNA splicing factor on chromosome 14. From generation 41 to generation 50 of HFGRII, the A->T mutation went from 3 to 51% of aligned reads. However, this was only supported by 3 and 21 reads respectively and could possibly be remaining artifact. Using the same filtering methodology in HFGRIII, we did not find a single segregating SNP that was not subtelomeric. Although such subtelomeric mutations could be an alignment error, they often occur in repeated gene families that recombine more frequently.

As orthogonal approaches to our filtering approaches, we also looked for mutations that would have went to fixation over the course of the selection or any that hitchhiked with the HFGRII cPRS mutation. Both analytic approaches did not find any candidate mutations that either fixed during the selection or were tightly linked to the HFGRII cPRS mutation. Without mutations sweeping to fixation, drug resistance might be achieved in these populations by multiple mutations in independent lineages or may not be due to SNPs or small INDELs and thus could have been missed by this metagenomic sequencing approach.

It was evident from our whole genome sequencing data that copy number variation (CNV) at the cPRS locus played a role in developing halofuginone resistance. We tracked the cPRS amplification in the two selections with qPCR relative quantification. We found that the cPRS gene amplification occurred by generation 50 in HFGRII and generation 32 in HFGRIII.

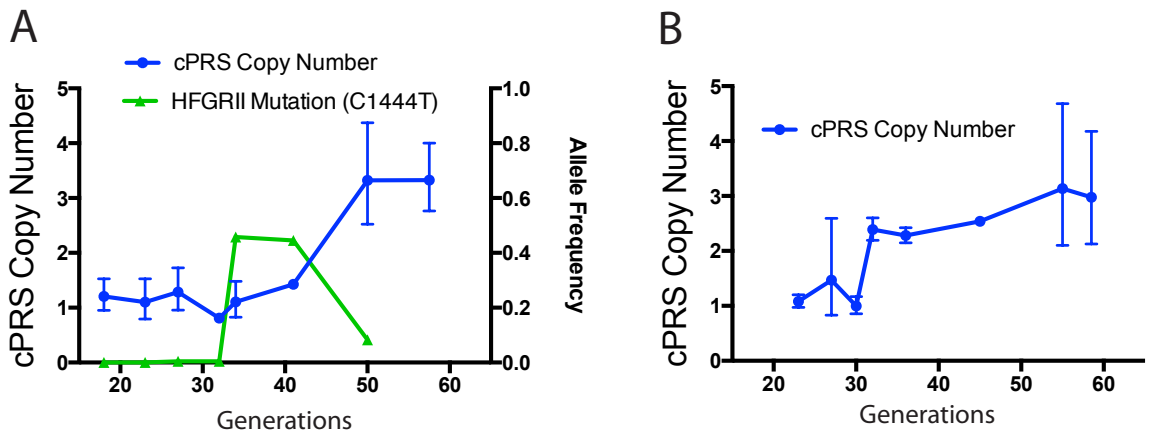

Figure 3.4.1: cPRS copy number and mutational variation of *in vitro* evolution experiments

Copy number was determined by ΔΔCt qPCR with SerRS as an endogenous control and allele balance was determined by analysis of next generation whole genome sequencing data from the HFGRII (a) and HFGRIII (b) *in vitro* evolution experiments.

From genetic analysis, we can identify adaptations at the cPRS locus from generation 32 and on, in both *in vitro* evolution experiments. However, acquisition of halofuginone resistance preceded cPRS copy expansion (Figure 3.4.1a,b). By cycle 27 in HFGRII, the bulk population had 18-fold decreased sensitivity to halofuginone (Figure 3.4.2).

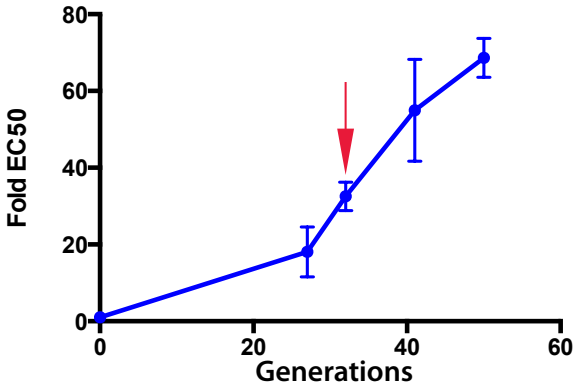

Figure 3.4.2: The acquisition of halofuginone resistance precedes genetic adaption in HFGRII

Resistance is quantified as the fold-increase in EC50 of the total population over the EC50 of the Dd2 parental line. The red arrow points to cycle 32, where the cPRS mutation first reaches an allele frequency of 0.57. EC50s were determined by a tritiated hypoxanthine incorporation dose-response assay.

To validate this phenomenon, we recreated the early steps of our evolution experiments but evaluated them much earlier on in the process of adaptation. We put wild type (WT) Dd2 parasites under constant halofuginone pressure (2.8nM). Within 8-9 generations, both replicate-treated Dd2 lines were more than 20-fold resistant compared to an untreated Dd2 line (Figure 3.4.3a). Since this Dd2 parasite line was the same used for our *in vitro* evolution experiment, we replicated these results in the unrelated parasite line 3D7 (Figure 3.4.3b). From here on we will refer to this phenomena as induced resistance.

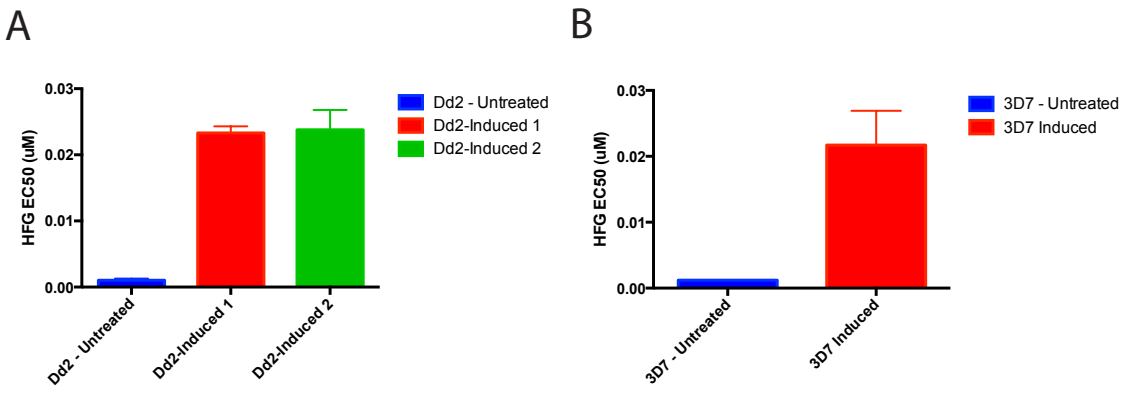

Figure 3.4.3: Short-term treatment of wild-type parasites results in immediate induction of halofuginone resistance

(a) Dd2 and (b) 3D7 induced parasites have increased halofuginone EC50 values determined by SYBR Dose-Response Assay.

Surprised that 20-fold resistance could be acquired only over 8 generations of exposure we conceived of two possible explanations for the results: non-genetic adaptation or fixation of prior-existing genetic diversity. We first investigated amino acid homeostasis in our induced parasites based on our knowledge of their effects on cell-based responses to halofuginone. In *Chapter 2* we found that increased environmental proline can alter halofuginone dose-response (Herman et al. *submitted*). Furthermore, proline is the only one of the three cPRS substrates that we believe competes with halofuginone for the cPRS binding pocket.

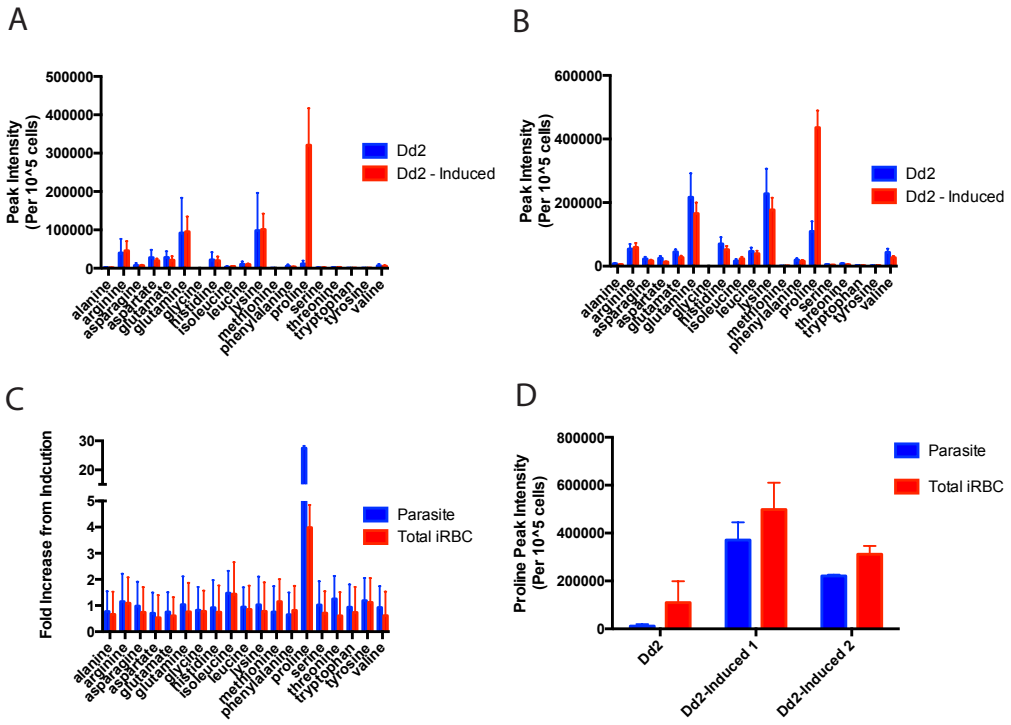

Figure 3.4.4: Induced Parasites Specifically Upregulate Intracellular Proline Concentration

(a)(b) Amino acid levels of purified Dd2 untreated and induced *P. falciparum* parasites (a) and total *P. falciparum* infected erythrocytes (iRBC) (b) Amino acid measurements are expressed as the integrated peak intensity per 10^5 cells.
(c) Fold-increase in amino acid concentration upon induction is expressed as a ratio of halofuginone pre-exposed over unexposed concentrations.
(d) Parasite and iRBC proline concentration in both biological-replicate induced parasites.

Of the 19 amino acids we measured with our LC-MS approach, proline was uniquely upregulated in induced parasites (Figure 3.4.4a) and total infected erythrocytes (iRBC) (Figure 3.4.4b); our iRBC measurements represent magnetically-purified red blood cells and thus represent the sum of both parasite and erythrocyte cytoplasmic proline pools. Induction produced a 3-5 fold increases in iRBC proline and 19-32 fold increases in purified parasites proline levels (Figure 3.4.4c). Our biological replicate inductions of Dd2 parasites showed similar increases in parasite and iRBC proline (Figure 3.4.4d).

Abrupt Induction of Halofuginone Resistance Occurs Through *clag* Gene Overexpression

Among 19 amino acids measured in induced and un-induced Dd2 parasites, we saw higher correlation between other amino acids and proline levels in the total iRBC samples than in purified parasites (Figure 3.4.5a). The three amino acids most highly correlated with proline were tyrosine, methionine, and isoleucine. Since all three amino are essential exogenous nutrients for *in vitro* growth [60] we thought a more general amino acid importation mechanism on the surface of the red blood cell could be involved. Thus, we chose to determine if the parasite-specific anion current (PSAC) that is responsible for the increased permeability of Plasmodium-infected erythrocytes was involved in induced halofuginone resistance. To probe this, we investigated the expression of the NPP/PSAC-associated *clag* gene family in induced parasites.

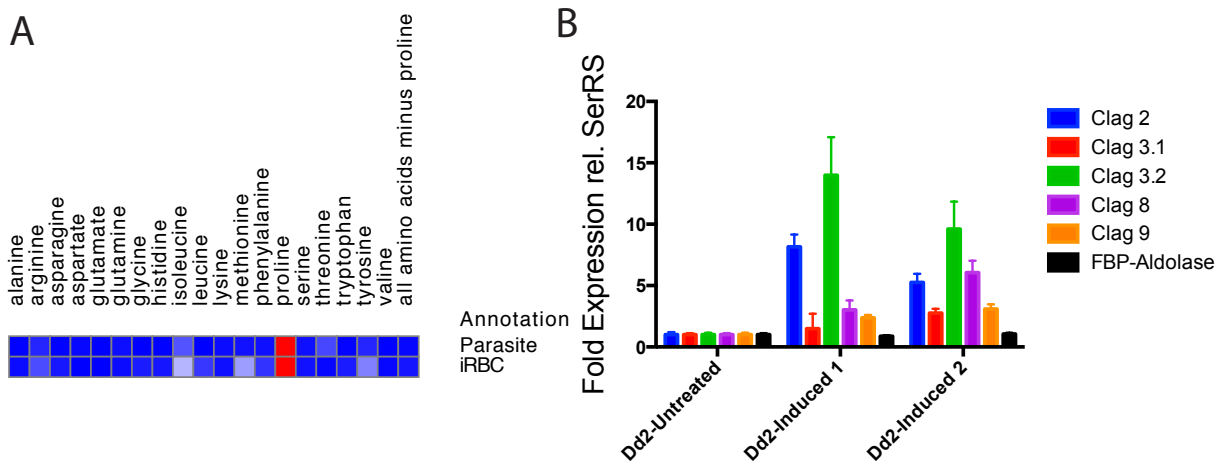

Figure 3.4.5: Stronger Correlation of Other Amino Acids with Proline in iRBC Leads us to *Clag* Overexpression

(a) Heatmap of R^2 correlation coefficients between proline concentration and a second amino acid in measurements of Dd2 untreated and Induced parasites. Correlation of amino acid fluctuations was examined separately for purified parasites and iRBCs. *P(two-tailed)<0.05. P-values for amino acids statistically significantly correlated with proline levels in iRBCs: Methionine p=0.0237, Isoleucine p=0.0379.

(b) Expression analysis of the Clag gene family in highly synchronous induced and untreated Dd2 early schizonts. FBP-Aldolase is included as a second control. SerRS was the endogenous control primer set used for ΔΔCt analysis.

We found that *Clag* 2 and *Clag* 3.2 expression to be robustly upregulated in Dd2 parasites with halofuginone-induced resistance. *Clag* 8 was also upregulated in both replicate Dd2 induced parasites, but to a lesser extent (Figure 3.4.5b).

Induced Halofuginone Resistance is Unlikely to have a Genetic Cause

Over three months, induced halofuginone resistance has been a stable phenotype. Both Dd2 and 3D7 parasites have remained resistant over these three months without halofuginone drug pressure. To address the possibility that preexisting genetic diversity could have been selected upon and fixed in 8 generations, we performed whole genome sequencing of Dd2 untreated and two biological replicate inductions of Dd2. We are still awaiting the sequencing results.

However, we have been able to characterize the cPRS locus of Dd2 induced and untreated strains. Resequencing of the entire cPRS gene did not identify any cPRS mutations in the induced parasites (Figure

3.4.6a). Similarly, we found no significant change in cPRS expression in Dd2 induced parasites (Figure 3.4.6b).

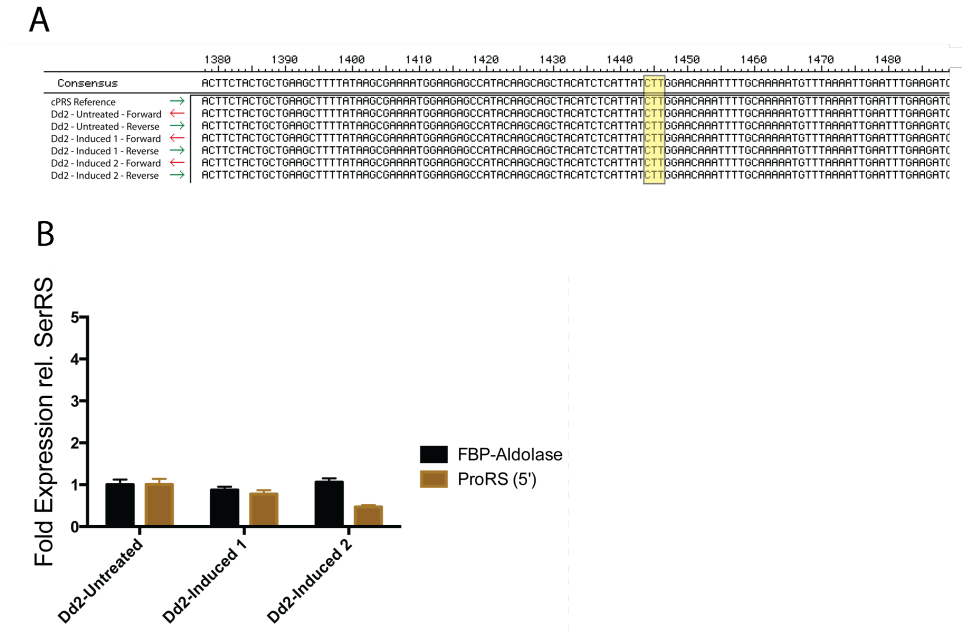

Figure 3.4.6: Induced Dd2 parasites have no evidence of genetic modifications at cPRS locus

(a) Sanger sequencing across the cPRS allele revealed that induced and untreated Dd2 strains have WT cPRS alleles. The codon where HFGRI (T14445A) and the HFGRII (C1444T) mutations occurred is highlighted in yellow.

(b) Expression of cPRS in synchronous early schizonts is invariant between untreated and induced Dd2 parasite lines.

LIKE DD2-INDUCED LINES, HFGII, AND HFGRIII *IN VITRO* EVOLVED LINES HAVE UNIQUELY INCREASED PROLINE POOLS

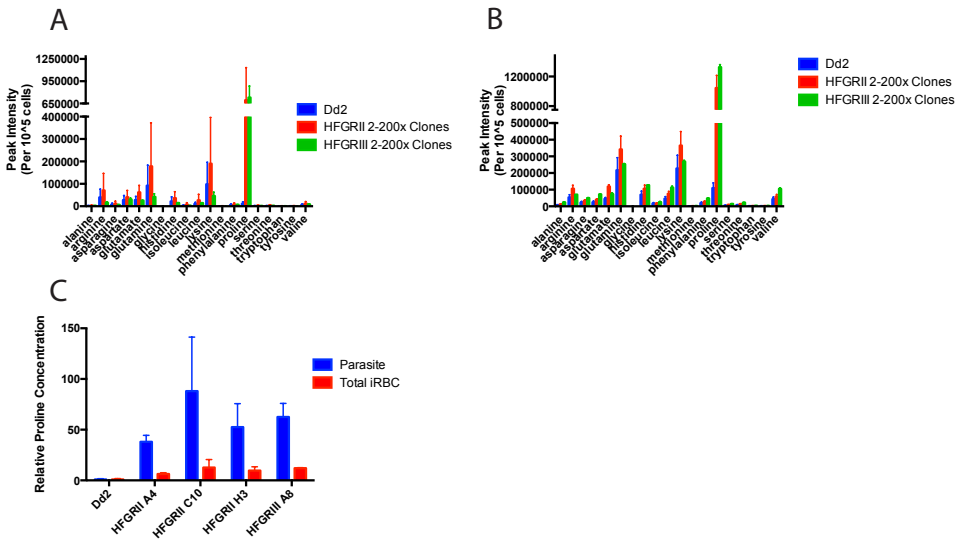

Figure 3.4.7: HFGRII and HFGRIII *in vitro* Evolved Halofuginone Resistant Lines Have Increased Proline Concentration

(a)(b) Concentration of 19 measured amino acids in (a) purified parasites and (b) infected RBCs from the parental Dd2 line and clones from *in vitro* selected lines HFGRII and HFGRIII. Data is displayed as integrated peak intensity per 10^5 cells.
(c) Relative proline concentration in clones from *in vitro* selected HFGR lines. Concentrations are relative to the parental Dd2 line.

We found that purified parasites cloned from the 2-200x selection time point (50 and 55 generations respectively) of HFGRII and HFGRII *in vitro* selected lines had dramatically increased proline concentration in purified parasites (Figure 3.4.7a) and iRBC (Figure 3.4.7b). Similar to induced Dd2 parasites, i*n vitro* evolved lines showed similar amino acid selectivity for increased proline and far greater enrichment of proline in purified parasites than total iRBCs (Figure 3.4.7c).

Copy Number Variation at cPRS Locus Contributes to HFG Resistance

Intrigued by our observations of cPRS locus amplification from whole genome sequencing, we confirmed this observation with qPCR over the span of the *in vitro* evolution experiments. While we verified the amplification of the cPRS locus in HFGRII (Figure 3.4.1a) and HFGRIII (Figure 3.4.1b), we also found an interesting difference in the temporality of this amplification. HFGRIII, the culture without cPRS mutations, had evidence of amplification 18 generations before HFGRII.

Although the HFGRIII 2-200x (Generation 55) parasite clones are from the same genetic background and grew in parallel in the same *in vitro* evolution experiment, we wanted to eliminate the chance that genetics factors beyond the cPRS locus could account for the HFG drug resistance. We are currently performing whole genome sequencing on the three clones and are still awaiting the sequencing results.

To explore the effect that cPRS copy number variation plays in resistance to halofuginone, we cloned by dilution the end point HFGRIII parasite population, HFGRIII 2-200x. We obtained 14 clonal lines and found an allele frequency spectrum dominated by parasites with 3 copies of cPRS (Figure 3.4.8). We chose 3 parasite clones with 1, 2, or 3 copies of cPRS (Figure 3.4.9a). We found that halofuginone resistance in our SYBR dose-response assay increased with the number of copies of cPRS (Figure 3.4.9b). Furthermore, the correlation between cPRS copy number and drug resistance was limited to halofuginone and not to any of 10 other antimalarial compounds we tested (Table 3.4.3).

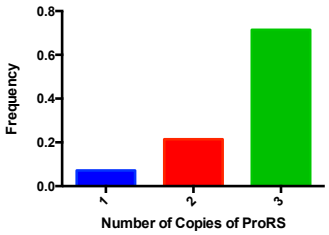

Figure 3.4.8: Copy number variation frequency spectrum at cPRS locus in HFGRIII 2-200x cloned parasites

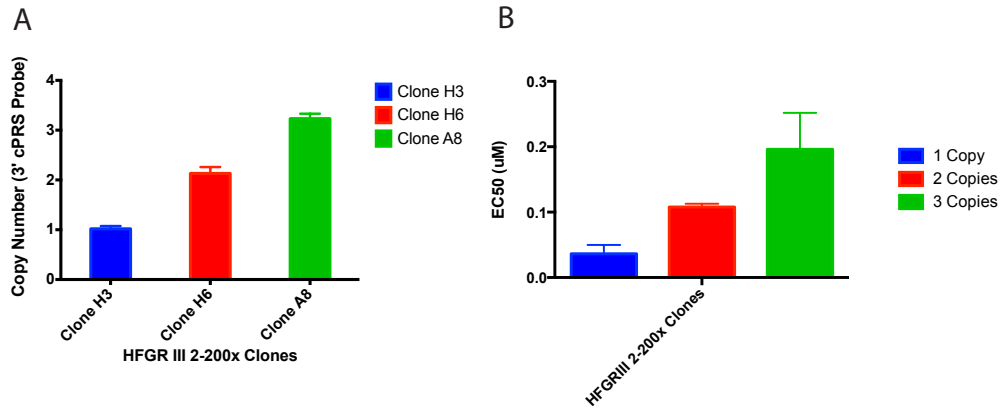

Figure 3.4.9: Amplification of cPRS confers resistance to halofuginone

(a) Copy Number variation determined by qPCR of three clones investigated for sensitivity to HFG using the 3′ cPRS assay. (b) SYBR assay confirms that more cPRS copies desensitize parasites to HFG.

Table 3.4.3: Correlation between cPRS copy number and drug resistance

Antimalarial Compounds	R^2
Amodiaquine	0.1811
Artemisinin	0.01341
Atovaquone	0.01929
Dihydroartemisinin	0.008082
Doxycycline	0.7748
Geldanamycin	0.3254
Guanabenz	0.2477
Halofuginone *	0.9963
Mefloquine	0.01006
Mg132	0.08533
WR 99210	0.04343

R^2 Pearson correlation coefficients of the relationship between cPRS copy number and the EC50 values of 11 antimalarial compounds. The parasites used for this analysis were HFGRIII 2-220x Clone H3 (1 Copy), H6 (2 Copies), and A8 (3 Copies). * Two-tailed t-test P-value <0.05.

3.5 Discussion

tRNA Synthetase inhibitors and Amino Acid Homeostasis

The past three years has seen an upswing in interest in tRNA synthetases as drug targets in eukaryotic parasites [128]. Exciting new work has demonstrated that small molecules that can inhibit isoleucine tRNA synthetase [58] lysine tRNA synthetase [129,130] and threonine tRNA synthetase [131], and proline tRNA synthetase (Chapter 2) in *P. falciparum*. This work has focused on target identification and validation of these inhibitors and has neglected the complex genus-specific mechanisms of amino acid homeostasis that greatly affect the potency and clinical future of antimalarials that target tRNA synthetases.

The malaria parasite has a dual proline supply in the erythrocytic stage. Within the red blood cell, *P. falciparum* parasites digest human hemoglobin, which is 4.9% proline. *P. falciparum* also imports amino acid from the extracellular milieu. There are several lines of evidence that support that *P. falciparum* uses both. Proline is one of seven amino acids that must be in the media used for *in vitro* cultivation of *P. falciparum* [60]. In addition, the new permeability pathway (NPP) / parasite-specific anion current (PSAC) that is responsible for the selective increase in permeability of early trophozoite infected red blood cells increases flux of many amino acids [61] including proline [62].

GENETIC FACTORS EXPLAIN PART BUT NOT ALL OF OBSERVED RESISTANCE

We approached the question of how the parasite evolves resistance to halofuginone from a conservative perspective. By observing two independent populations, we were able to see snap-shots of evolution. Within the cPRS locus, we saw two different genetic mechanisms of drug resistance: mutation and amplification. In Chapter 2, we identified the nonsynonymous C1444T mutation in the cPRS gene that arose during the HFGRII *in vitro* selection. In both HFGRII and HFGRIII we saw amplification of the cPRS locus. Here, we have shown that amplification of the cPRS locus results in increased halofuginone resistance (Figure 3.4.9, Table 3.4.3).

However, these two genetic pieces of evidence only partially explained the acquisition of resistance we mapped in our *in vitro* evolution experiments. We saw a 20-fold increase in halofuginone dose-response (Figure 3.4.2) before the SNP in HFGRII or amplification in HFGRIII reached a high enough frequency to be detected by our deep-coverage whole genome sequencing or qPCR CNV assay.

We adopted two approaches to explore other mechanisms for the acquisition of drug resistance: one genetic and one non-genetic. Looking for additional genetic contributors outside of the cPRS locus, we performed whole genome sequencing of snap-shots taken along the course of two evolution experiments. We found that no SNPs or small INDELs fixed in HFGRII or HFGRIII over the selection. Also, in HFGRII we found that no SNPs or small INDELs hitchhiked also with the C1444T cPRS. Using a series of filters to distinguish segregating SNPs and INDELs from noise regardless of fixation in the population, we found one other mutation in HFGRII that only occurred in the last two genetic snap-shots. Thus, a potential mutation in PF3D7_1402100 could further explain the high level resistance we found at the end of HFGRII, but not the early adaptation unexplained by genetic adaption at the cPRS locus.

The second approach assumed that epigenetic adaptations could explain the 'missing resistance' from our genetic story. To probe the early evolutionary dynamics we had yet to understand in our long-term evolutionary experiments, we treated wild-type strains Dd2 and 3D7 with 2.8nM (4xEC50) halofuginone. We found both acquired halofuginone drug resistance within 8-9 generations (Figure 3.4.3a,b).

The abrupt adaptation itself implies a non-genetic phenomenon is the most likely explanation. The initial population size of 10^9 parasites in each of these induction experiments argues against the possibility that a novel mutation (present at an allele frequency of $1/10^9$) arising in the first generation would have enough fitness advantage become fixed in the population after 7 additional generations. Additionally, acquisition of this induced resistance phenotype in two separate strains argues against pre-existing parasite sub-populations with a HFG-resistance trait that could fix and cause the rise in halofuginone resistance we have observed. To rule out the pre-existing or de-novo mutation hypotheses, we are performing whole genome sequencing of the two induced Dd2 lines and their parental strain.

Using our induced resistance parasite lines, we sought to understand the non-genetic acquisition of resistance to halofuginone. Our attention turned to amino acid homeostasis because proline is one of the three substrates of cPRS. We knew from previous testing that increased proline levels in culture media increased halofuginone EC50 in SYBR dose-response assays (Chapter 2). Based on this evidence we measured intracellular amino acid levels in our Dd2 parasites with induced halofuginone resistance.

Intracellular Proline Concentration Linked to Halofuginone Resistance

We measured the concentration of 19 amino acids in induced and untreated Dd2 parasites and found proline to be uniquely upregulated. We examined the metabolomics picture of these parasites by measuring both purified *P. falciparum* parasites and *P. falciparum* infected erythrocytes. This provided further insight into the dynamics of proline accumulation that may contribute to induced halofuginone resistance. Both purified parasite and total iRBC showed increased proline concentrations upon induction (Figure 3.4.4 a,b).

However, total iRBC samples from induced parasites show slightly upregulated levels of multiple amino acid; these concentrations correlated with more strongly with proline in iRBC than purified parasites (Figure 3.4.5a). The magnitude of proline enrichment is also substantially different between purified parasites and iRBC; induction resulted in a 3-5 fold increase in iRBC proline and a19-32 fold increase in parasite proline .

To validate that the increased proline pools observed in our halofuginone-induced parasites also occurred in our *in vitro* evolution experiments, we measured levels of the same 19 amino acids in end point clones of HFGRII and HFGRIII selections. We confirmed our suspicion that clones from both halofuginone evolved lines had elevated proline levels (Figure 3.4.7 a, b).

Based on the parasite's two sources of proline, we created two working models to explain the underlying mechanisms of observed amino acid homeostasis alterations. In the first, halofuginone induction modulates hemoglobin degradation regulation. Following this hypothesis, the parasite would have to upregulate hemoglobin degradation to increase the parasite proline pool. However, to achieve the proline-specific enrichment that we have observed, the parasite would have to specifically efflux non-proline amino acids into the erythrocyte and then from the erythrocyte into the extracellular environment. Amino acid efflux transporters have been identified in prokaryotes such as *Corynebacterium glutamicum* and *Escherichia coli* [132] but have yet to be described in eukaryotes or *Apicomplexa* specifically. Additionally, the selective advantage for *P. falciparum* to contain non-proline amino acid efflux machinery remains to be demonstrated. Thus, we view this first model as unlikely.

Our second working model is based on increased and selective importation of proline from the extracellular milieu. The difference between iRBC and parasite measurements in selectivity and magnitude of proline enrichment supports a two-step model of proline import. In this model, a subset of amino acids, including proline, are transported across the erythrocyte membrane by a *P. falciparum*-altered mechanism. Then, proline is transported across the parasitophorous vacuole and parasite membrane. This model is consistent with two separate transport or transport-effector mechanisms activated by halofuginone-induced resistance.

CLAG Overexpression linked to Induction of Halofuginone Resistance

Based on this model, we investigated the expression of *clag* genes in our parasite with induced resistance. *Clag* 3 has been identified as a genetic determinant of the PSAC channel [20]. Pillai et al. reported up regulation of a larger *clag* repertoire (*Clag* 3.2 and *Clag* 2) when they selected for *Clag* 3.2 expression by

growing Dd2 parasites in custom media and *clag* 3.1-inhibitor ISPA-28 [133]. Two groups recently found *clag* 3 expression to be down regulated in *P. falciparum* parasites resistant to blasticidin S [63,64].

We found that *clag* 2 and 3.2 had strongly increased expression in parasites with halofuginone induced-resistance (Figure 3.4.5 b). Our observations demonstrate that Plasmodium parasites use *clag* genes to regulate amino acid transport as a mechanism of drug resistance. More strikingly, these results implicate *clag 2* and clag 3.2 genes in regulation of PSAC importation specificity that has not been reported before.

We hypothesize that upregulation of *clag* gene expression in response to halofuginone causes increased intracellular proline, which inhibits the halofuginone activity at the cPRS. We recognize that it is unlikely that only *clag* 2, 3.2, and 8 are responsible for the proline-specific regulation of importation at the red blood cell surface. It remains to be shown whether non-*clag* effectors of the PSAC channel or of other erythrocyte surface receptors are involved in HFG-induced resistance. We also recognize that we not addressed the mechanism of parasite surface proline import. There is a large diversity of amino acid transporters; there are over 2-dozen families and superfamilies recognized with greatly varying specificity and selectivity for amino acids and their derivatives [134]. We have identified nine *P. falciparum* genes with homology to different families of amino acid transporter proteins (AATs). We will address both outstanding issues with RNA-seq based expression studies we are currently undertaking of Dd2 parasites with HFG-induced resistance.

The amino acid homeostatic mechanisms witnessed in these halofuginone experiments have demonstrated that proline levels are regulated in response to external pressures. It is possible that this complex epigenetic regulation of intracellular solutes could be unique to proline-focused drug pressure. However, it is more likely a general mechanism of drug-resistance to tRNA synthetase inhibitors including mupriocin and cladosporin.

General Model of Multi-Step Evolution of Resistance to Halofuginone

At first glance our 50 plus generation halofuginone *in vitro* evolution experiments and the rapid induced resistance we found after 18 days appear discordant. However, our in *vitro* evolution experiments used

much higher concentrations of halofuginone. This created an entirely different fitness landscape under which the malaria parasites adapted and resulted in different magnitudes of resistance. After the full course of *in vitro* evolution, strains are as much as 300-fold resistant to halofuginone. However, induced Dd2 or 3D7 parasites show only 20-fold resistance.

To explain the multistep mechanisms of halofuginone drug resistance, we propose a multi-step adaptation process that maximizes fitness in increasing concentrations of halofuginone. In the first phase of our *in vitro* evolution, resistance is acquired by altering cellular amino acid homeostasis; specifically, intracellular and intraerythrocytic proline concentration are adapted in response to halofuginone pressure. This phenomenon is analogous to the induced resistance phenotype we found with low-dose constant drug treatment.

The second phase of drug resistance represents alterations in the cPRS in mutually exclusive ways. We have witnessed either target site mutations or early target amplification in this second temporal phase.

However, the third phase of drug resistance encompasses amplification of the WT target loci in the presence of increasing selective drug pressure regardless of prior mutation (Figure 3.5.1).

We stress the sequential acquisition nature of these adaptations; a target site mutation in cPRS may provide increased fitness only in the presence of halofuginone with elevated intracellular proline.

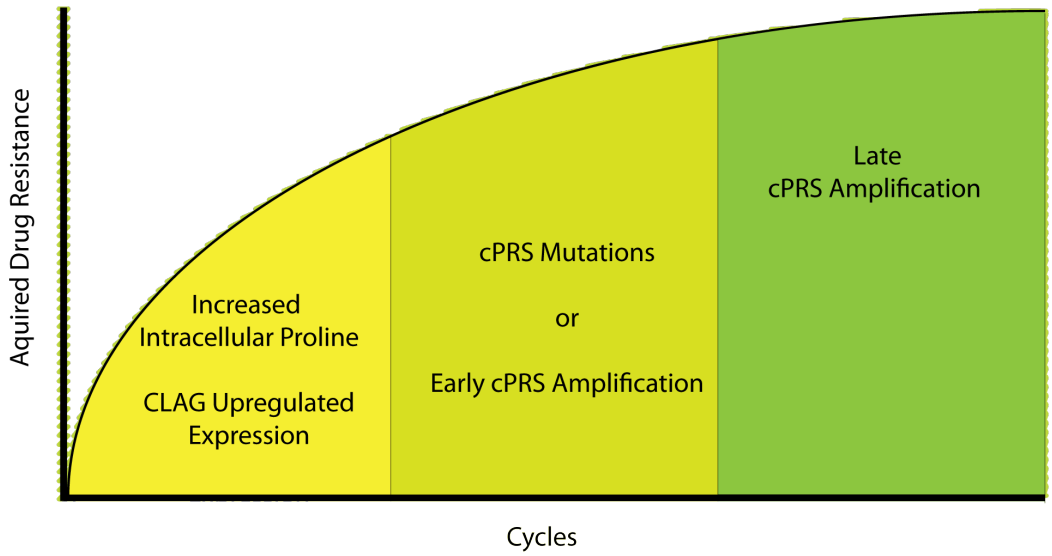

Figure 3.5.1: A Model of Step-wise Acquisition of Halofuginone Drug Resistance

Mapping resistance mechanisms is essential to furthering malarial drug discovery. Identifying resistance mechanisms inform the future usefulness of an antimalarial compound. Further, this model of halofuginone resistance will inform the rational design of combination therapy. The most obvious of which is the combination of febrifugine derivatives with PSAC channel inhibitors.

Implications of Evolutionary Trajectory on the Fitness of Competing Alleles

Genomic sequencing of time points along the HFGRII evolution trajectory revealed a mutation in the cPRS that increased in the prevalence from 0.6% in cycle 27 to 57% in cycle 34. However, instead of fixing in the population, the allele remained at an intermediate frequency for another 7 generations before being out competed by a parasite with an amplified WT cPRS locus. The anticorrelation of the HFGRII cPRS SNP and CNV implies clonal competition and argues that cPRS amplifications are more fit at higher halofuginone drug pressures than the HFGRII cPRS mutant allele.

Chapter 4: Analysis of Allelic Replacements of Halofuginone Resistance Mutations at the cPRS Locus

4.1 ATTRIBUTION

Authors: Jonathan D. Herman[1,2], Daniel P. Rice[3,4], Ulf Ribacke[2], Amy Deik[1], Huihao Zhou[6], Eli Moss[1], Paul Schimmel[9], Michael Desai[3,4], Clary B. Clish[1], Ralph Mazitschek[1,2,7], and Dyann F. Wirth*[1,2]

Affiliations:

[1] The Broad Institute, Infectious Diseases Initiative, Cambridge, MA 02142, USA

[2] Harvard School of Public Health, Department of Immunology and Infectious Disease, Boston, MA 02115, USA

[3] Department of Organismic and Evolutionary Biology, Harvard University, Cambridge MA 02138

[4] FAS Center for Systems Biology, Harvard University, Cambridge MA 02138

[5] Department of Cell and Molecular Biology, Microbiology, Uppsala University, 751 24 Uppsala, Sweden

[6] The Skaggs Institute for Chemical Biology, Department of Molecular Biology, The Scripps Research Institute, 10550 North Torrey Pines Road, La Jolla, California 92037, USA.

[7] Massachusetts General Hospital, Center for Systems Biology, Boston, MA 02142, USA

We gratefully acknowledge financial support for this work by the Gates Foundation (DFW and RM) and the National Institute of Health (DFW) (AI084031).

J.D.H. designed and performed HFGRII and HFGRIII *in vitro* selections. J.D.H. characterized the three selections and their clones. J.D.H. and U.R. designed the cloning scheme for transgenic parasites. J.D.H. cloned the constructs, transfected and cycled the parasites, and phenotypically characterized them. U.R. and J.D.H. designed the Allelic Discrimination assay and competitive growth assays. J.D.H. performed and analyzed the data from the competitive growth assays. J.D.H. designed and prepared the samples for the metabolite profiling experiment. A.D. ran and quality-controlled the mass-spec analysis of metabolites. C.C. and J.D.H. analyzed the metabolite experimental data. J.D.H. designed and performed the HFG induced resistance and clag expression experiments.

4.2 INTRODUCTION

We have previously described two mutations found from drug-resistance selections in the cytoplasmic prolyl tRNA synthetase (cPRS), HFGRI and HFGRII that confer halofuginone drug resistance in a yeast heterologous system. Here we describe the two-step process necessary for evolution of the HFGRI and HFGRII halofuginone resistance mutation. Using a reverse-genetic approach we found that HFGRI on its own leads to halofuginone hypersensitivity in *P. falciparum*. However, AR-HFGRI's hypersensitivity was lost when exposed to sufficiently high (>=2.8nM) halofuginone pressure during a competition assay or before a SYBR

dose-response assay. Upon overexpressing *clag* 2 and *clag* 3.1, AR-HFGRI parasites halofuginone EC50 increased 40-fold. We found a similar upregulation of *clag* 2 and 3.2 in AR-HFGRII parasites exhibiting resistance to halofuginone. Thus from identifying an epistatic relationship between cPRS drug resistance alleles and *clag* gene expression we have found evidence for a two-step process for the evolution of drug resistance mutations in *P. falciparum*.

4.3 Materials and Methods

Whole Genome Sequencing of Transfected Parasites

Genomic DNA extracted from bulk population cultures of the two independent halofuginone resistance selected lines was extracted and sheared with a Covaris S 220. Illumina-compatible libraries were prepared on the IntegenX Apollo 324 and sequenced on an Illumina HiSeq 2000. All sequenced populations included in this analysis reached average fold-coverage across the *P. falciparum* genome greater than 60x.

qPCR – Copy Number Analysis

Genomic DNA was prepared from saponin-lysed *P. falciparum* parasites using the Qiagen Blood Mini- or Midi Kits. qPCR analysis was performed on an Agilent 7900HT Fast Real-Time PCR. System using unlabeled primers and Power SYBR Green master mix and. Primers used for copy-number analysis are in Table 4.3.1 (target locus primers) and Table 4.3.2 (control locus primers). Copy number was calculated with the ΔΔCt method according to the Applied Biosystems user bulletin 2.

Table 4.3.1: qPCR Control Primers

Gene Name	Direction	PlasmoDB ID	Sequence (5′ to 3′)
fructose-bisphosphate aldolase	Forward	PF3D7_1444800	TGTACCACCAGCCTTACCAG
fructose-bisphosphate aldolase	Reverse	PF3D7_1444800	TTCCTTGCCATGTGTTCAAT
B-tubulin	Forward	PF3D7_1008700	CGTGCTGGCCCCTTTG
B-tubulin	Reverse	PF3D7_1008700	TCCTGCACCTGTTTGACCAA
Seryl tRNA Synthetase	Forward	PF3D7_0717700	TATCATCTCAACAGGTATCTACATCTCCTA
Seryl tRNA Synthetase	Reverse	PF3D7_0717700	TTTGAGAGTTACATGTGGTATCATCTTTT

Table 4.3.2: qPCR Primers for cPRS Target

Gene Name	Region of Gene	Direction	PlasmoDB ID	Sequence (5′ to 3′)
Prolyl tRNA synthetase (cPRS)	5'	Forward	PF3D7_1213800	TGCTATAAGACCAACAAG TGAAACA
Prolyl tRNA synthetase (cPRS)	5'	Reverse	PF3D7_1213800	ACGTACCACAGTATTCCAT TGATTT
Prolyl tRNA synthetase (cPRS)	3'	Forward	PF3D7_1213800	CCAAACAAACAGTGAAAC GACAT
Prolyl tRNA synthetase (cPRS)	3'	Reverse	PF3D7_1213800	TAGGTGGTTGATCTAACG GGATAC

IN VITRO DRUG SENSITIVITY AND DOSE-RESPONSE ANALYSIS BY SYBR GREEN

The SYBR Green I method was used as previously described[82]. In brief, we grew *P. falciparum* parasites for 72 hours in 384 well plates at 1% hematocrit and 1% starting parasitemia. Growth was assessed by SYBR Green staining of parasite DNA. All dose-response assays were carried out with twelve-point curves with technical triplicate. DMSO stocks of drugs used were dispensed by the HP D300 Digital Dispenser. Fluorescence measurements were collected on a SpectraMax M5 (Molecular Devices) and analyzed on GraphPad Prism version 5 and EC_{50} values were determined with the curve-fitting algorithm log(inhibitor) vs. response – Variable slope.

PARASITE CULTURE AND TRANSGENESIS

Malaria culture was performed as described by Trager *et al*. [81]. Dd2 is a chloroquine resistant *in vitro* cultured parasite cloned from the Laos derived W2-MEF parasite obtained from MR4.

To generate transfection plasmids for 3′ allelic replacement, we PCR amplified 1209:2241 nucleotides of PfcPRS from Dd2, and two halofuginone-resistant *in vitro* HFGRI and HFGRII evolved lines with the primers 5′GGACCGCGGCCGCAGAATTTTTATGGCAAGAAG′3 and 5′GGACCCTCGAGTTAATAACTTCTACCAAATAAAC′3. These 3′ fragments were subcloned into a pGEM3Z-based (Promega) plasmid with hDHFR selectable marker driven by a CAM promoter, PfHSP 86

3′UTR. The 3′ fragment of cPRS was inserted at NotI and XhoI sites such that it is not transcribed episomally. 3D7 parasites were electroporated with pcPRSWT, pcPRSHFGRI, or pCPRSHFGRI plasmids and transgenic parasites were selected via homologous recombination by cycling on and off WR99210 drug pressure until integration was confirmed by PCR and transcription of the correct allele was confirmed by Allelic Descrimiation qRtPCR.

INTEGRATION-SPECIFIC PCR

The plasmid-specific amplicon was amplified using Plasmid-Forward and Plasmid-Reverse primers. The un-integrated chromosomal locus was amplified using Chromosomal-Forward and Chromosomal-Reverse. The Integrated chromosomal locus was amplified using Chromosome-Forward and Plasmid-Reverse. The primers are described in Table 4.3.3 and the PCR scheme is described in Figure 4.4.1.

PCR Conditions for the Integration-specific and plasmid-specific PCR reactions are as follows: 95°C for 4 minutes and then 40 amplification cycles (95°C for 30s, 57°C for 30s, 68°C for 180s) and then a final extension at 68°C for 300s. Amplification of the unmodified chromosomal locus follows the same conditions except for the use of an annealing temperature of 48°C instead of 57°C.

Table 4.3.3: PCR Primers for Analysis of 3' Allelic Replacement Transgenic Parasites

Gene Name	Type of Region Amplified	Direction	PlasmoDB ID	Sequence (5′ to 3′)
Prolyl tRNA synthetase (cPRS)	Native Chromosomal Locus	Forward	PF3D7_1213800	CAAACAACTTAAGATTTGTTGACGA
Prolyl tRNA synthetase (cPRS)	Native Chromosomal Locus	Reverse	PF3D7_1213800	TGAATTTTAAATGAAAAATGGGGTA
Prolyl tRNA synthetase (cPRS)	Unrecombined Plasmid	Forward	PF3D7_1213800	AGGAAACAGCTATGACCATGATTAC
Prolyl tRNA synthetase (cPRS)	Unrecombined Plasmid	Reverse	PF3D7_1213800	ATATTGGGGTGATGATAAAATGAAA

Competition Assay and Allelic Discrimination qPCR Readout

AR-WT #38, AR-HFGRI #25, and AR-HFGRII #71 clones were used in these fitness competition assays. Tightly synced parasites (10-14 hours post invasion) were mixed in a 1:1 ratio to achieve a 1% parasitemia culture and maintained in competition for 5 generations in quadruplicate. Each cycle RNA was harvested, cultures were cut back to 1% parasitemia by flow cytometry, and drug pressure was maintained. RNA was also harvested from individual transfectant parasites on Day 0. RNA was extracted using RNeasy 96-well plate extractors, DNase treated, and then purified through a second set of plates. First strand cDNA synthesis was made with SuperScript III (Life Technologies). Absence of contaminating DNA and the success of reverse transcriptase reaction was confirmed by comparison of Seryl tRNA synthetase Ct values of Rt+ and Rt- samples run in quadruplicate on ABI 7900 HT Fast Real-Time PCR machine. Transcribed allele balance of each parasite was determined by analysis of the individual samples pre-mixture (Cycle 0) and parasite prevalence over the five generations was determined by cPRS Allelic Discrimination Assay.

cPRS Allelic Discrimination qPCR Assay

We custom designed two allelic discrimination genotyping assay at Codon 482 of cPRS to differentiate between two SNPs we previously identified to confer resistance to halofuginone (Table 4.3.4). MGB-binding probes (Life Technologies) were designed to either the WT allele or two MT alleles (HFGRI and HFGRII).

To calibrate the assay artificial mixtures of plasmid DNA with WT and MT cPRS alleles were mixed in a decrement of 10% to make an eleven-sample set spanning 100% of each allele. Six ten-fold dilutions were made of the set of mixtures and were used to calibrate the Allelic Discrimination qPCR assay with each point of this matrix run in duplicate. The primers and probes used in the Allelic Discrimination assay to track WT versus HFGRI and WT versus HFGRII are described in Table 4.3.4. Choice of which dilution of the calibration curve to use was made for each individual sample basis on a Euclidian distance minimization algorithm. Allele balance of sample was calculated based on the log transformation of the ratio of fluorescence signal intensities of the chosen calibration curve. Allelic discrimination assays were run with TaqMan Universal PCR Master Mix with no AmpErase UNG (Applied Biosystems) on an ABI 7900 HT Fast

Real-Time PCR machine with the amplification conditions as follows: 95°C for 10 minutes, followed by 40 cycles of a two-step amplification of 95°C for 15 seconds and 60°C for 1 minute.

Table 4.3.4: cPRS allelic discrimination assay primers and probes

Primers/Probe	Direction	Fluorophore	Sequence (5′ to 3′)
cPRS Locus Amplification Primer	Forward		AAAATGGAAGAGCCATACAAGCA
cPRS Locus Amplification Primer	Reverse		TACAACCCCATGATGTTTGATGA
WT Probe		FAM	TCATTAT**ct**TGGAACAAA
HFGRI Allele (L482F) Probe		VIC	TCATTAT**ca**TGGAACAAA
HFGRII Allele (L482H) Probe		VIC	TCTCATTAT**tt**TGGAACAAA

Flow Cytometry

Flow cytometry of *P. falciparum* infected erythrocytes was carried out as based on SYBR Green I staining of parasite nuclei as previously described [126]. Modifications to the Bei et al. protocol include staining of iRBC with SYBR Green I at a 1:2000 concentration, acquisitions of non-single cells were pre-filtered by for cells that fell on the y=x line in a plot of forward scatter area vs. height. All Flow Cytometry was collected on a MACSQuant Flow Cytometer (Miltneyi Biotec) and analyzed with MacQuantify and FlowJo 8.8.6 software (Tree Star).

LC-MS analysis of amino acids and polar metabolites

Highly synchronous (within 4 hours) early schizonts were magnetically purified with MACS CS columns (Miltenyi Biotec). A small aliquot was also made for flow cytometry. The rest of the purified samples were divided into two equal volumes: one for saponin lysis (0.025%) and one for whole iRBC extraction. Each sample was washed 2x in PBS, and then suspended in 10 uL PBS. Polar metabolites were extracted using nine volumes of 74.9:24.9:0.2 (v/v/v) acetonitrile/methanol/formic acid containing stable isotope-labeled internal standards (0.2 ng/µL valine-d8 (Isotec); and 0.2 ng/µL phenylalanine-d8 (Cambridge Isotope Laboratories)). Profiles of amino acids were measured using LC-MS as described previously[127]. Briefly, positive ionization, multiple reaction mode (MRM) data were acquired using a 4000 QTRAP triple quadrupole mass spectrometer (AB SCIEX) coupled to an 1100 Series pump (Agilent) and an HTS PAL

autosampler (Leap Technologies). Cell extracts (10µL) were injected onto a 150 x 2.1 mm Atlantis HILIC column (Waters). The column was eluted isocratically at a flow rate of 250 µL/min with 5% mobile phase A (10 mM ammonium formate and 0.1% formic acid in water) for 1 minute followed by a linear gradient to 40% mobile phase B (acetonitrile with 0.1% formic acid) over 10 minutes. The ion spray voltage was 4.5 kV and the source temperature was 450°C. MultiQuant 1.2 software (AB SCIEX) was used for automated peak integration and metabolite peaks were manually reviewed for quality of integration and compared against a known standard to confirm identity. Stable isotope-labeled internal standards were used to eliminate samples with poor data quality. Metabolite peaks signals were normalized by flow cytometry-determined cell counts and compared to PBS and uninfected red blood cell control measurements. Pearson correlation analysis was performed in prism and heat maps were generated with Gene-e (Broad Institute).

qPCR – Gene Expression Analysis

Total RNA was extracted by the Trizol extraction method, DNAse treated, and re-purified with Qiagen RNeasy mini columns. First strand cDNA synthesis was made with SuperScript III (Life Technologies). Absence of contaminating DNA and the success of reverse transcriptase reaction confirmed by comparison qPCR of Rt+ and Rt- with the control Seryl tRNA synthetase primer set in quadruplicate and was run on ABI 7900 HT and fold expression was calculated. cDNA concentrations were then balanced by SerRS Ct to minimize PCR efficiency biases. Samples were run in quadruplicate and run with two control primer sets for validation of expression analysis. PCR amplification was performed as follows: 15 minutes at 95 °C followed by 40 cycles of two-step amplification of 94 °C for 30s and 52 °C for 30s. All primers used for expression analysis (Tables 4.3.5, 4.3.1, and 4.3.2) were validated for specificity and efficiency with these exact PCR conditions.

Table 4.3.5: qPCR primers for expression analysis of the clag gene family

Gene Name	Direction	PlasmoDB ID	Sequence (5′ to 3′)
Clag 2	Forward	PF3D7_0220800	CTCTTACTACTTATTATCTATCTCTCA
Clag 2	Reverse	PF3D7_0220800	CCAGGCGTAGGTCCTTTAC
Clag 3.1	Forward	PF3D7_0302500	ACCCATAACTACATATTTTCTAGTAATG
Clag 3.1	Reverse	PF3D7_0302500	TCTGAACTAGGAGGCCAACC
Clag 3.2	Forward	PF3D7_0302200	ACCCATAACTACATATTTTCTAGTAATG
Clag 3.2	Reverse	PF3D7_0302200	TTCAGCAGCAAGTCCGTGA
Clag 8	Forward	PF3D7_0831600	GTTACTACAACATTCCTGATTCAG
Clag 8	Reverse	PF3D7_0831600	AATGAAAATATAAAAATGCTGGGGGAT
Clag 9	Forward	PF3D7_0935800	TACCATTAGTGTTTTATACACTTAAGG
Clag 9	Reverse	PF3D7_0935800	CCAAAATATGGCCAAGTACTTGC

4.4 RESULTS

Table 4.4.1: Summary of cPRS mutations in drug resistance selected lines HFGRI and HFGRII

Selected Line	Dd2 Parental Strain	HFGRI	HFGRII
Nucleotide Change Observed in cPRS	-	A1445T	C1444T
Amino Acid Change Observed in cPRS	-	L482H	L482F
Corresponding Allelic Replacement (AR) Strain	AR-WT	AR-HFGRI	AR-HFGRII

HFGRII MUTATION AT THE CPRS CONFERS RESISTANCE TO HALOFUGINONE IN ALLELIC REPLACEMENT EXPERIMENTS

We previously performed drug-resistance selections with halofuginone and found two mutations in the cytoplasmic prolyl tRNA synthetase (*Chapter 2*) and summarized in Table 4.4.1. We confirmed in a heterologous yeast model that cPRS mutant allele HFGRII, from drug resistance selected parasite HFGRII, conferred high-level resistance to halofuginone analogue halofuginol in is a dose-dependent manner (SFigure 2.5.8). To validate the effect of these alleles in *P. falciparum* we set out to genetically engineer syngeneic parasites that only differed by their cPRS allele type. To achieve this goal, we performed 3′ single crossover allelic exchange experiments as depicted in Figure 4.4.1a in wild type 3D7 *P. falciparum*

parasites. We confirmed integration in our cPRS cloned transfectants parasites by PCR (Figure 4.4.1b). Notably, our transection control parasites AR-WT #38 where we replaced the wild type chromosomal copy with the wild type allele validated that we can integrate a plasmid at the cPRS locus. Furthermore, we verified that all allelic replacement AR-WT parasites had an indistinguishable dose-response to halofuginone from its 3D7 parental strain (Figure 4.4.1c).

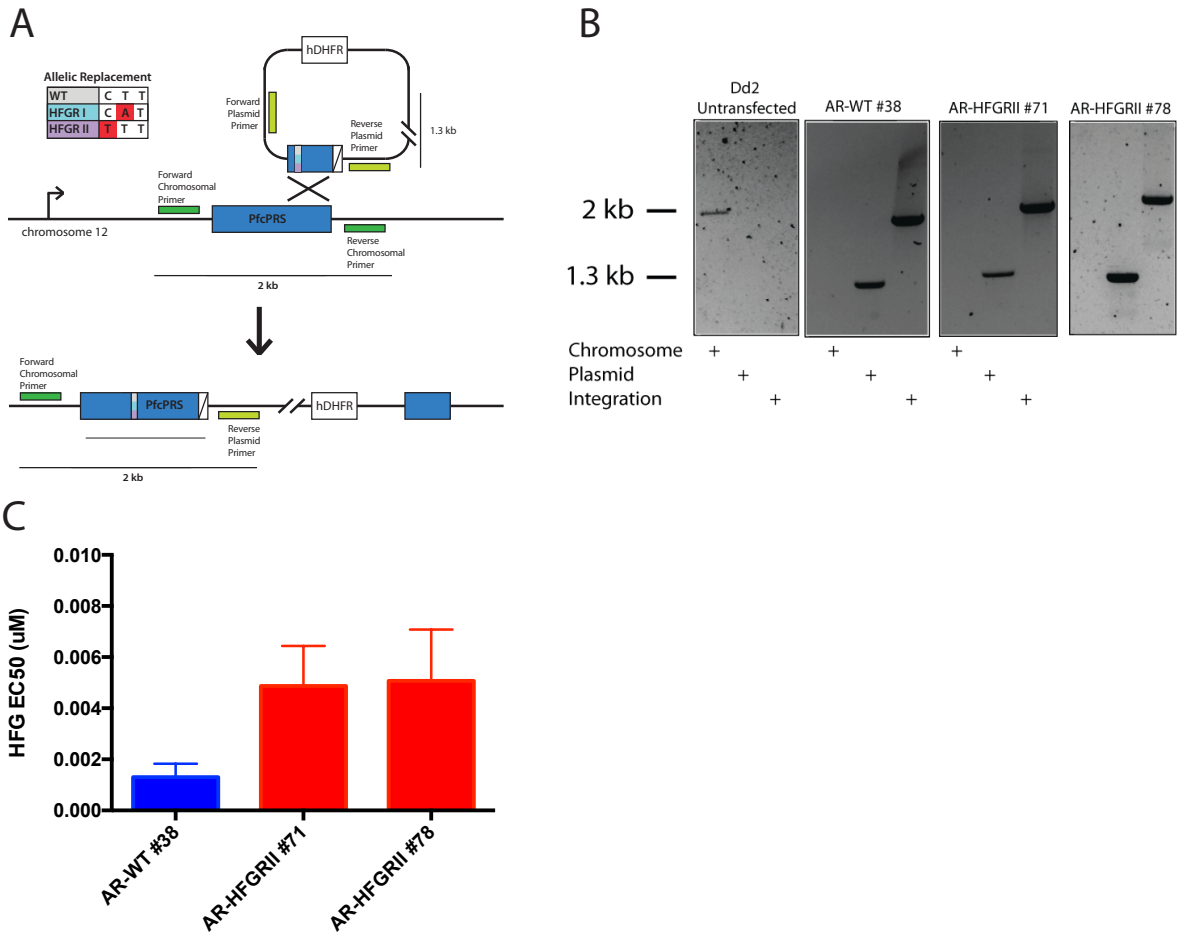

Figure 4.4.1: cPRS HFGRII transgenic parasites are more resistant to halofuginone
(a) A model of 3′ allelic replacement transgenesis at cPRS via single homologous recombination.
(b) PCR confirmation of integration and absence of unrecombined locus in AR-WT and AR-HFGRII clones with modified cPRS loci.
(c) Halofuginone EC50s of AR-WT and AR-HFGRII clones. Error Bars reflect SD.

In our transfectants with the cPRS HFGRII mutant allele, we confirmed integration by PCR (Figure 4.4.1b). We found that both AR-HFGRII clones we characterized had a five-fold increased resistance to halofuginone (Figure 4.4.2c) in our 1.5-cycle SYBR green-based growth inhibition assay.

Encouraged by the results with the HFGRII allelic replacements, we went forward with allelic exchange experiments with the cPRS HFGRI allele. The HFGRI allele showed a stronger resistance phenotype in our heterologous yeast model (SFigure 2.5.8) so we hypothesized that AR-HFGRI parasites would be more resistant than AR-HFGRII parasites.

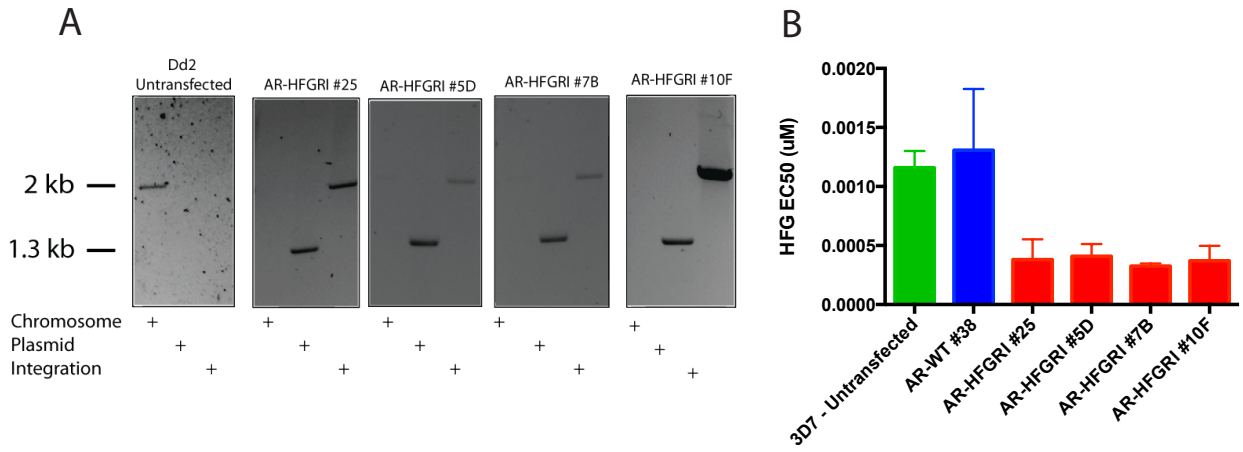

Figure 4.4.2: cPRS HFGRI transgenic parasites are hypersensitive to halofuginone

(a) PCR confirmation of integration and absence of unrecombined locus in AR-HFGRI clones with modified L482F cPRS locus.

(b) Halofuginone EC50s for the transfectant parasite clones expressed in uM units. Halofuginone EC50s of 3D7 untransfected, AR-WT, and AR-HFGRII clones. Error Bars reflect SD.

We first went forward and obtained one transfectant clone, AR-HFGRI #25. We confirmed it had integrated the plasmid and lacked any unrecombined native locus (Figure 4.4.2a). When we investigated the halofuginone dose-response of our HFGRI transfectants, we found it was uniquely hypersensitive to halofuginone and no-other antimalarial tested including artemisinin, atovaquone, amodiaquine, dihydroartemisinin, doxycycline, mefloquine, and sulfadoxine. Alarmed by this sensitization to halofuginone, we then went back to an early freeze of the bulk transfected line that yielded the AR-HFGRI #25 and re-selected with WR and obtained three additional clones that were PCR-positive for integration (Figure 4.4.2b): 5D, 7B, and 10F.

We drug-phenotyped our additional AR-HFGRI clones and found they were all more sensitive to halofuginone than the wild type transfected and untransfected controls (Figure 4.4.1c). Since this observation was inconsistent with the phenotype of the halofuginone resistance-selection parasites with

corresponding alleles, we set out to characterize the genetic changes leading to this surprising phenotype. First we looked at the cPRS RNA transcription levels in the transfectant parasites clones with qPCR probes to the 5′and 3′ untranslated regions of the cPRS locus.

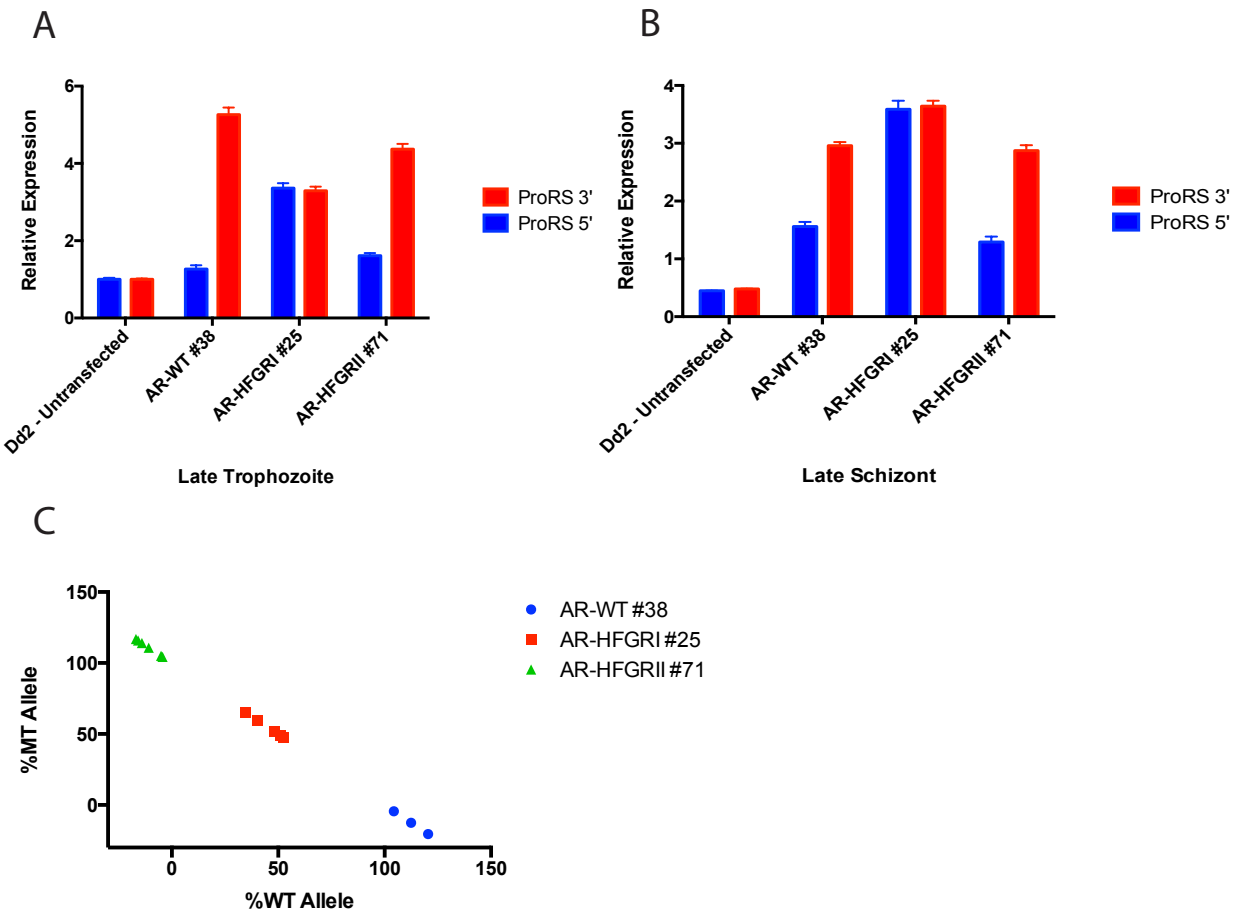

Figure 4.4.3: Expression analysis reveals co-allelic expression and amplification in AR-HFGRI not present in other transfectants

(a) cPRS gene expression of untransfected Dd2 parasites and transfectants AR-WT #38, AR-HFGRI #25 and AR-HFGRII #71 in Late Trophozoites (LT) stage parasites.
(b) cPRS gene expression of untransfected Dd2 parasites and transfectants AR-WT #38, AR-HFGRI #25 and AR-HFGRII #71 in Late Schizont (LS) stage parasites.
(c) Expressed allele in transfectant parasites AR-WT#38, AR-HFGRI #25, and AR-HFGRII #71 parasites determined by allelic discrimination qrtPCR assay. AR-WT#38 and AR-HFGRI #25 were analyzed with the WTvsHFGRI assay. AR-HFGRII#71 was analyzed with the WTvsHFGRII assay.

From previous experience with the 3′ single-strand break based modification strategies, we expected to see more 3′ RNA than 5′ RNA because of the 3′ cPRS fragment on the donor plasmid. If the plasmid concatermizes as often occurs before integration, much more 3′ cPRS transcript can be made than 5′. We

saw this pattern of 3′ transcript predomination in AR-WT and AR-HFGRII transfectants in both parasite stages investigated (Figure 4.4.3a,b). However, we interestingly saw equal expression levels of 5′ and 3′ cPRS transcript in AR-HFGRI #25. In addition, AR-HFGRI transfectants expressed between 2-3-times more full-length RNA than untransfected Dd2 parasites. This furthered our suspicion that AR-HFGRI transfectant parasites might have amplified their cPRS locus.

With the hypothesis in mind that AR-HFGRI #25 might have a duplicated locus, we next determined which cPRS allele our transfectants expressed with allelic discrimination qrtPCR. As shown in Figure 4.4.3c, AR-WT #38 and AR-HFGRII #71 each expressed 100% of the wild type and HFGRII mutant-type alleles respectively. However, AR-HFGRI #25 expressed approximately equal amounts of wild type and HFGRI mutant-type cPRS alleles. This evidence for co-allelic expression in AR-HFGRI #25 convinced us to look more deeply into the genomic architecture of the cPRS locus in these transfectants.

At first, we took a southern blot approach to map the recombined locus but could not determine the details of the genetic map from multiple digestion schemes and two different probes. As a second approach, we used qPCR to look for evidence of copy number variation at the cPRS locus.

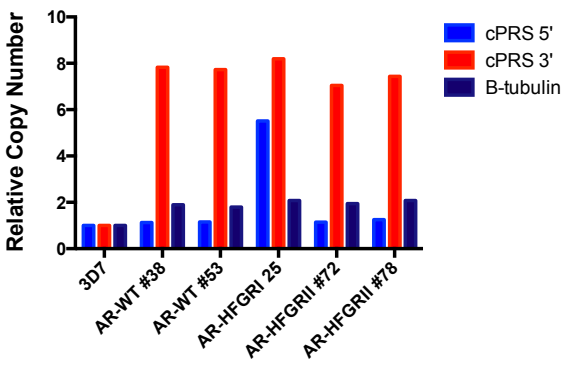

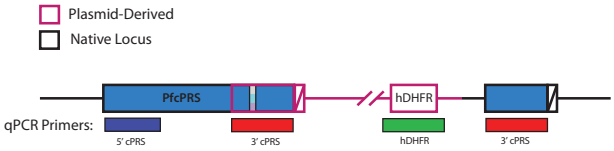

Strain	cPRS 5'	cPRS 3'	hDHFR
HFGRI C5	1.07	1.03	0
AR-HFGRI 25	5.95	7.79	5.077
AR-HFGRI 5D	6.56	8.94	4.009
AR-HFGRI 7B	7.37	8.08	4.839
AR-HFGRI 10F	3.73	4.84	1.788

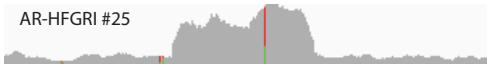

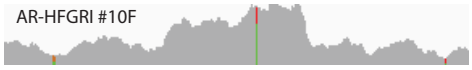

Figure 4.4.4: Mapping the Recombined cPRS Loci in transfected parasites with qPCR

(a) cPRS gene copy number analysis of untransfected 3D7 parasites along with transfectants AR-WT #38, AR-HFGRI #25, and AR-HFGRII #71 clones by qPCR relative to a 3D7 untransfected control. SerRS was used as the endogenous control for ΔΔCt analysis.

(b) Model of integrated locus with location of qPCR primers and the relative copy number of each region of the transfected locus in HFGRI resistance-selected line and the four cloned transfectant clones with the HFGRI cPRS allele. The magenta outlined locus in the model represents plasmid-derived DNA; black-outlined loci represent chromosome 12-derived material. cPRS copy number was determined relative to 3D7 untransfected control. hDHFR copy number was determined in relation to an unrelated transfected parasite externally confirmed to have a single copy. All ΔΔCt analysis was performed with a SerRS endogenous control.

(d) (e) A 30kB view of cPRS locus of AR-HFGRI #25 (d) and AR-HFGRI #10F (e) from whole genome sequencing data. Read pile-ups were visualized with the Integrated Genome Viewer. 5′ of the gene is to the left, and 3′ of the gene is to the right. The red and green lines represent the proportion of mutant-type to wild type aligned reads at the T1445A locus. The chromosomal coordinates for this view are Pf3D7_12_v3:587,476-595,131.

From previous experience with the 3′ single-crossover based modification strategies, we expected to see more 3′ copies than 5′ copies as seen in the integration scheme in Figure 4.4.1a. We found that both sets of clones from AR-WT and AR-HFGRII parasites had this expected pattern (Figure 4.4.2a): 1 copy of 5′ cPRS and >1 copy of 3′ cPRS. This confirms that AR-WT and AR-HFGRII clones are single-integrant, single cPRS copy parasites. However, AR-HFGRI #25 showed a surprising increase in both ends of the cPRS locus confirming that the cPRS has been amplified. We confirmed the amplification of the cPRS locus of AR-HFGRI#25 with whole genome sequencing (Figure 4.4.4d).

We went back to the original HFGRI resistance selected parasite where we found the HFGRI L482H cPRS mutation and confirmed that it has a single copy of cPRS (Figure 4.4.4c). We realized that a transfectant

strain with both an amplification and change in allele type would complicate our understanding of how the HFGRI cPRS allele contributes to halofuginone resistance. To investigate whether it is possible to get single cPRS copy AR-HFGRI transfectant, we first tried to transfect Dd2 WT parasites with the same plasmid used for the AR-HFGRI lines characterized above. In both transfections, parasites failed to grow back after 70+ days. As a second approach, we mapped the cPRS locus by-qPCR of the three other AR-HFGRI clones we obtained (Figure 4.4.2b). We found that all of the AR-HFGRI clones amplified their cPRS locus but each had a unique amplification scheme (Figure 4.4.4c).

P. falciparum Parasites Overexpressing cPRS Alleles Could not Be Produced

Intrigued that all of the transfected HFGRI parasites that came up had amplified cPRS loci, we transfected parasites with HSP86-driven episomal overexpression plasmids with WT, HFGRI, or HFGRII alleles. In all of our 3 transfections of each construct, parasites did not return after 70 days.

Competition Assay Reveals that AR-HFGRI Transfectants Acquire Resistance at High Concentrations of Halofuginone

We were still unsure how to reconcile the hypersensitive phenotype of HFGRI allelic replacement experiments with the drug-resistance selections and yeast allelic replacement data. In parallel with our genetic dissection of the transfectant parasites, we looked for another approach beyond our 1.5 cycle growth assay to interrogate the halofuginone phenotype of these parasites. We chose growth competition assays as an orthogonal approach to confirm the halofuginone hypersensitivity phenotype we saw with our AR-HFGRI transfectants.

This second approach focused on explaining the selective advantage that cPRS alleles confer in competitive growth over 5 generations rather than the 1.5 generations of our previous assay. We grew AR-WT #38 in competition with either AR-HFGRI #25 in the presence or absence of halofuginone at multiple concentrations. Interestingly, AR-HFGRI #25 displayed a fitness disadvantage in low concentrations of halofuginone (1.4nM) as would be expected from our SYBR growth assays (Figure 4.4.3a); AR-HFGRI #25 was less fit in the presence of 1.4nM than in the absence of halofuginone entirely. However, when

presented with greater concentrations of halofuginone (4.2 nM and 7 nM) AR-HFGRI #25 parasites were strongly favored (Figure 4.4.3b).

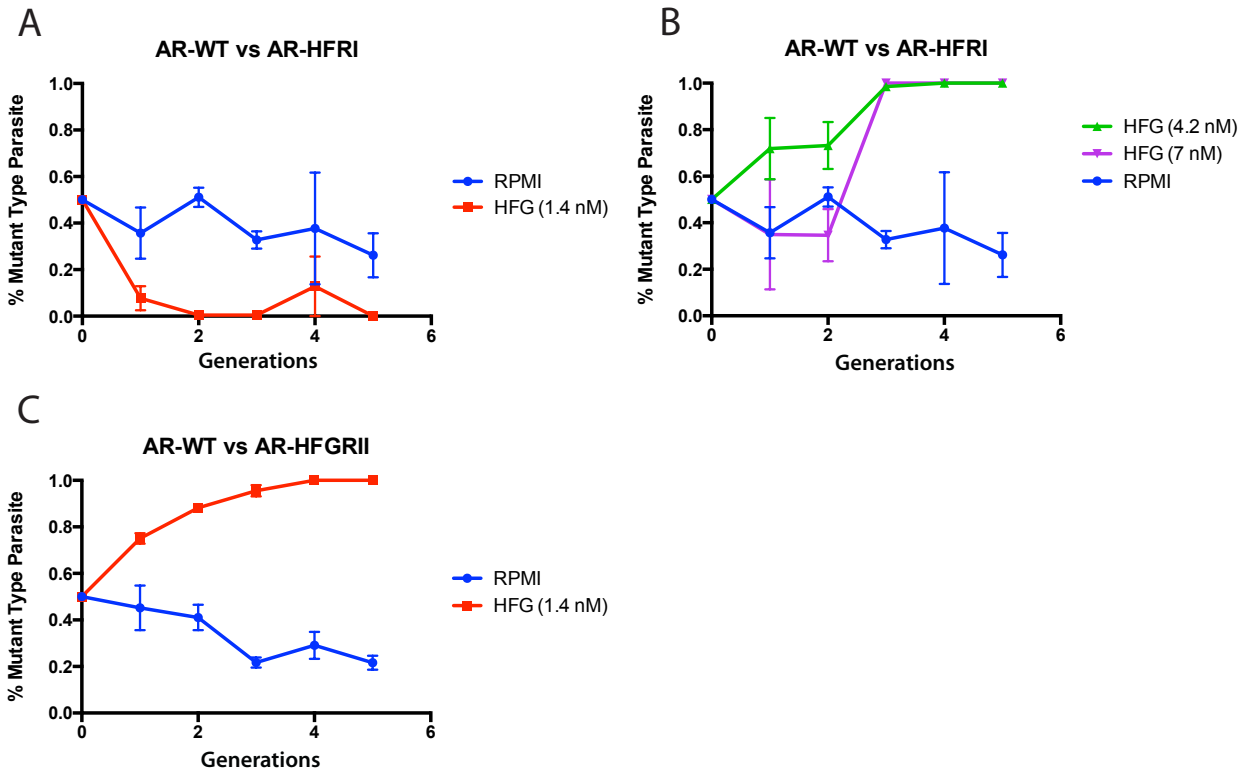

Figure 4.4.5: HFGRI and HFGRII cPRS alleles confer advantage only in the presence of halofuginone
(a) (b) Competitive growth assay of AR-WT #38 versus AR-HFGRI #25 transfected parasites in the presence and absence of low-dose halofuginone (1.4nM) (a) or high-dose halofuginone (b). Error bars in (a) and (b) represent standard error.
(c) Competitive growth assay of AR-WT #28 versus AR-HFGRII #71 parasites in the presence and absence of halofuginone. Error bars in (a) reflect SD and in (b) represent SE.

AR-HFGRII Transfectants are Resistant to Halofuginone at Baseline in Competitive Growth

Due to the discrepancy we found between AR-HFGRI's halofuginone fitness between our 1.5 and 5 generation assays, we were curious to see if similar discrepancies existed for our AR-HFGRII line. We grew AR-WT #38 in competition with AR-HFGRII #71 transgenic parasites over 5 generations in the presence or absence of halofuginone. Confirming the 1.5-cycle growth assay (Figure 4.4.1b), AR-HFGRII #71 parasites proved more fit in the presence of halofuginone (Figure 4.4.5b). We also performed similar competition experiments between AR-WT #38 and AR-HFGRII#71 at 4.2 and 7nM HFG but growth in replicate cultures

was fully inhibited. The HFGRII cPRS allele was mildly deleterious in the absence of halofuginone (normal unmodified RPMI). Thus, we confirmed that AR-HFGRII parasites didn't require higher halofuginone concentrations to 'awake' a resistance phenotype.

HFGRI BUT NOT HFGRII CPRS ALLELE REQUIRES HALOFUGINONE PRE-TREATMENT TO MAKE P. FALCIPARUM RESISTANT TO HALOFUGINONE

To explain the conflicting data from the two different measurements of halofuginone phenotype, we employed a model of epistatic: HFGRI is a resistance mutation in one background and a sensitizing mutation in another and depending on time/dose of halofuginone exposure can convert from one to another.

We were grappling with these AR-HFGRI transfectants at the same time that were came across the HFG-induction phenotype described in Chapter 3. We hypothesized that the same conditions that cause the induction of resistance in wild-type Dd2 parasites could help us understand the epistatic control of the cPRS resistance mutation HFGRI. The evidence that AR-HFGRI parasites need high concentrations of halofuginone to acquire resistance in a competitive growth assay (Figure 4.4.5b) further supported this hypothesis. Thus, we treated both WT and HFGRI transfectant parasites with 2.8nM halofuginone. As quickly as 3 generations after treatment, AR-HFGRI transfectants acquired dramatically increased resistance to halofuginone by our 1.5 cycle growth assay (Figure 4.4.6a). All three clones of AR-HFGRI had greater than a 40-fold increase in halofuginone resistance whereas AR-WT experienced a 5-fold increase (Table 4.4.2). This acquired resistance has been stable over 60 days after removal of drug pressure from AR-HFGRI induced lines.

When we performed the same induction experiments with AR-HFGRII transfectants, we saw no change in halofuginone resistance (Figure 4.4.6b and Table 4.4.2). This result was internally consistent with the competitive growth assays – AR-HFGRII's halofuginone resistance pre-existed external drug pressures.

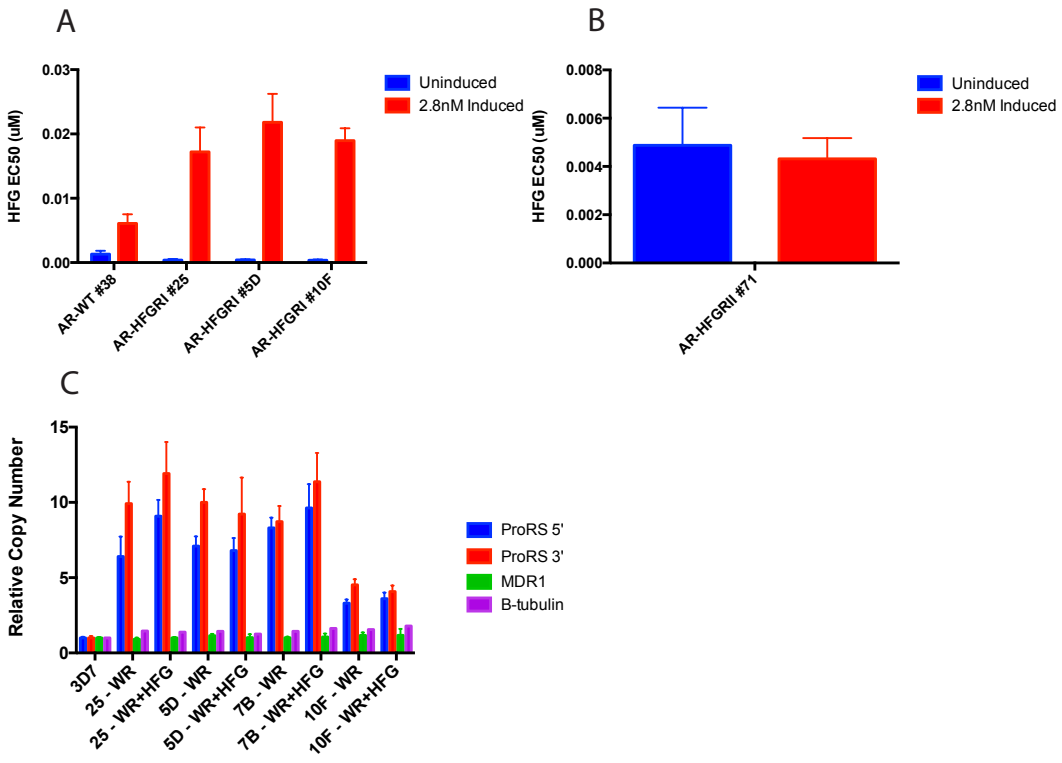

Figure 4.4.6: Pre-Exposure of AR-HFGRI transfectants to halofuginone induces resistance but does not in AR-HFGRII

(a) Halofuginone EC50s of AR-WT and AR-HFGRI transfectants with and without pre-exposure to 2.8nM halofuginone.

(b) Halofuginone EC50s of induced and un-induced AR-HFGRII #71 clone. Error Bars reflect SD.

(c) Relative Copy Number of cPRS and MDR1 in Induced and untreated transfectants. B-tubulin is provided as an additional control.

Table 4.4.2: Fold-increase in HFG EC50 after pre-exposure with 2.8nM HFG in transfectants

	Fold Increase in Halofuginone EC50 Upon Induction
AR-WT #38	5
AR-HFGRI #25	45
AR-HFGRI #5D	53
AR-HFGRI #10F	51
AR-HFGRII #71	0.9

We wanted to eliminate the possibility that the phenotypic change in resistance caused by our induction protocol was due to a change in the architecture of the cPRS locus. With a similar qPCR-based

methodology we found that all four clones of AR-HFGRI showed no change in cPRS copy number upon halofuginone induction (Figure 4.4.4b). We also eliminated MDR1 amplification, a common drug-resistance mechanism in *P. falciparum*, as a potential explanation of the induction of resistance (Figure 4.4.4b).

Pre-exposure Causes the Overexpression of Multiple *clag* Genes AR-HFGRI

Taking a page from our findings in Chapter 3, we preformed expression analysis of the *clag* gene family in our AR-HFGRI transfectants. Expression of the epigenetically regulated *clag* gene family are associated with the NPP/PSAC channel that is responsible for importation of many salts and nutrients including amino acid across the cell membrane of infected erythrocytes.

We found that AR-HFGRI, a transgenic parasite from the 3D7 background, upregulated *clag* 2 and *clag* 3.1 expression upon exposure to halofuginone (AR-HFGRI #25 – Uninduced vs. AR-HFGRI #25 – Induced in Figure 4.4.7). Clag 8 and 9 expression on the other hand were not remarkably upregulated (Figure 4.4.7) upon halofuginone induction.

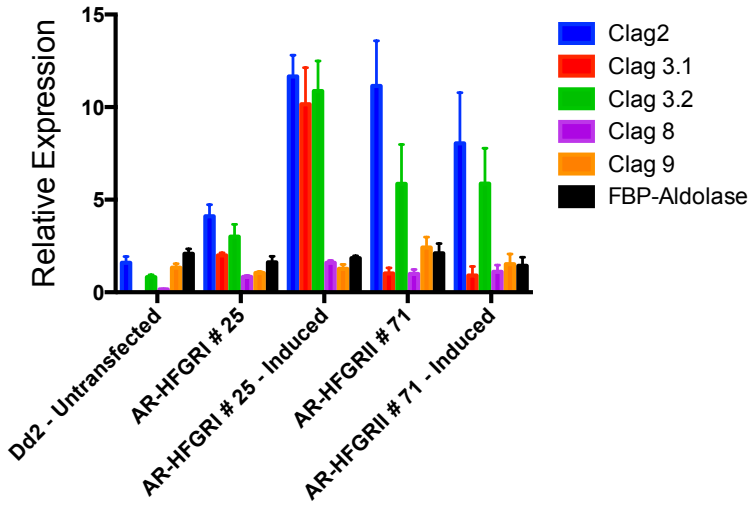

Figure 4.4.7: Overexpression of *clag* 2 and *clag* 3.2 associated with halofuginone pre-treatment of AR-HFGRI #25 parasites but not in AR-HFGRII #71
(a) Replicate Expression Studies of Clag gene family in Halofuginone treated and naïve AR-HFGRI and AR-HFGRII early schizont stage parasites. FBP-Aldolase is included as a second control and Dd2 is provided as untransfected control. SerRS was used as the endogenous control primer set used for ΔΔCt analysis.

AR-HFGRII Parasites Endogenously Upregulate their Clag Gene Expression

Next looking at *clag* gene expression in AR-HFGRII parasites, we found that un-induced AR-HFGRII parasites have already upregulated their expression of *clag* 2 and *clag* 3.2 (Figure 4.4.7). When further pre-treated with halofuginone, we did not witness any increase in *clag* expression of AR-HFGRII parasites. Thus, both AR-HFGRII and AR-HFGRI parasites demonstrate epistasis between cPRS HFGR mutations and *clag* gene expression.

4.5 Discussion

Previous Evidence for cPRS HFGRI and HFGRII Mutations in Drug Resistance

In Chapter 2, we performed two drug-resistance selections with intermittent halofuginone pressure and found two mutations in the cytoplasmic prolyl tRNA synthetase. We named the mutations for the selection in which they were first identified, HFGRI and HFGRII. The nonsynonymous T1445A mutation in HFGRI was validated to be a halofuginone and halofuginol-resistance conveying mutation in a heterologous yeast system. The nonsynonymous C1444T was also demonstrated to confer resistance to halofuginol in transgenic yeast. Though nucleotide 1444 and 1445 are not in the tRNA charging domain of cPRS, our structural modeling identified it as proximal to the proline-binding pocket (Chapter 2). Here in this paper, we sought to validate HFGRI as a halofuginone resistance mutation in *P. falciparum* and characterize the properties of parasites expressing the HFGRI cPRS allele.

Evidence for The Epistatic Nature of HFGRI Mutation from Our Allelic Exchange Experiments

We employed a 3' allelic replacement single crossover approach typical in *P. falciparum* genetics to introduce HFGRI and HFGRII into a syngenic environment. We quickly realized our monogenic model of cPRS mutations as the sole determinant of halofuginone resistance was an oversimplification from the AR-HFGRI transfectants. AR-HFGRI transgenic parasites took twice as long as AR-Dd2 to recrudesce after transfection. When we characterized all three parasite lines, they had equivalent growth rates in semi-

quantitative assays. This indicated to us that a second adaptation/mutation likely had to be acquired for AR-HFGRI to achieve normal growth in an *in vitro* environment. When we characterized the recombined cPRS locus in our transfectant lines, we found one of these adaptations was amplification of the modified cPRS locus (Figure 4.4.4.a).

Drug phenotyping of the three sets of transgenic parasites confirmed the multi-factorial nature of drug resistance. Though AR-HFGRI parasites were more sensitive than AR-WT in our 1.5 cycle dose-response assay (Figure 4.4.2b), they were more resistant is a 5-cycle competitive growth assay only at higher doses of halofuginone (Figure 4.4.45a,b). Taken in total, these data indicated that the HFGRI cPRS allele is not sufficient to confer halofuginone resistance in *P. falciparum*. Rather the HFGRI allele is part of a larger cellular program for resistance.

HFGRI cPRS Allele Has A Strong Affect on Cell Physiology

As a counter-point AR-HFGRII parasites did not amplify their cPRS locus and did not have a halofuginone phenotype that was dependent on external stimuli. This led us to believe that for reasons unappreciated, HFGRI had a much stronger effect on *P. falciparum* cell physiology than HFGRII.

To understand whether the cPRS amplification was a rare event or necessity for our HFGRI allelic exchange experiments, we went back to an early freeze of the uncloned transfected AR-HFGRI line that yielded the AR-HFGRI #25 and re-selected with WR. Each of the three clones we isolated was similarly hypersensitive to halofuginone and possessed an amplified cPRS locus. If all of the AR-HFGRI parasites had the same amplification pattern, we could conclude that a single amplification event and the clones I obtained were unmodified progeny. However, the organization of the amplified locus was unique in each clone. This phenomenon would be consistent with multiple independent amplification or a single initial amplification and subsequent modification/de-amplifications by the individual progeny. Either way, both models argue for the essentiality of copy number variation the cPRS locus of AR-HFGRI parasites and the strong effect the HFGRI has had on cell physiology in our transgenesis experiments.

ROLE OF *CLAG* EXPRESSION IN HFGRI-MEDIATED RESISTANCE TO HALOFUGINONE

To elucidate the larger program necessary for HFGRI resistance, we set out to model the phenotypic change elucidated by our competitive growth assays (Figure 4.4.5a,b). AR-HFGRI parasites were less fit in 1.4nM HFG, but strongly selected for in 4.2nM HFG and higher concentration. We formulated two hypotheses based on this data. The first was that exposure to a certain dose of halofuginone re-programed AR-HFGRI and created the cellular environment where HFGRI could contribute to resistance. The second was that a sub-population of resistant AR-HFGRI parasites pre-existed the competition assay and were selected for only in exposure to high concentrations of halofuginone.

To address the first hypothesis, we set out to replicate the phenotypic change in AR-HFGRI by pre-treating the cultures with halofuginone. We estimated that the inflection point between a sensitive and resistant program was 2.8nM. Pre-treated HFGRI transfectants with this mid-level concentration acquired 45-53-fold increase (Table 4.4.1), thus supporting our first hypothesis. This acquired resistance was present in multiple clones of AR-HFGRI, thus decreasing the likelihood that fixation of a subpopulation could explain the acquisition of resistance. Furthermore, we sequenced both the untreated and HFG treated AR-HFGRI #25 clone and in the process of analyzing the sequences to identify any genetic polymorphisms that could differ between the two.

It has been know for some time that the new permeability pathway (NPP) / parasite-specific anion current (PSAC) that is responsible for the selective increase in permeability of early trophozoite infected red blood cells increases flux of many amino acids [61] including proline [62]. More recently, *clag* 3 has been identified as a genetic determinant of the PSAC channel [20]. In Chapter 3, we found that overexpression of *clag* 2 and *clag* 3.2 played an important in the acquisition of induced halofuginone resistance. Based on this premise, we looked into whether pre-treatment of AR-HFGRI with halofuginone changed *clag* gene expression and found upregulation of *clag* 2 and *clag* 3.1 in two replicate studies. This is congruent with recent findings by Pillai et al. who saw up regulation of a larger *clag* repertoire (*clag* 3.2 and *clag* 2) when they selected for *clag* 3.2 expression by growing Dd2 parasites in custom media and *clag* 3.1-inhibitor ISPA-28 [133].

HFGRII Transfectants Upregulate *clag* Expression without Induction

We wanted to investigate whether the epistatic we found between *clag* expression and cPRS allele phenotype in AR-HFGRI parasites is generalizable. Thus, we set out to determine if induction phenotype, i.e. induction of halofuginone resistance we found in Chapter 3, in our AR-HFGRII transfectants. When we induced AT-HFGRII transfectant parasites with halofuginone pre-treatment, we surprisingly saw no difference in dose-response. This lack of an induction phenotype distinguished AR-HFGRII from AR-HFGRI and wild type parasites.

We wondered if that meant that the HFGRII mutation some how disentangled *clag* genes from their involvement in halofuginone resistance. By measuring the expression of AR-HFGRII of the *clag* family of genes, we determined that AR-HFGRII transfectants over-express *clag* 2 and *clag* 3.2 endogenously (Figure 4.4.5a). This observation further confirmed *clag* involvement in the halofuginone resistance of AR-HFGRII. Even further, the unaltered *clag* 2 and 3.2 expression levels in AR-HFGRII induced parasites provides better evidence *clag* overexpression is involved in phenotypic halofuginone resistance rather than just an associated phenomena triggered by HFG-treatment.

Halofuginone Resistance Mutations at cPRS requires Elevated *Clag* Expression

The model we have built from our investigations of transgenic parasites with the HFGRI and HFGRII cPRS alleles is based upon multi-factorial resistance in which HFGRI is not the first but a second step. From many unexpected observations that were not foretold by work in a yeast model system, we propose a model of epistasis between cPRS allele type and *clag* expression in our phenotype of resistance to halofuginone.

AR-HFGRI parasites without altered *clag* gene expression are sensitized to halofuginone (Figure 4.4.5a) and a HFGRI cPRS mutation without second-site adaptation would never fix under the selective force of halofuginone (Figure 4.4.4a). We have confirmed in our genetic experiments that upon *clag* -overexpression parasites with the HFGRI allele are strongly selected for by halofuginone (Figure 4.4.4b).

Thus, the genetic requirement of a pre-existing environment for cPRS resistance mutations is in direct agreement with the observation-based model of evolution of halofuginone resistance we presented in Chapter 3. Synthesizing the two independently derived models of resistance, we posit a re-interpretation of our three steps: First non-genetic re-regulation of *clag* expression predominates and importantly sets the stage for cPRS mutations to evolve. In step two, genetic adaptation occurs either through cPRS mutations that are selected for in a newly permissive environment or through cPRS amplification. In the third step, cPRS amplification become more favored in ever-increasing halofuginone pressures and outcompetes cPRS mutations.

Reconciling the Differences Between AR-HFGRI and AR-HFGRII

At this point, we cannot experimentally explain certain differences that resulted during our transfection experiments. It is not known why AR-HFGRI parasites needed an outside stimulus to upregulate *clag* 2 and *clag* 3.2 expression and AR-HFGRII parasites upregulated *clag* 2 and *clag* 3.1 expression de novo. Hopefully, whole genome sequencing of the transfectants will identify any mutations outside of the cPRS that were acquired to all parasites to proliferate with the HFGR cPRS alleles and give us the step towards understanding the more complex regulatory mechanisms at play.

Larger Implications and Limitations of Current Mechanistic Model

This two-step model for evolution of a drug resistance mutation in *P. falciparum* has two greater implications for the field of drug resistance. First, it shows there are relevant markers of drug sensitization or pre-resistance that could be used be used to track and intervene before permanent drug resistance fixes in a population. Second, the multiple steps required to evolve drug resistance can inform the design of future rational drug combinations. These experiments we present here argue that inhibitors of amino acid import would make the HFGRI and HFGRII mutants evolutionarily inaccessible.

We do acknowledge that we have yet to provide a mechanistic link between *clag* gene overexpression and cPRS mutations in these transfectants. Our underlying hypothesis is that *clag* gene overexpression is

involved with amino acid homeostasis regulation as we have seen in out wild type induced lines. However, we are currently pursuing this approach to determine whether a proline-specific or non-specific re-regulation of amino acid levels are responsible for the epistatic between cPRS and *clag* genes.

Chapter 5: Conclusion and Future Directions

4.1 Conclusions and Future Directions

Lack of an effective vaccine and recurrent drug resistance are the two main reasons a treatable disease such as malaria remains responsible for more than 1,238,000 deaths a year [6]. Despite much work to find new approaches to vaccine development, our greatest success in malaria vaccine development in 2014 is RTS,S/AS01: a vaccine with less than a 50% efficacy in children under 17 months old [26]. A big hindrance to our progress is that any malaria vaccine needs to outperform natural immunity.

Drug development and abating drug resistance remains a promising direction for research and development to combat malarial disease and death. This is why we have focused on identifying new drug targets and understanding the potential resistance pathways that may thwart this new class of drugs.

To that end, we labored in Chapter 2 to discover a new target for antimalarial development – a druggable chokepoint in the parasite's cellular physiology. Through drug resistance selection with halofuginone, a derivative of an ancient Chinese medicinal remedy for fever, we found that the cytoplasmic prolyl tRNA synthetase (cPRS) is a new promising target for antimalarial development. Further, we have discovered a related molecule, halofuginol, is active *in vivo* against liver and red blood cell stages of malaria and lacks the gastrointestinal toxicity of halofuginone. Thus, halofuginol proves that targeting the cPRS is a viable and promising route for future development of dual-stage anti-malarial drugs.

To better support our argument that halofuginol is a promising *in vivo* active antimalarial, we need to more thoroughly explore the dosing regimens needed in our mouse model. Specifically, we should explore the dose at which gastrointestinal toxicity similar to halofuginone occurs with

halofuginol and determine if it is possible to achieve a dose in our mouse model of erythrocytic infection that can provide a single dose radical cure (SERC).

In the future, we hope to perform protein-based high-throughput screens to find additional small molecule scaffolds that target three of the enzymatic functions of cPRS: activation of proline, charging of proline onto proline tRNAs, and editing of mischarged proline tRNAs.

In Chapter 3, we delve more deeply into the halofuginone resistance mechanisms that *P. falciparum* can evolve, but more generally into understanding the sequential, multi-step nature of the evolution of drug resistance in malaria. In addition to the evidence that cPRS mutations contribute to halofuginone resistance in Chapters 2 and 4, in Chapter 3 we show that copy number variation at the locus is a drug resistance mechanism. More significantly, we have found evidence that both genetic and non-genetic mechanisms are essential for halofuginone drug resistance. We found that short-term treatment of *P. falciparum* parasites with halofuginone induced non-genetic resistance that led to the upregulation of *clag* family genes and increased proline levels within the parasite. Interestingly, this is the first example of substrate-specific regulation of solutes that has involved the *clag* gene family. Thus we have found evidence for a highly regulated amino acid homeostasis that can be perturbed by the cPRS inhibitor, halofuginone.

Because of the recent and surprising nature of the results we present in Chapter 3, we have some experiments that were ongoing at the time of submission of this dissertation. To further strengthen the evidence that cPRS confers halofuginone resistance, we want to ensure that loci outside of the cPRS could contribute to the resistance we saw in the three clones we characterized from HFGRIII 2-200x. Thus, we are currently performing whole genome sequencing of the three clones and will look for any SNPs or CNVs that differ among the trio. A fundamental assumption of our three-step

model is that induction of halofuginone resistance via upregulation of *clag* gene family members and cytosolic proline occurs as a first step. We base this assumption on three observations: first that parasites at the end of *in vitro* evolution replicates HFGRII and HFGRII have strongly upregulated cytosolic proline. Our second piece of data is that induced wild type Dd2 parasites overexpress *clag* gene family members and upregulate cytosolic proline. Third, induced wild type parasite had a similar level of drug resistance as observed in HFGRII before cPRS mutations or CNVs appeared. To confirm this model, we need to thaw our early time points in both selections and validate the temporality of non-genetic resistance to halofuginone.

Our current evidence shows the linkage of high cytosolic proline, *clag* family gene upregulation, and non-genetic abrupt development of drug resistance. However, our model is still incomplete. First, we cannot yet prove that the elevated proline levels are due to increased proline importation, though this is hinted towards by the *clag* gene expression data. Thus, we are planning on two experimental approaches: first we will track proline importation in induced and untreated parasites with C14-labeled proline. Second, we will use aspartic protease inhibitors to probe the involvement of hemoglobin degradation in induction of halofuginone resistance. Also, we recognize that *clag* gene overexpression can only explain the increased proline levels in the erythrocyte cytoplasm. We are hopeful that RNA-seq gene-expression studies that are ongoing will help elucidate the genes involved in parasite membrane and parasitophorous vacuole contribution to proline uptake in the parasite cytoplasm.

The evidence of *clag*-mediated halofuginone resistance has caught us by surprise. Certain questions that directly arise from our findings address the fundamental understanding we have of how *clag* genes contribute to and regulate PSAC–mediated transport.

The finding specific enrichment of proline through a *clag*-involved mechanism is very interesting and leads us to many follow up questions and observations. We would like to understand how specific import of single amino acids is achieved by *clag*-involved PSAC machinery. As of now, *clag* 3 and more recently *clag* 2 have been implicated as genetic determinants of PSAC importation. However, the composition of the PSAC channel, its subunits, and its modifiers are still unexplored. We feel that the specific enrichment of proline we have seen in the non-genetic induction of halofuginone resistance is a unique observation and can be utilized to further probe the specificity of PSAC and additional determinants of this specificity within and beyond the *clag* gene family.

Our finding of *clag* involvement has opened up many future directions to further drug discovery and the approaches we combine antimalarials for clinical therapy. We are very interested to know whether the *clag*-related resistance is a phenomena specific to proline regulation and selective pressures created by cPRS inhibitors, or is it more generalizable to inhibitors of other tRNA synthetase.

We have created a three-step model of the evolution of drug resistance with *clag*-medicated non-genetic and genetic mechanisms. Our three replicate evolutions experiments HFGRI, II, and III have provided us with a three-step model. However, we hope to pursue a much larger number of replicate experiments of artificial evolution to ensure the robustness of the N=3 conclusions. In addition, in these future *in vitro* evolution experiments we will disentangle the acquisition of improved fitness from escalating selective pressure, i.e. elevated drug dose. Thus by performing separate selections at constant drug pressures over time, we will be able to attribute any clonal competition to differential fitness in the same environment, rather than observing the selective fitness of mutants in environments other than those in which they arose.

In Chapter 4, we were able to show that cPRS drug resistance mutations found in halofuginone-selected lines, HFGRI and HFGRII, are epistatic with *clag* gene overexpression and require preexisting cellular adaptation to confer resistance. This finding further validates the model of drug resistance we have described in Chapter 3. However, the recent nature of these findings has not allowed us to perform all of the follow experiments we need to connect the *clag* regulation we saw in Chapter 3 with our transfectants strains. We need to perform metabolic studies of the WT, HFGRI, and HFGRII transfectants with and without induction to understand if amino acid levels are altered as a result of *clag* gene overexpression as we found in wild type Dd2 parasites. Additionally, we hope to shine more light on the genetic architecture of the cPRS locus in the AR-HFGRI clones. We are currently using the PRICE Genome Assembler to de novo assemble the cPRS locus and identify the number of full length amplifications that are likely transcriptionally active in each clone.

We have confirmed that in the right cellular environment, cPRS mutations HFGRI and HFGRII confer resistance to halofuginone. The deeper implications of our work with allelic exchange experiments in Chapter 4 arise from the requirement of specific cellular adaptations to allow cPRS mutations to confer resistance to halofuginone. A common model employed to understand the evolution of drug resistance and its fitness costs is that of compensatory mutation: evolution of drug resistance results in organisms with decreased fitness in the absence of drug pressure [42,43]. Additional 'compensatory' mutations are acquired to rescue the fitness of the drug-resistant organisms. This was our null hypothesis going into our work with halofuginone.

Once we identified that cPRS was the target of halofuginone, we looked with our metagenomic sequencing approach for additional mutations that would fix along or after fixation of the cPRS mutation in HFGRII. Rather than finding post-cPRS compensatory mutations, we found that

preexisting cellular adaptations were required for cPRS mutations to be selected for by halofuginone pressure. In both AR-HFGRI and AR-HFGRII, halofuginone resistance was epistatically linked with *clag* gene overexpression. AR-HFGRI parasites with normal *clag* expression patterns were even less fit in the presence of halofuginone than wild type. Thus, we have created a model of pre-adaptation of cellular environment that allows the evolution and fixation of a cPRS resistance allele that is otherwise deleterious. This model has larger implications for understanding the initial steps of evolutionary adaptation that is required for later and more permanent genetic events.

In terms of drug discovery, our findings from Chapter 3 and 4 are very informative for re-orienting rational based drug discovery and drug combination design. From my first pass analysis of the evolutionary trajectory of halofuginone resistance, I surmised that this fine mapping of evolution showed us that combining PSAC inhibitors and halofuginone would be an apt approach. However, it took me a while to realize the new approach implicit in this statement. A newly developing theme of much cancer and infectious disease research is to focus on developing therapies that will target the common resistance pathways with mutant specific drugs; this approach has been investigated in *P. falciparum* with DHODH and pfCRT inhibitors [135] and has been extensively explored in clinical treatment of imatinib-resistant chronic myeloid leukemia with second-generation BCR-ABL kinase inhibitors (Reviewed in Weisenberg et al) [136].

Our findings in Chapter 4 show that pre-conditioning of the cellular environment via *clag* gene family overexpression is essential for the drug resistance evolution of cPRS mutations. Thus, by combining cPRS and PSAC inhibition we are suggesting that we can block the early non-genetic adaption that precedes the evolution of genetic resistance. Thus rather than targeting the resistant

enzyme and making it less fit, we are proposing to eliminate the evolutionary path that would lead to target site mutations at the cPRS.

Appendix

6.1 Supplementary Figures and Tables from Chapter 2

2.5 Supplementary Materials

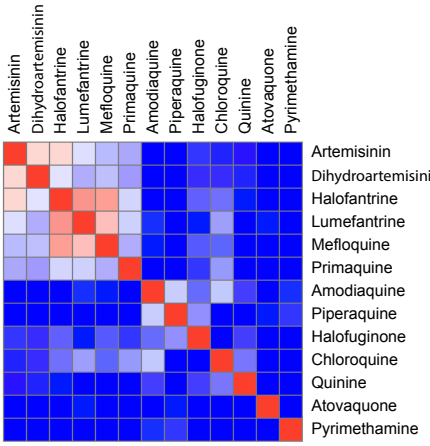

SFigure 2.5.1: Halofuginone is not cross-resistant with common anti-antimalarials
Linear correlation of EC50 values among 31 culture adapted *P. falciparum isolates* from Senegal found little relationship between in-vitro resistance to halofuginone and resistance to 12 standard antimalarials. Correlations are represented by R^2 values in a heatmap matrix (R^2=1 is red, highly correlated; R^2=0 is blue, uncorrelated).

A

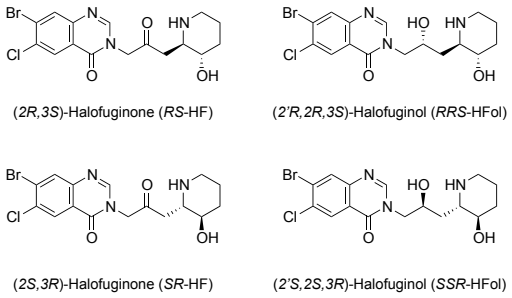

B

	Strains			
Antimalarial	**Dd2**		**HFGR I**	
	EC50 (nM)	95% CI	EC50 (nM)	95% CI
Halofuginone	0.81	0.73 - 0.89	252	211 - 301
(2R,3S)-Halofuginone	0.197	0.187 - 0.208	78.3	66.7 - 91.8
(2S,3R)-Halofuginone	3.6	3.48 - 3.73	1075	949 - 1218
Halofuginol	5.839	5.390 - 6.325		
(2'R,2R,3S)-Halofuginol	3.05	2.87 - 3.25	>1000	-
(2'S,2S,3R)-Halofuginol	142	140 - 149	18300	4725 - 70890
epi-Halofuginol	~ 576.3	-		
Febrifugine	2.37	1.87 - 2.33	987	904 - 1482
MAZ1310	86	80.9 - 91.4	>100000	-

SFigure 2.5.1: Enatiomer-Specific Potency of Halofuginone and Halofuginol
(A) Structures of halofuginone and halofuginol enantiomers. **(B)** EC50 values of febrifugine and analogs for erythrocytic stage Dd2 wild-type and halofuginone-resistant strains. Values are representative of three replicate SYBR dose-response assays.

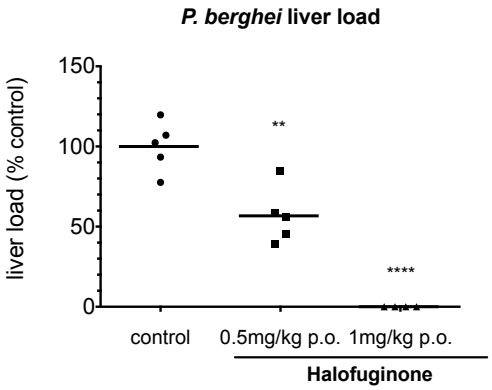

SFigure 2.5.3: *In vivo* potency of halofuginone in liver stage *P. berghei* infection model
Relative parasitemia in mouse livers 44 h after infection with *P. berghei* sporozoites. Mice were treated 1hr post infection with halofuginone (0.5mg/kg p.o. and 1mg/kg p.o.) and vehicle, respectively. Parasite load was quantified relative to vehicle control by qRT-PCR of *P. berghei* 18S rRNA. Data are displayed as mean relative to vehicle treated control, with the mean of the control group set to 100%. p values (**p < 0.01, ****p < 0.0001) were calculated from multiple animals by ordinary one-way ANOVA (Graphpad PRISM).

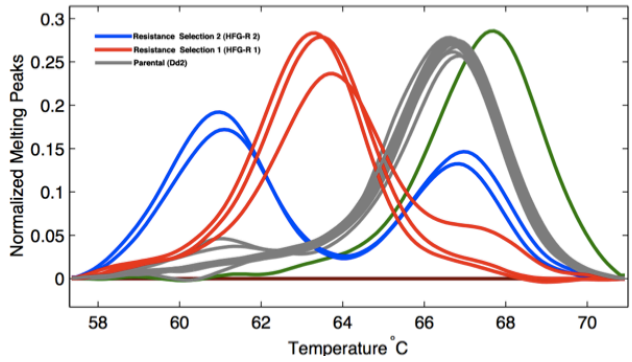

SFigure 2.5.4: High resolution melt assay of *Pfc*PRS identifies mutant loci
A high-resolution melt genotyping assay identified two different mutant alleles within the Class II core tRNA synthetase domain of *Pfc*PRS in the drug-resistance selected lines.

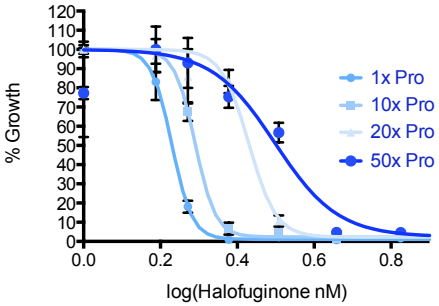

SFigure 2.5.5: Dose dependent inhibition of *P. falciparum* growth is dependent on the concentration of free proline
Proline concentration relative to RPMI media. Error bars reflect s.d. of triplicate experiments.

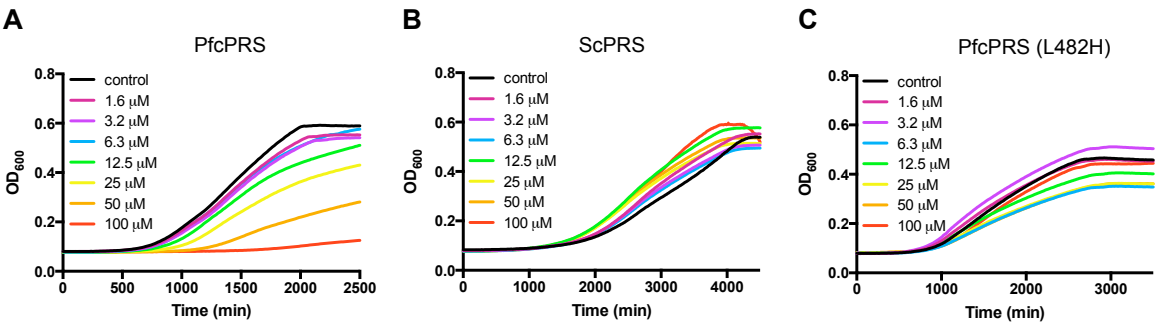

SFigure 2.5.6: Transgenic *S. cerevisiae* expressing wild type PfcPRS is sensitivity to halofuginone
Representative growth curves for -/-YHR020w *S. cerevisiae* recombinantly expressing PfcPRS **(A),** ScPRS **(B)** and mutant (L482H) PfcPRS **(C)** in presence of varying concentrations of halofuginone.

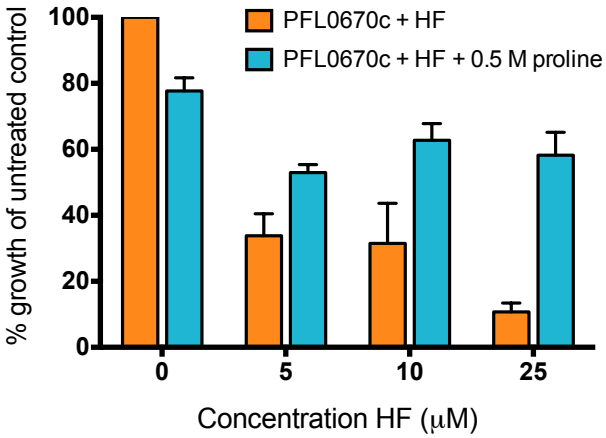

SFigure 2.5.7: Dose dependent inhibition of PfcPRS-expressing yeast growth by halofuginone is abolished by addition of proline
% Growth was normalized to untreated control. Error bars reflect s.d. of triplicate experiments.

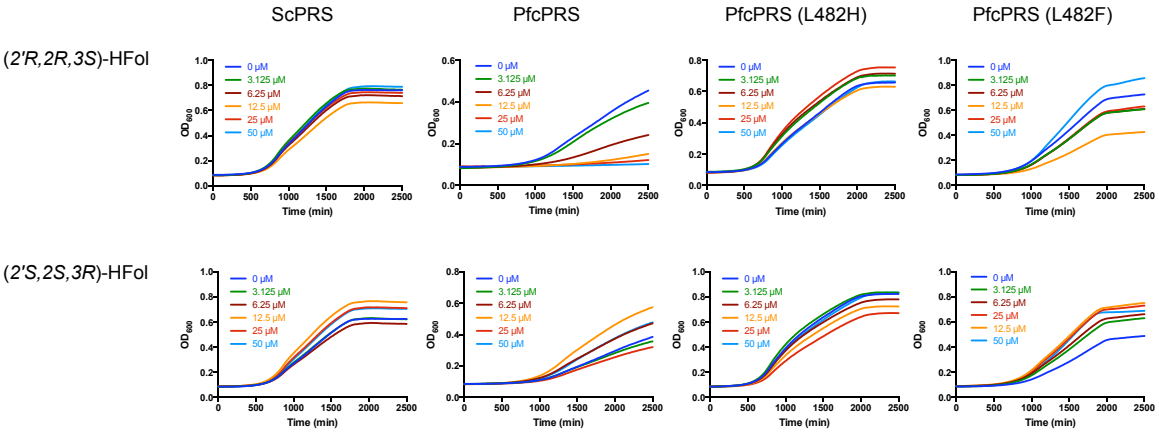

SFigure 2.5.8: Dose dependent inhibition of *S. cerevisiae* expressing wild type PfcPRS by halofuginol
Representative growth curves for -/-YHR020w *S. cerevisiae* recombinantly expressing ScPRS, PfcPRS, PfcPRS(L482H) and PfcPRS(L482F) PfcPRS in presence of varying concentrations of respective halofuginol enantiomers.

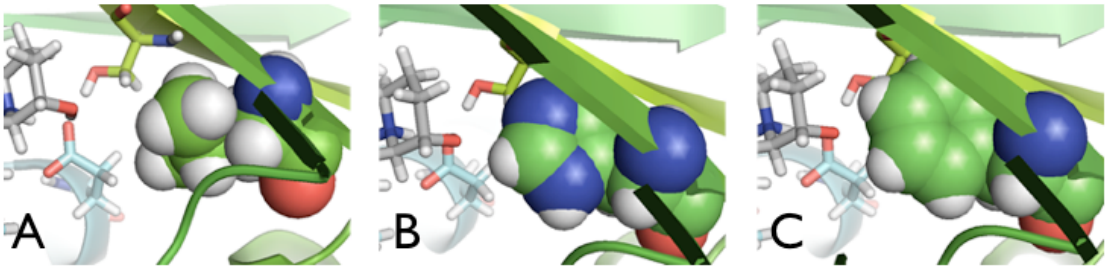

SFigure 2.5.9: Molecular models of Leu482 resistant mutatations
Effect of the mutation of Leu482 **(A)** to histidine **(B)** and phenylalanine **(C)**, on the interactions of halofuginone (gray sticks) in the active site of cPRS. Residue 482 is shown in sphere representation. Leu482 is directly adjacent to the proline binding pocket, and although it does not directly participate in the hydrogen bonding network formed between halofuginone and the respective PRS, it does support the binding geometry of the interacting amino acid residues. The histidine in L482H mutant provides an alternative hydrogen bonding acceptor, thus destabilizing the network. Mutation to phenylalanine, on the other hand, induces steric repulsion with residues nearby, again disrupting the interactions in the binding pocket.

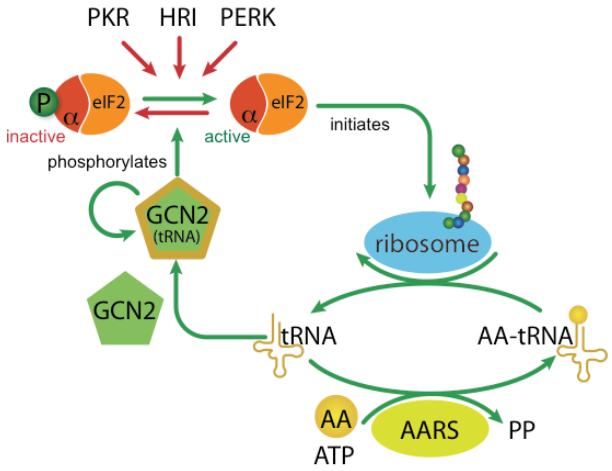

SFigure 2.5.10: Amino Acid Response Pathway
Aminoacyl tRNA (aaRS) synthetases charge unloaded tRNAs with their cognate amino acids (AA), which in turn are used as substrates by the ribosome during protein biosynthesis. Inhibition of aaRS (or lack of amino acids) results in accumulation of uncharged tRNAs that bind and activate GCN2. Active GCN2 phosphorylates the a-subunit of the eukaryotic initiation factor eIF2. Phosphorylated eIF2α can no longer initiate the ribosome assembly, resulting in inhibition of translation.

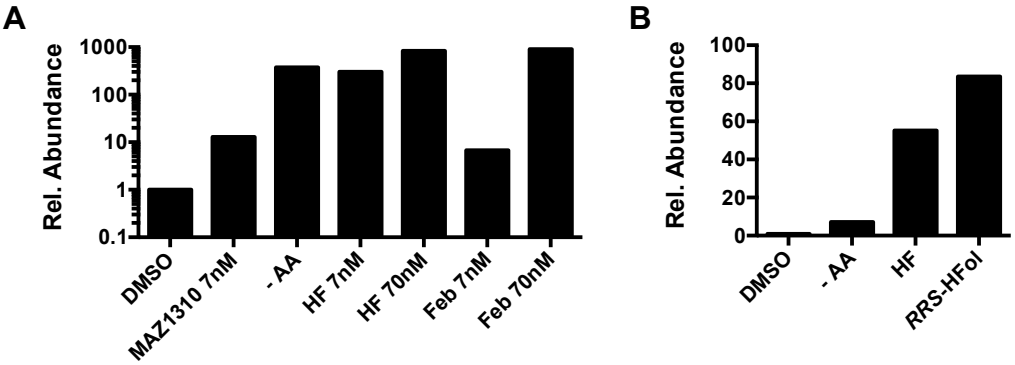

SFigure 2.5.11: Quantification of peIF2α protein levels in the western blots from Figure 2.4.4a
Western blots in Figure 2.4.4a were of asynchronous Dd2 cultures treated with halofuginone and febrifugine **(A)** and from Figure 2.4.4b of 3D7 asynchronous cultures treated with halofuginone and (*2'R,2R,3S*)-halofuginol (*RRS*-HFol). Protein abundance is represented as relative to untreated control (DMSO) after normalization to the histone H3 loading control.

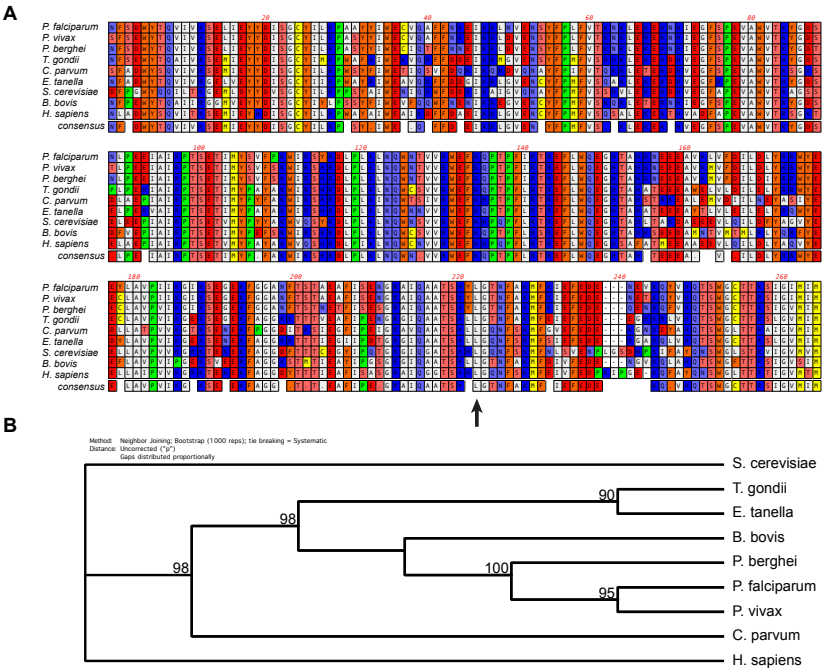

SFigure 2.5.12: Multiple protein sequence alignment of the Class II Core Domains of Proline tRNA Synthetases from diverse species
(A) Sequences of the class II core tRNA synthetase domains were aligned by a ClustalW algorithm.A Black arrow indicates the conserved residue L482. **(B)** A neighbor joining tree assembled of the class II core domains. Tree metrics represent an unrefined P value calculated by a bootstrapping algorithm with 1000 replicates.

Torins are potent antimalarials that block replenishment of *Plasmodium* liver stage parasitophorous vacuole membrane proteins

Kirsten K. Hanson[a,1], Ana S. Ressurreição[b], Kathrin Buchholz[c], Miguel Prudêncio[a], Jonathan D. Herman-Ornelas[c], Maria Rebelo[a], Wandy L. Beatty[d], Dyann F. Wirth[c], Thomas Hänscheid[a], Rui Moreira[b], Matthias Marti[c], and Maria M. Mota[a,1]

[a]Instituto de Medicina Molecular, Faculdade de Medicina, Universidade de Lisboa, 1649-028 Lisboa, Portugal; [b]iMed.UL, Faculdade de Farmácia, Universidade de Lisboa, 1649-003 Lisboa, Portugal; [c]Department of Immunology and Infectious Diseases, Harvard School of Public Health, Boston, MA 02115; and [d]Washington University School of Medicine, St. Louis, MO 63110

Edited* by Louis H. Miller, National Institutes of Health, Rockville, MD, and approved May 23, 2013 (received for review April 2, 2013)

Residence within a customized vacuole is a highly successful strategy used by diverse intracellular microorganisms. The parasitophorous vacuole membrane (PVM) is the critical interface between *Plasmodium* parasites and their possibly hostile, yet ultimately sustaining, host cell environment. We show that torins, developed as ATP-competitive mammalian target of rapamycin (mTOR) kinase inhibitors, are fast-acting antiplasmodial compounds that unexpectedly target the parasite directly, blocking the dynamic trafficking of the *Plasmodium* proteins exported protein 1 (EXP1) and upregulated in sporozoites 4 (UIS4) to the liver stage PVM and leading to efficient parasite elimination by the hepatocyte. Torin2 has single-digit, or lower, nanomolar potency in both liver and blood stages of infection in vitro and is likewise effective against both stages in vivo, with a single oral dose sufficient to clear liver stage infection. Parasite elimination and perturbed trafficking of liver stage PVM-resident proteins are both specific aspects of torin-mediated *Plasmodium* liver stage inhibition, indicating that torins have a distinct mode of action compared with currently used antimalarials.

host-parasite interactions | malaria | protein trafficking | *P. falciparum*

The population at risk for developing malaria is vast, comprising some 3.3 billion people particularly in sub-Saharan Africa and Southeast Asia, with mortality estimates ranging from 655,000 to 1,200,000 (1). Widespread resistance has limited the therapeutic utility of most existing antimalarial drugs, and artemisinin, the highly efficacious cornerstone of artemisinin combination therapies, appears to be at risk for the same fate (2). The need for new antimalarial chemotherapeutic strategies is thus acute.

Plasmodium spp., the causative agents of malaria, have a complex life cycle with alternating motile-nonreplicative and sessile-replicative forms in both mammal and mosquito. In the mammalian host, *Plasmodium* invades and replicates inside two very distinct cell types: hepatocytes and red blood cells (RBCs). In mammals, the *Plasmodium* life cycle is initiated by a motile sporozoite that invades a hepatocyte, where it resides for 2–14 d, multiplying into >10,000 merozoites in a single cycle (3). Once released into the bloodstream, each of these motile merozoites will infect an RBC and, within 1–3 d, generate 10–30 new merozoites, which will contribute to the continuous cycle of blood stage infection that causes the symptoms, morbidity, and mortality of malaria.

These two stages of mammalian infection, despite taking place in distinct cell types and having an orders-of-magnitude difference in parasite replication, do share common features. In both, the motile "zoite" invades the host cell through formation of a parasitophorous vacuole (PV). Both stages grow and replicate exclusively within the confines of the PV, and the parasitophorous vacuole membrane (PVM), which is populated with parasite proteins, constitutes the physical host–parasite interface throughout development. Unlike the vacuoles of many intracellular pathogens including *Leishmania*, *Chlamydia*, *Mycobacteria*, and *Legionella* (4, 5), the *Plasmodium* vacuole, like that of Toxoplasma *gondii*, does not fuse with host lysosomes and is not acidified (6). This is not unsurprising in the context of *Plasmodium* development in an RBC, which lacks endomembrane system trafficking and, indeed, lysosomes. The highly polarized hepatocyte, however, has extensive vesicular transport networks (7) and can target intracellular pathogens residing in a vacuole (8), suggesting that the exo-erythrocytic form (EEF) may need to resist host cell attack.

Although the PVM is thought to be critical for *Plasmodium* growth in both the hepatocyte and the RBC contexts, its cellular roles remain elusive. The importance of several *Plasmodium* PVM-resident proteins, however, has been conclusively demonstrated in both blood and liver stages. Attempts to generate exported *(exp)1* and *Plasmodium* translocon of exported protein (*ptex)150* knockout parasites in *Plasmodium falciparum* failed (9, 10), revealing that these are both essential proteins for the blood stage, whereas *Plasmodium berghei* and *Plasmodium yoelii* mutants lacking *up-regulated in sporozoites (uis)3* or *uis4* fail to complete liver stage development (11, 12). These PVM-resident proteins, and thus the PVM itself, are performing functions that are crucial for *Plasmodium* growth, but delineating the functions of individual PVM-resident proteins has proven as difficult as identifying the cellular processes mediated by the PVM.

Significance

***Plasmodium* parasites have two distinct intracellular growth stages inside the mammalian host—the first stage, which is clinically silent, in liver hepatocytes, and the second, which causes the symptoms of malaria, in red blood cells. This study reports the discovery of a class of antimalarial compounds called torins, which are extremely potent inhibitors of both intracellular stages of *Plasmodium*. We show that torins block trafficking of liver stage parasite proteins to the physical host–parasite interface, called the parasitophorous vacuole membrane (PVM), and that without continuous trafficking of PVM-resident proteins, the parasite is subject to elimination by its host hepatocyte.**

Author contributions: K.K.H., D.F.W., and M.M.M. designed research; K.K.H., K.B., M.P., J.D.H-O., M.R., and W.L.B. performed research; A.S.R. and R.M. contributed new reagents/analytic tools; K.K.H., K.B., M.P., J.D.H-O., M.R., W.L.B., D.F.W., T.H., M.M., and M.M.M. analyzed data; and K.K.H. and M.M.M. wrote the paper.

The authors declare no conflict of interest.

*This Direct Submission article had a prearranged editor.

Freely available online through the PNAS open access option.

[1]To whom correspondence may be addressed. E-mail: khanson@fm.ul.pt or mmota@fm.ul.pt.

This article contains supporting information online at www.pnas.org/lookup/suppl/doi:10.1073/pnas.1306097110/-/DCSupplemental.

The one process in which both the centrality of the PVM is known and evidence for the participation of specific PVM proteins exists is the export of parasite proteins to the RBC. A cohort of parasite proteins that are involved in extensive physiological and structural modifications of the infected RBC (iRBC) is exported into the iRBC cytoplasm and beyond (13). Five proteins have been identified as components of PTEX, the proposed export machinery at the iRBC PVM (9). Although liver stage protein export has been shown for the Circumsporozite (CS) protein (14) and PTEX components are expressed in *P. falciparum* EEFs (15), a role for parasite protein export into the hepatocyte remains speculative; the host hepatocyte may not require the extensive structural remodeling that the iRBC does.

Conversely, however, the hepatocyte, with its extensive vesicular transport network, intuitively constitutes a more hostile host environment than the RBC, and there is evidence that the liver stage PVM may play a crucial role in preventing host cell-mediated parasite killing, as it does in Toxoplasma *gondii* (16). Support for a protective role for the liver stage PVM comes from knockout parasites that fail in the earliest steps of PVM formation and remodeling. Sporozoites lacking the p52/p36 gene pair invade hepatocytes successfully, but fail in PVM formation (17, 18) and are severely reduced in abundance midway through liver stage development. Parasites lacking *slarp*/*sap* (19, 20), a regulator of early liver stage development, fail to express UIS4 and exported protein 1 (EXP-1), along with other parasite proteins, and are also eliminated at the beginning of infection.

Acquisition of resources from the host-cell environment, an unambiguous requirement for an obligate intracellular parasite like *Plasmodium*, is a function ascribed to the PVM in both mammalian stages. The PVM allows the free passage of molecules (21, 22), presumably through proteinaceous pores, which may contribute to acquisition of host nutrients and disposal of parasite waste products. Members of the early transcribed membrane protein (ETRAMP) family, single-pass transmembrane proteins conserved among *Plasmodium* spp., which are highly expressed and developmentally regulated in both blood and liver stage parasites (23, 24), could be candidates for mediating uptake of host resources. Such a role in lipid uptake has indeed been proposed for the *P. berghei* ETRAMP UIS3 on the basis of its interaction with host-cell L-FABP (liver fatty acid binding protein) (25).

Although *Plasmodium* parasites must use host resources to support their own growth in both mammalian stages, the single cycle replicative output of the liver stage parasite is vastly greater than that of the blood stage, which may reflect a similarly increased need for host resources. In this respect, the hepatocyte constitutes far superior "raw material" compared with the RBC; hepatocytes are not only metabolically active, but also highly versatile cells, which are capable of altering uptake, storage, production, and degradation of a wide array of macromolecules in response to cellular and organismal requirements. The presence of a growing *Plasmodium* parasite is sensed by the host hepatocyte, which responds with activation of cellular stress responses and altered metabolism (26, 27). The mammalian target of rapamycin (mTOR) kinase integrates signals from amino acids, stress, oxygen, energy, and growth factors and responds by altering cellular protein and lipid synthesis, as well as autophagy (28). As such, we sought to determine how inhibition of host mTOR signaling would affect *Plasmodium* liver stage development. Here we show that torins, a single structural class of mTOR inhibitors, are highly potent antiplasmodial compounds targeting both mammalian stages in vitro and in vivo. Independent of host-cell mTOR, torins impair trafficking of *Plasmodium* liver stage PVM-resident proteins, revealing the fast turnover of these proteins at the liver stage PVM, and provoke elimination of liver stage parasites.

Results

Torins Potently Inhibit *Plasmodium* Liver and Blood Stages. We first tested whether *Plasmodium* infection could be modulated by inhibition of host mTOR signaling using two unrelated mTOR inhibitors (see Table S1 for structures, reviewed in ref. 29): rapamycin, a naturally occurring macrolide that is an allosteric mTOR inhibitor, and Torin1, a tricyclic benzonaphthyridinone developed through medicinal chemistry efforts as an ATP-competitive inhibitor (30). We plated two human hepatoma cell lines, Huh7 and HepG2, and infected the cells with GFP-expressing *P. berghei* sporozoites. Two hours after infection, by which time sporozoite invasion is completed, cells were switched into medium containing 250 nM of either rapamycin or Torin1. Control cells were treated with DMSO alone (vehicle control). Infection parameters were quantified by flow cytometry 48 h after sporozoite addition. In both cell lines, the effects of the two mTOR inhibitors were strikingly different. Treatment with rapamycin led to a modest increase in the proportion of infected cells (number of GFP+ cells) (Fig. 1*A*), or parasite development (Fig. 1*B*), as indicated by the geometric mean of the GFP signal intensity, which correlates with parasite development (31). Treatment with Torin1, however, eliminated the vast majority of parasites in both cells lines (Fig. 1*A*; HepG2 $P < 0.0001$) and blocked the development of those few that remained (Fig. 1*B*; HepG2 $P < 0.0001$). These results were confirmed by microscopy, and representative examples of control, rapamycin-treated, and the rare remaining Torin1-treated EEFs are shown in Fig. 1*C*.

A Torin1 analog with properties more amenable to large-scale synthesis and in vivo use was recently reported (32). We next synthesized and tested this analog, Torin2, for antiplasmodial activity. Dose–response analysis revealed that Torin2 is an ~100-fold more potent an inhibitor of *Plasmodium* liver stage growth than Torin1; the calculated cellular EC_{50} of Torin1 and Torin2 for parasite development was 106 nM 95% confidence interval (CI) 101–107 nM and 1.1 nM (95% CI 0.95–1.33 nM), respectively (Fig. 1*D*). Furthermore, a single dose of 10 mg/kg Torin2, administered to mice 2 h after infection with 10,000 sporozoites, led to a highly significant reduction in *Plasmodium* liver load (Fig. 1*E*, $P < 0.0001$) 40 h postinfection. In a controlled physiological infection model with infection initiated by 500 *P. berghei*-GFP sporozites, the same 10 mg/kg dose of Torin2 was curative. Control mice became blood stage positive by flow cytometry detection of GFP from day 4 to 6 postinfection, but none of the Torin2-treated animals ever developed blood parasitaemia by day 11 (Fig. 1*F*). The flow cytometry data were confirmed by microscopic examination of thin blood smears for all of the Torin2-treated animals.

The discrepancy between the extremely potent inhibition of *P. berghei* EEFs by the torins and the slight (and opposing) effects of rapamycin led us to wonder whether the antiplasmodial activity of the torins was really mediated by host mTOR. As a first step in addressing this, we tested if the inhibitory effects of the torins would extend to *P. falciparum* asexual blood stages, as the mature enucleate RBCs in which *P. falciparum* replicates have no catabolic capacity for mTOR to stimulate. Torin1 (200 nM) and Torin2 (10 nM) were added to synchronized *P. falciparum* 3D7 ring stages, and parasite replication and reinvasion were assessed by flow cytometry 48 h later. iRBCs were identified based on SYBR green labeling of *P. falciparum* DNA. Strikingly, both Torin1 and Torin2 blocked parasite development and completely prevented reinvasion, as evidenced by the static parasitemia, compared with the DMSO-treated control (Fig. 2*A*, $P < 0.0001$ for both Torin1 and Torin2 vs. control). Using a different cytometry-based assay and the P2G12 clone of *P. falciparum* 3D7 (33), we performed dose–response assays and determined the Torin2 EC_{50} for asexual blood stages to be 1.4 nM (95% CI 1.31–1.59 nM) (Fig. 2*B*). Torin2 is also highly potent against early gametocytes, with a slightly lower EC_{50} of 6.62 nM (95% CI 4.59–9.54 nM). (Table S1). We next

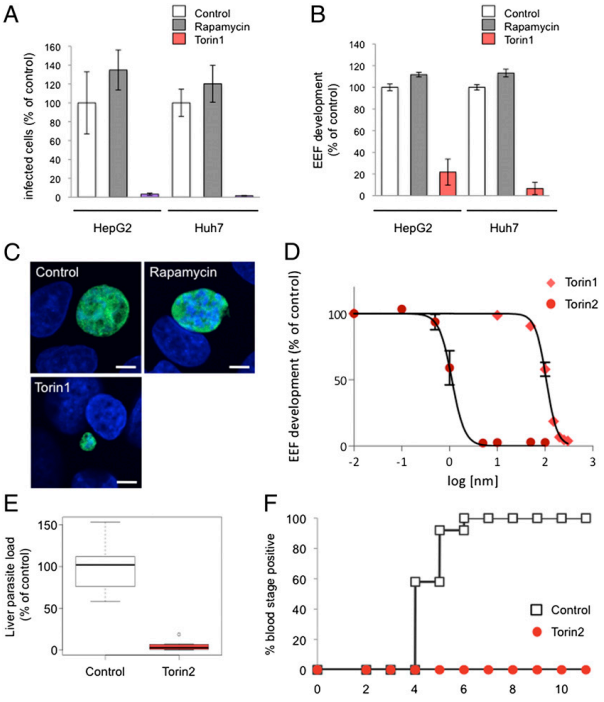

Fig. 1. Torins are antiplasmodial compounds with nanomolar potency against *Plasmodium* liver stages and are capable of curing infection. (*A–C*) Effect of mTOR inhibitors, rapamycin, and Torin1 on *P. berghei* liver stage infection. HepG2 or Huh7 cells infected with *P. berghei*-GFP sporozoites on the day after seeding. Torin1, rapamycin, or DMSO (vehicle as control) were added 2 h after infection and remained present until 48 h after sporozoite addition, when samples were processed for flow cytometry (*A* and *B*) or microscopy (*C*). Data from technical triplicates of the DMSO control were averaged, and the mean was set to 100%; all samples were then normalized to this value. Mean ± SD from one representative experiment is shown. (*A*) The number of GFP+ events detected represents the number of infected cells. (*B*) The geometric mean of the GFP signal, known to correlate with parasite growth, represents EEF development. (*C*) Representative confocal images. Huh7 cells were fixed and labeled with anti-PbHSP70 (*P. berghei* heat shock protein 70) (EEF, green) and DAPI (nuclei, blue). (*D*) Dose-dependent effects of Torin1 and Torin2 on *P. berghei* liver stage infection. HepG2 cell infection analyzed by flow cytometry 48 h later, as in *B*. Each data point represents $n = 3$ biological triplicates. Four-variable curve fitting was carried out using GraphPad Prism. (*E*) Effect of a single Torin2 oral dose on parasite liver load. C57BL/6 mice were infected i.v. with 10,000 Pb-GFP sporozoites and given 10 mg/kg Torin2 suspended in sunflower oil or an equivalent dose of sunflower oil alone 2 h after infection. Each point represents a single animal ($n = 3$ independent experiments); mean ± SD is indicated for each group. (*F*) Effect of a single Torin2 oral dose on prepatency period. C57BL/6 mice were infected i.v. with 500 Pb-GFP sporozoites and given 10 mg/kg Torin2 suspended in sunflower oil or an equivalent dose of sunflower oil alone 2 h after infection. Animals were monitored daily for appearance of parasitaemia in the blood by flow cytometry. Data are from three independent experiments with a total of 12 animals in each group.

tested whether Torin2 would be capable of antimalarial activity against the blood stage of *P. berghei* in vivo. C57BL/6 mice infected with *P. berghei*-GFP iRBCs were treated with a single oral dose of 10 mg/kg Torin2 on day 4 after infection when the parasitaemia had reached 3%. All control mice succumbed to experimental cerebral malaria by day 7, whereas the majority of the Torin2-treated group did not (Fig. 2*C*), a highly significant difference in survival ($P < 0.0001$). The single Torin2 dose also led to a highly significant blunting of parasitaemia (Fig. 2*D*, $P < 0.0001$). Overall, our data demonstrate that torins are similarly effective and potent against both blood and liver stage *Plasmodium* parasites in vitro and in vivo. Thus, the mediator of the antimalarial activity must be present in both of these host–parasite settings.

Inhibition of Host mTOR Signaling by Other Means Does Not Phenocopy the Antiplasmodial Effects of Torins. The ability of torins to potently target both liver and blood stages of *Plasmodium* infection suggested a direct effect on the parasite and not on host mTOR. We sought to further test this hypothesis using chemical and genetic means to reduce host mTOR activity in hepatoma cells.

First, we evaluated the ability of PP242, another highly specific ATP-competitive mTOR inhibitor that is structurally unrelated to the torins (34), to inhibit *Plasmodium* liver stages. Treatment with 2.5 μM PP242 [concentration showing complete inhibition of mTORC1 and mTORC2 signaling in cellular assays (34)] did not reduce either infected hepatocyte number or *Plasmodium* liver stage growth (Fig. 3 *A* and *B*). Likewise, addition of PP242 to *P. falciparum*-synchronized 3D7 ring stages had no impact on blood stage development and reinvasion (Fig. 3*C*).

We next turned to siRNA knockdown of mTORC1 components in hepatoma cells. siRNA oligonucleotide pools targeting human m*Tor* or *raptor* transcripts were introduced by reverse transfection and the knockdown cells infected with GFP-expressing *P. berghei* sporozoites 48 h later. siRNA-mediated knockdown of neither mTOR nor raptor could phenocopy the dramatic reduction of infected cells or parasite development observed with Torin2 treatment (Fig. 3 *D* and *E*). EEF morphology 24 h after infection was also comparable across the control, mTOR, and raptor knockdown cells (Fig. 3*F*). Taken together, our data strongly suggest that the target mediating the antiplasmodial effects of torins is not the host cell mTOR kinase, but rather is parasite-encoded.

Torin2 Is Not Permissive to Generation of Drug-Resistant Parasite Lines in Vitro. To identify the target of Torin2, we attempted to generate drug-resistant mutants in *P. falciparum* blood stage parasites. We first determined that the multidrug-resistant Dd2 strain of *P. falciparum* retained Torin2 sensitivity, with an EC_{50} of 0.7 nM (95% CI 0.48–1.02 nM) in asexual blood stage growth assays (35). We then performed resistance selection with clonal Dd2 ring stage parasites, exposing them to 10× EC_{50} (7 nM) Torin2 for 8 d. When parasites failed to recrudesce 60 d after this treatment, we varied the length of selection to optimize the mutation-selection window. We achieved parasite recrudescence in 4 of 32 independent selection attempts and only with exposure times of 48 h or less (summarized in Table 1). Remarkably, the four selected strains all failed to display any resistance phenotype by SYBR dose–response or decrease in time to recrudescence in subsequent repetitions of the selection protocol (Table 1). We, and others, have used these selection

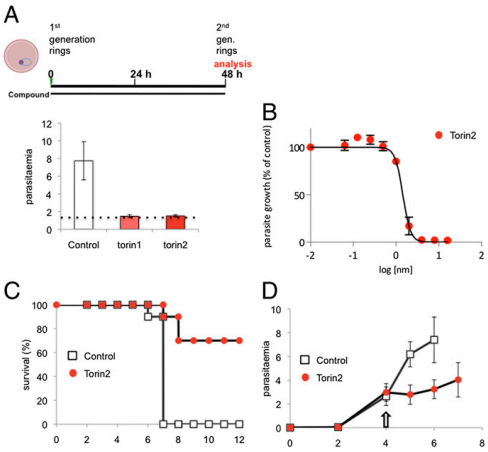

Fig. 2. Torins potently inhibit *Plasmodium* blood stage infection. (*A*) Effect of Torin1 and Torin2 in *P. falciparum* blood stage in vitro cultures. Synchronized *P. falciparum* 3D7 ring stage parasites were treated with 200 nM Torin1, 10 nM Torin2, or DMSO (vehicle control); reinvasion was analyzed after SybrGreen labeling of parasite DNA 48 h later. Data represent mean ± SD of three independent experiments. Starting parasitaemia are represented by dotted line. (*B*) Dose-dependent effect of Torin2 on *P. falciparum* blood growth. Data represent mean ± SD of three independent experiments. (*C* and *D*) Effect of a single 10-mg/kg oral dose of Torin2 administered on day 4 after infection of C57BL/6 mice with 1×10^6 Pb-GFP–parasitized RBC on survival (*C*) and parasitemia (*D*). Animals were monitored daily for malaria-associated pathology (experimental cerebral malaria symptoms), and parasitaemia was analyzed by flow cytometry. (*C*) Cumulative survival curve for three independent experiments; $n = 10$ mice for control and Torin2-treated groups. (*D*) Parasitaemia; each point represents the mean ± SD from three independent experiments.

methodologies to raise resistance to antimalarials that act on a variety of targets within the parasite's cytosol and mitochondria (36, 37). In contrast, Torin2 pressure has thus far failed to induce a stable resistance phenotype after varied, repeated attempts, suggesting that additional unbiased approaches will be necessary to elucidate the drug target(s).

***Plasmodium* Growth Is Inhibited by Torin2 Throughout Liver Stage Development.** With the evidence leaning toward torins acting directly on *Plasmodium* spp., we sought to gain insight into the killing mechanism by asking when the target(s) of Torin2 antiplasmodial activity are present in liver stages. We first varied compound treatment windows to target different stages of parasite invasion and development during liver stage infection. Initially, we checked whether Torin2 treatment of HepG2 cells 2 h before sporozoite addition could impact either sporozoite invasion or EEF development. Torin2 pretreatment did not alter either parasite numbers or development, as assayed 24 h after infection (Fig. S1*A*). We next tested if Torin2 treatment concomitant with sporozoite addition would affect parasite invasion and again found no effect; comparable amounts of cells were infected (GFP+) after 2 h, demonstrating that sporozoite invasion occurs normally in the presence of Torin2 (Fig. S1*B*). Next, sporozoites were allowed to complete invasion of HepG2 cells, and then 10 nM Torin2 was added for varying time periods (as schematized in Fig. 4*A*) corresponding roughly to "early PVM remodeling" (2 h), trophozoite (6 h), and schizont (24 h) stages of intrahepatocyte development. Infection was analyzed 50 h after sporozoite addition by flow cytometry, and none of the Torin2 treatment periods was found to significantly increase HepG2 cell death (Fig. S1*C*). As previously shown, continuous incubation of infected cells with 10 nM Torin2 after sporozoite invasion results in near-complete parasite elimination (Fig. 4*A*). Remarkably, a mere 4-h incubation with 10 nM Torin2 from 2 to 6 h after infection was also capable of eliminating more than 90% of all parasites (Fig. 4*A*); Torin2 treatment from 6 to 24 h postinfection was similarly effective (Fig. 4*A*). The very few developing EEFs under the 2- to 6- or 6- to 24-h conditions showed slightly reduced development compared with the control (Fig. 4*B*). Interestingly, when Torin2 treatment was initiated only after the start of schizogony (24–50 h), fewer parasites were eliminated, with parasite numbers about 60% of the control (Fig. 4*B*). However, in this treatment group, EEF development showed the strongest inhibition—to 30% of control levels (Fig. 4*B*); on an individual level, these parasites show aberrant development and fail to form merozoites (Fig. S1*D*). Our data demonstrate that Torin2 is a potent inhibitor of all phases of *Plasmodium* EEF development through late schizogony. Torin2-treated parasite elimination, however, occurred efficiently only when EEFs were exposed to Torin2 before the onset of schizogony.

Torin2 Treatment Leaves the PVM Structurally Intact, but Lacking PVM-Resident Proteins. A number of gene-knockout parasite lines that successfully invade hepatocytes exist, but fail during PVM establishment or remodeling and are rapidly eliminated (11, 12, 17–20, 38). Given this phenotypic parallel to the effects of Torin treatment, which also does not affect the invasion

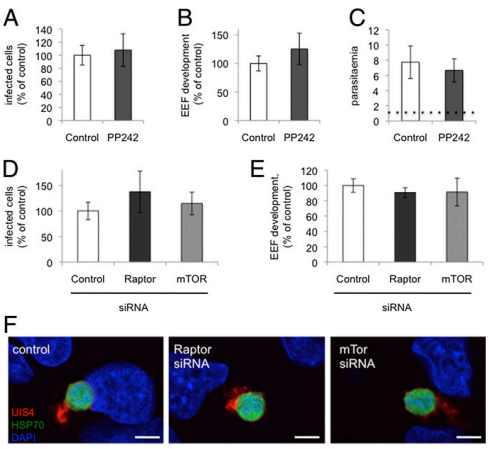

Fig. 3. mTOR inhibition by other means does not phenocopy the antiplasmodial effect of torins. (*A* and *B*) Effect of PP242 on inhibition of liver stage infection. Infected HepG2 cells were treated with 2.5 uM PP242 2 h after spozoroite addition, and the infection was analyzed by flow cytometry 48 h later, as in Fig. 1. Data represent mean ± SD three independent experiments. (*C*) Effect of PP242 on blood stage infection. Synchronized *P. falciparum* 3D7 rings were treated with 2.5 μM PP242 or DMSO (identical control data set as in Fig. 2*A*), and reinvasion was analyzed after SybrGreen labeling of parasite DNA 48 h later. Data represent mean ± SD of three independent experiments. (*D–F*) Effect of siRNA-mediated knockdown of raptor or mTOR on liver stage infection. Validated siRNA pools were reverse-transfected into HepG2 cells, which were infected with sporozoites 2 d later and analyzed by flow cytometry as described above or with immunofluorescence analysis (IFA) 24 h after sporozoite addition. (*F*) Representative images with PbHSP7 (green), UIS4 (red), and DAPI (blue).

Table 1. Torin2 is refractory to repeated attempts at resistance selection in vitro

Selection strategy	Recrudescence of parasites	Days to recrudescence (first/second/third round)*	Fold EC_{50} (nM)**
10× EC_{50}, 192 h	0/8	NA	NA
10x EC_{50}, 144 h	0/4	NA	NA
20x EC_{50}, 48 h pulsed three times	0/4	NA	NA
20x EC_{50}, 48 h	1/7	26/24/30	1.04
20x EC_{50}, 36 h	1/3	26/23/30	0.93
20x EC_{50}, 24 h	2/4	22/24/31	1.14
20x EC_{50}, 12 h	0/2	NA	NA

Asexual Dd2 parasites were subjected to varied step-wise intermittent selection protocol with10x EC_{50} Torin2.

*Number of days for each independent selection to return to 1% parasitemia. The time to recrudescence for subsequent rounds of selection is expressed separately for the first/second/third round of selections and expressed as the average of the number of days when multiple independent selections were performed with identical protocols.

**Parental Dd2 strain EC_{50} is 0.7 nM (0.48,1.02). Values expressed as fold change over Dd2 EC_{50}.

process itself, but leads to parasite elimination, we wondered if Torin2 treatment might be altering the parasite PVM, or alternatively, if infected cells were selectively rendered nonviable by a brief Torin2 treatment. To this end, we used a live imaging setup to address two questions: (*i*) Are infected cells viable after Torin2 treatment? and (*ii*) Is the PVM maintained intact after Torin2 treatment? To that end, we infected HepG2 cells with *P. berghei*-GFP sporozoites and used the vital dye tetramethylrhodamine, ethyl ester (TMRE), which labels mitochondria with an intact membrane potential, to assess host-cell mitochondrial activity and unambiguously identify intracellular EEFs. Additionally, we used the vital DNA dye Hoechst 33258, which freely labels host-cell DNA or free sporozoites, which lack a PVM, but is unable to label the DNA of developing EEFs until maturation-induced PVM changes occur late in liver stage development (39). Torin2 was added 2 h after infection, and the cells were imaged 6 h later, after TMRE and Hoechst 33258 labeling. Based on our earlier data (Fig. 4*B*), the vast majority of Torin2-treated EEFs are ultimately nonviable after such a treatment. In both control and Torin2-treated cells, the 8-h EEFs developed in host cells with normal nuclear morphology and active mitochondria (Fig. S2*A*). Importantly, the EEF nuclei are not labeled by Hoechst 33258 in either drug-treated or control cells (Fig. S2*A*), although the nuclei of extracellular sporozoites that have failed to invade clearly are an indication that Torin2-treated EEFs reside in an intact PVM. To confirm this interpretation, we used transmission electron microscopy (TEM) to investigate PVM integrity in EEFs that were exposed to Torin2 from 2 to 8 h after infection. As expected, the 8-h control EEFs were uniformly PVM-positive (Fig. 5*A*). Torin2-treated parasites were also clearly surrounded by a PVM in all cases (Fig. 5*A*) and tended to have more parasite PM waviness and intracellular complexity (e.g., membranous whorls) than the control parasites observed.

Given that the PVM appeared intact in Torin2-treated infected cells, we next checked whether *Plasmodium* proteins known to localize to the PVM were altered after exposure to Torin2. UIS4, which is already transcribed in mature salivary gland sporozoites (40), is localized to the PVM throughout development inside the hepatocyte (11). Using UIS4-specific antiserum, we confirmed that 2 h after infection UIS4 was already localized to the PVM; the peak UIS4 signal is clearly outside of the parasite soma delineated by *P. berghei* heat shock protein 70 (HSP70) antibody staining (Fig. 5*B*). Torin2 treatment initiated 2 h after infection is thus acting upon developing parasites already enclosed in UIS4-positive PVMs. Surprisingly, we found that 6 h of Torin2 treatment completely abolished the PVM localization of UIS4. In stark contrast to both the pretreated 2-h parasites and the 8-h control parasites, UIS4 is found exclusively within the parasite soma in Torin2-treated parasites (Fig. 5*B*).

Torins are potent antiplasmodials throughout liver stage development, so we next investigated whether or not Torin2 treatment could induce mislocalization of PVM-resident proteins in more mature parasites. Infected HepG2 cells were treated with 10 nM Torin2 during a 12-h window starting 16 h after infection, and localization of both UIS4 and EXP1, another known PVM-resident protein [also called Hep17 (41)], was assessed in 28 h EEFs. As expected, UIS4 and EXP1 were localized almost completely outside of the parasite soma in control 28-h EEFs (Fig. 5*C*). Again, Torin2 treatment led to a dramatic mislocalization of UIS4, with signal largely found in the parasite soma in 28-h EEFs (Fig. 5*C*), although some residual UIS4 could also be observed in the host-cell cytoplasm. EXP1 localization was also completely perturbed by Torin2 treatment, with a PVM (control) to soma (Torin2-treated) shift paralleling that of UIS4 (Fig. 5*C*). Additionally, Torin1 treatment also induces mislocalization of UIS4 to the parasite soma (Fig. S2*B*). These data imply that torins act against *Plasmodium* by altering the localization of PVM-resident proteins.

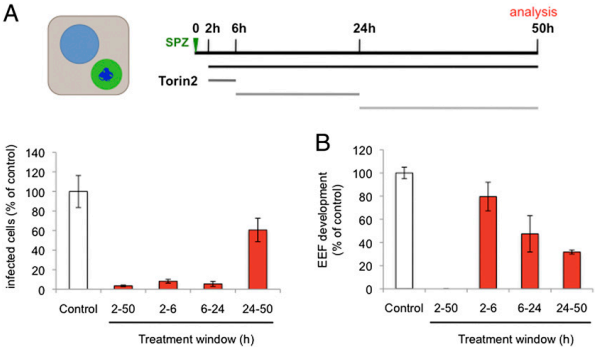

Fig. 4. *Plasmodium* growth is inhibited by Torin2 throughout liver stage development. (*A* and *B*) Effects of Torin2 throughout *P. berghei* liver stage development in vitro. Infected HepG2 cells were treated with 10 nM Torin2 or DMSO (vehicle control) as indicated in the schematic illustration, and the infection analyzed by flow cytometry 50 h after sporozoite addition, as in Fig. 1. Data represent mean ± SD of quadruplicates from one representative experiment with all conditions processed in parallel.

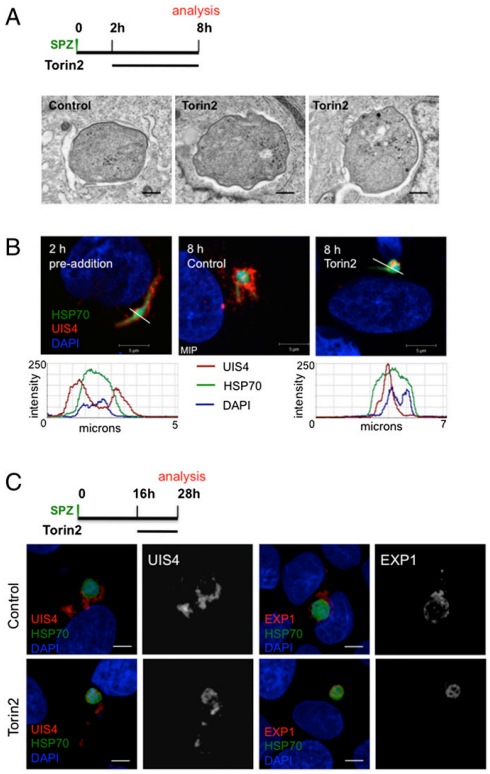

Fig. 5. Torin2 treatment leaves the PVM structurally intact but lacking PVM-resident proteins. (*A* and *B*) Effect of Torin2 treatment on the PVM and UIS4 localization in young liver stage trophozoites. Schematic illustrates experimental setup. (*A*) Representative images of TEM of 8-h EEFs after Torin2 or DMSO (control) treatment. (*B*) IFA at 2 h (control, single confocal slice) and at 8 h in control [maximum intensity projection (MIP)] and Torin2-treated cells [single confocal slice (HSP70, green; DAPI, blue; UIS4, red)]. Fluorescence intensity graphs of the trajectory indicated by the white lines in the preaddition and Torin2-treated images show the relative spatial intensity peaks of the three fluorophores. (*C*) Effect of Torin2 treatment on UIS4 and EXP1 during early liver stage schizogony. Schematic illustrates experimental setup. MIPs of the entire EEF are shown for *A*–*C*.

EEF Elimination and PVM-Resident Protein Mislocalization Are Not General Aspects of Liver Stage Inhibition by Antimalarials, Indicating a Distinct Mechanism of Action for Torins. Although a comprehensive study of the activity of currently used antimalarials against rodent liver stage parasites has been carried out (42), we lack such information on a phenotypic level, leading us to wonder whether parasite clearance is the inevitable outcome for EEFs that are rendered nonviable during the first hours of intrahepatocyte development. To address this, we first confirmed the elimination of Torin2-treated parasites in HepG2 cells by microscopy; continuous exposure to Torin2 initiated after sporozoite invasion results in a complete absence of developing EEFs 48 h later. We then compared Torin2 side by side with the recently identified antiplasmodial decoquinate, which has the same mechanism of action (MoA) as atovaquone (43, 44), the most potent antimalarial in clinical use effective in the liver stage (42). We chose to focus on decoquinate as its potency is more similar to that of Torin2 than that of atovaquone. Treatment of infected HepG2 cells 2 h after sporozoite invasion with either 10 nM Torin2 or 26 nM decoquinate (10× EC_{50}) resulted in complete *Plasmodium* inhibition. Torin2 eliminated EEFs, as expected (Fig. 6*A*, $P < 0.0001$), whereas decoquinate led to a modest reduction in the number of EEFs present 50 h after infection (Fig. 6*A*, $P < 0.05$). Furthermore, a 6-h treatment with decoquinate from 2 to 8 h after infection was phenotypically equivalent to the 2- to 50-h treatment (Fig. S3). Despite the persistence of decoquinate-treated EEFs, they appear to be arrested very early in development (Fig. 6*A*, $P < 0.0001$), a phenotype we have confirmed by microscopy in primary mouse hepatocytes (Fig. 6*B*). EEF elimination is thus not a default outcome of parasite nonviability early in development, but rather reflects a specific aspect of the torin-treated EEF phenotype. This provides an intriguing parallel to the phenotypes described for those mutant parasites that successfully invade hepatocytes, but fail during PVM establishment or remodeling and are rapidly eliminated (17–20).

We next checked if the mislocalization of PVM-resident proteins induced by the torins could be a previously unnoted feature of pharmacological inhibition/killing of *Plasmodium* liver stages, also provoked by known antimalarials active against the liver stages. We tested this hypothesis by evaluating UIS4 and EXP1 localization in infected cells treated with representative members of the classes, in terms of both chemical structure and MoA, of currently known antimalarials (42). Primaquine, pyrimethamine, and decoquinate were individually added to HepG2 cells 20 h after infection at 10× EC_{50} concentrations. Ten hours later, coverslips were fixed and processed for immunofluorescence. Compared with the control and Torin2 conditions (Fig. 6*C*), decoquinate-treated parasites retained robust anti-UIS4 labeling of the PVM but, notably, EXP1 staining was nearly abolished (Fig. 6*C*), a feature we also noted in mouse primary hepatocytes (Fig. 6*B*). In the primaquine- and pyrimethamine-treated cells, both PVM-resident proteins were properly localized (Fig. 6*C*). Additionally, PVM-resident proteins remain properly localized in cells treated with the known liver stage inhibitors genistein (45), lopinavir (46), and cyclosporin A (47), as well as with the PI3K inhibitor LY294002 and rapamycin (Fig. S4). Furthermore, Torin2 treatment from 2 to 4 h postinfection is sufficient to mislocalize UIS4, but is reversible, in terms of both parasite growth and UIS4 localization at 48 h postinfection (Fig. 6*D*). Additionally, cycloheximide treatment (10 μg/mL), which blocks translation and is a potent antiplasmodial compound (48), during the same 2 h window is uniformly lethal for the developing EEFs, which do not grow after this time period; this lethality is not accompanied by a penetrant defect in UIS4 localization as assayed at either 4 or 50 h after infection (Fig. 6*D*). Thus, PVM-protein mislocalization is definitively not a consequence of parasite death.

As such, we conclude that both parasite elimination and altered localization of PVM resident proteins are specific phenotypes of torin-mediated *Plasmodium* liver stage inhibition, which strongly indicates that torins have a distinct MoA from currently used antimalarials.

***Plasmodium* Liver Stage Parasites Require Replenishment of PVM-Resident Proteins for Viability.** As the alteration of PVM-resident protein localization was not a general consequence of antimalarial activity against EEFs, we sought to determine the mechanism by which Torin2 provokes the mislocalization of these proteins.

Trafficking of blood stage *P. falciparum* proteins to specific organelles, the vacuolar space, PVM, and beyond into the iRBC itself has been a subject of intense study (49). Brefeldin A (BFA), an inhibitor of eukaryotic ADP-ribosylation factor (ARF) GTPases and the retrograde Golgi-ER trafficking that they mediate in many species, including *Plasmodium* (50), blocks export of knob-

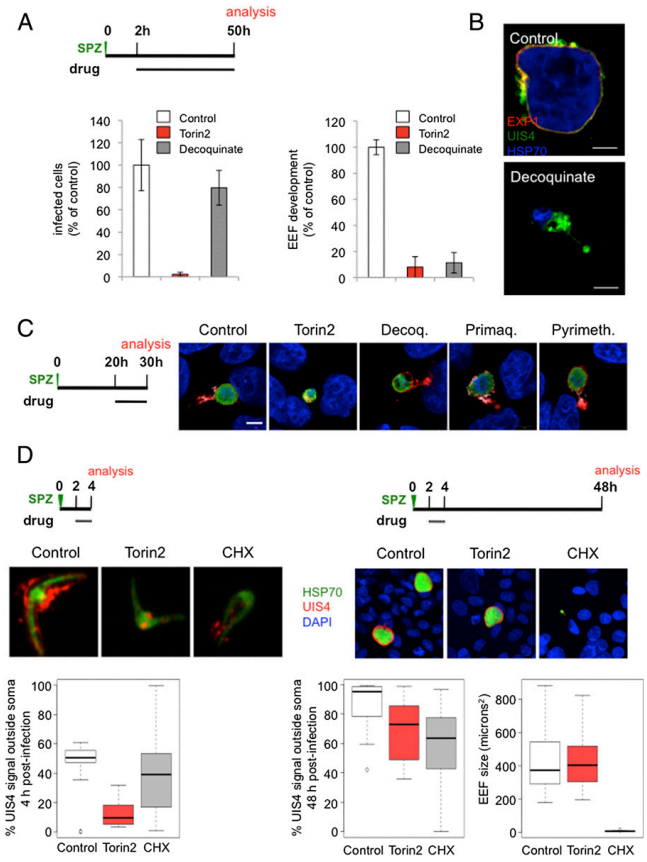

Fig. 6. EEF elimination and PVM-resident protein-trafficking defects are torin-specific phenotypes, not general aspects of liver stage inhibition by antimalarials. (*A* and *B*) Effects of decoquinate and Torin2 on EEF numbers and development. (*A*) Schematic of treatment and analysis. Infected HepG2 cells analyzed by flow cytometry at 50 h after sporozoite addition. Mean of $n = 3$ biological experiments, each condition in triplicate. (*B*) Mouse primary hepatocytes infected ex vivo with EXP1 (red), UIS4 (green), and HSP70 (blue) labeling. (*C*) Effect of current antimalarial classes active against the liver stage at the onset of schizogony. Schematic illustrates experimental setup; representative confocal images shown with UIS4 (red), EXP1 (white), PbHSP70 (green), and DAPI (blue) labeling. (*D*) Effects of 2 h Torin2 or cycloheximide treatment on UIS4 localization and EEF development. Schematic illustrates experimental setup. Representative confocal images of control (DMSO), Torin2-, and cycloheximide-treated EEFs labeled with anti-UIS4 (red), anti-PbHSP70 (green), and DAPI (blue) 4 and 48 h postinfection. Quantification of the proportion of UIS4+ pixels not overlapping PbHSP70 in 20 EEFs from each condition at 4 and 48 h postinfection; quantification of EEF area 48 h postinfection.

associated histidine-rich protein (KAHRP), *P. falciparum* erythrocyte membrane protein 1 (PfEMP1) (51), and EXP1 (52) among other proteins in blood stage parasites. Nothing is known about the trafficking pathways used by the liver stage parasite, so we tested whether UIS4 trafficking to the PVM proceeds through a BFA-sensitive pathway. We added BFA to HepG2 cells 2 h after infection, when UIS4 is already present in the PVM. After BFA (5 μM) treatment for 6 h postsporozoite invasion, UIS4 is found inside the parasite soma as in Torin2-treated parasites (Fig. 7*A*). Compared with Torin2 treatment, which causes UIS4 to accumulate in discrete intracellular puncta (Fig. 7*A*) during the same window, BFA causes UIS4 to accumulate in what appears to be a more continuous distribution within the parasite soma. As UIS4 colocalizes with the microneme marker thrombospondin-related anonymous protein (TRAP) in mature salivary gland sporozoites (40) and as TRAP is maintained in puncta throughout the majority of liver stage development (53), we tested whether UIS4 relocalized into TRAP-positive structures upon Torin2 or BFA treatment. The data clearly show that UIS4 and TRAP do not substantially colocalize in control, BFA-, or Torin2-treated cells (Fig. S5*A*).

Most strikingly, BFA treatment, which blocks only protein secretion, phenocopied the complete loss of PVM-localized UIS4 seen in the Torin2-treated parasites (Fig. 7*A*). We quantified the distribution of UIS4 and found that, on average, 62% of the UIS4 signal is present outside of the parasite soma in 8-h control EEFs, whereas BFA or Torin2 treatment resulted in >95% overlap of UIS4 and HSP70 in the parasite soma (Fig. 7*B*). We extended these results to *P. berghei* EEFs developing inside murine primary hepatocytes ex vivo (Fig. S5*B*); UIS4 and EXP1 trafficking to the PVM is BFA- and Torin2-sensitive in young liver stage schizonts (Fig. S5*B*), and both PVM-resident proteins are also concomitantly depleted from the PVM.

Taken together, our data support a model (Fig. 7*C*) in which Torin2 treatment prevents secretion of liver stage PVM-resident proteins, leading to their accumulation inside the EEF soma. This block in secretion causes the PVM to be left devoid of PVM-resident proteins, particularly in trophozoites, which leads to parasite elimination by the host hepatocyte.

Discussion

This study reports that torins, developed as ATP-competitive mammalian mTOR kinase inhibitors, are extremely potent inhib-

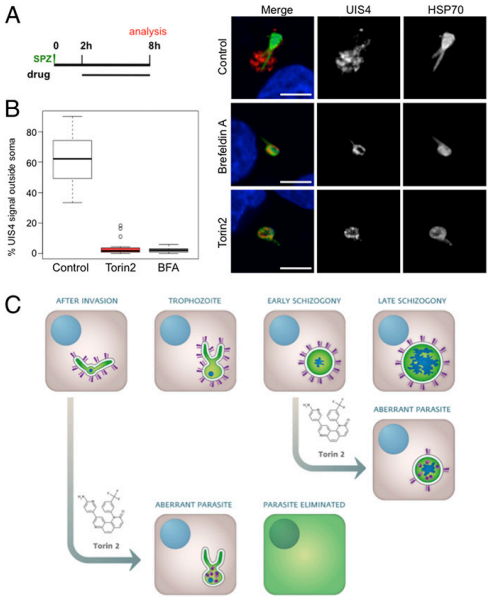

Fig. 7. *Plasmodium* liver stage parasites require replenishment of PVM-resident proteins for viability. (*A* and *B*) Comparative effects of Torin2 and BFA on UIS4 trafficking to the PVM in young liver stage trophozoites. Schematic illustrates experimental setup. (*A*) Representative confocal images of control (methanol, BFA vehicle), Torin2-, and BFA-treated EEFs labeled with anti-UIS4 (red), anti-PbHSP70 (green), and DAPI (blue). (*B*) Quantification of the proportion of UIS4+ pixels not overlapping PbHSP70 in 20 EEFs from each condition. DMSO and methanol, the vehicle controls for Torin2 and BFA, respectively, are grouped together as control. (*C*) Model of Torin2 liver stage MoA.

itors of both the liver and blood stages of *Plasmodium* parasites. Although we first tested Torin1 (together with rapamycin) to investigate the role of host hepatocyte mTOR signaling in liver stage *Plasmodium* infection, our data as a whole provide extremely strong support for a parasite-encoded target mediating the antiplasmodial activity of the torins. We present three lines of evidence that suggest that host-cell mTOR is not the mediator of the antiplasmodial activity of the torins. First, unrelated small-molecule mTOR inhibitors (rapamycin and PP242) or siRNA-mediated reduction of mTOR signaling both fail to inhibit *Plasmodium* liver stage infection. Strong evidence that host mTOR is uninvolved comes from the nonequivalence of PP242 and torins. Both cause complete inhibition of mTORC1 and mTORC2 activity (30, 32, 34). The chemical structures of the two compounds are not at all similar although, as we show here, neither are their effects on liver or blood stage *Plasmodium* infection. Second, torins inhibit both liver and blood stage parasites, with Torin2 maintaining a near identical EC_{50} for the two stages and for different *Plasmodium* species. Although it is easy to envisage mechanisms by which reduction of host hepatocyte mTOR signaling could alter liver stage *Plasmodium* development, this is not the case for the iRBC. The mature RBC lacks the capacity for both protein and lipid synthesis, as well as gene expression, and although mTOR has been found in the RBC "hidden proteome," no evidence of functional protein exists (54). Third, torins are able to alter the localization of *Plasmodium* proteins during liver stage infection, an effect very unlikely to be mediated by a host protein. As a whole, our data point unequivocally to a *Plasmodium*-encoded molecule or molecules, conserved across the genus and expressed in all mammalian stages, as the target of the antiplasmodial activity of Torin1 and Torin2.

Sequence homology queries of current *Plasmodium* genome assemblies show that no *Plasmodium* orthologs of mTOR exist, and indeed the PI3K-like protein kinase family, of which mTOR is a member, is not found (55, 56). The *P. berghei* proteins showing the highest sequence similarity to human mTOR are the single predicted phosphatidylinositol-3-kinase (PI3K) (PBANKA_111490) and the two predicted phosphatidylinositol-4 kinases (PI4Ks) (PBANKA_110940 and PBANKA_072200), which show conservation primarily in the kinase catalytic domain. Although little is known about the activity of the two predicted *Plasmodium* PI4Ks, PbPI3K is an essential gene (57), and treatment with the known PI3K inhibitors wortmannin and LY294002 reduced PI3P production by PfPI3K in vitro and inhibited blood stage parasite growth (58). LY294002 does not phenocopy Torin2 inhibition of *P. berghei* liver stages, however, and the inhibition of *P. falciparum* replication by wortmannin and LY294002 (58) is much more modest than what we observed with either Torin1 or Torin2.

Our data clearly show that Torin2 is a potent antimalarial with in vivo activity against both liver and blood stages, capable of curing liver stage infection with a single, well-tolerated oral dose. Still, given its demonstrated potent inhibition of human mTOR, we cannot, and do not, see Torin2 itself as a lead compound; further medicinal chemistry elaboration will be necessary to realize a torin analog as a suitable antimalarial lead. Nevertheless, torins represent a new antimalarial chemotype that certainly warrants further medicinal chemistry investigation due to the following highly desirable properties: (i) versatility: Torin2 targets both liver and blood stages, and is active against immature gametocytes; (ii) speed of action: torins render P. falciparum parasites nonviable in a single blood stage cycle and short treatment windows are sufficient to kill liver stage parasites; (iii) distinct MoA from currently utilized antimalarials: none of the compounds in current clinical use which are active against Plasmodium liver stages provoke PVM trafficking defects; and (iv) Torin2 retains potency against the multidrug resistant Dd2 strain of P. falciparum, and is not amenable to in vitro resistance generation, in contrast to most antimalarials in current clinical use and leading candidates (36, 37, 59–63). Additionally, the mediator(s) of the antiplasmodial activity of the torins is clearly druggable in vivo during both mammalian stages.

Although the value of torin analogs for human antimalarial use will rely on future medicinal chemistry elaboration, the utility of torins for probing PVM function and protein-trafficking pathways in the *Plasmodium* EEF is immediate. *Plasmodium* parasites contain many unusual cellular compartments and have evolved strategies to direct proteins not only to these but also to destinations outside of the parasite soma—from the PV to the host-cell membrane itself. The transport pathways that the blood stage parasite uses to direct proteins to these diverse locations has been a subject of intense study; whereas specific trafficking pathways and molecular determinants ultimately mediate protein movement to discrete locations—i.e., the vacuolar space, the Maurer's clefts in the iRBC cytoplasm, the digestive vacuole, or the PVM—most secreted proteins seem to initially follow a common, canonical BFA-sensitive ER-Golgi route in the blood stage parasites (49). As such, it is perhaps not surprising that UIS4 and EXP1 trafficking to the liver stage PVM requires the canonical BFA-sensitive ER-Golgi transport route, as we have demonstrated. Still, it highlights the fact that the parasite does use this, and undoubtedly other core pathways, throughout all mammalian stages. It remains to be determined whether the EEF uses the same parasite-encoded molecules for acquisition of host hepatocyte resources that the blood stage parasite uses in remod-

elling the "inert" RBC or whether components of the host hepatocyte vesicular trafficking networks are co-opted by the parasite.

Comparing BFA- and Torin2-treated EEFs, we find clear commonalities and subtle differences in phenotype. When either drug is added after sporozoite invasion and intial UIS4-positive PVM establishment, both treatments result in complete loss of UIS4 at the PVM 6 h later, as well as intracellular accumulation of UIS4. BFA blocks ER to Golgi trafficking by inhibiting the P. falciparum orthologue of Arf1 (64). BFA-treated blood stage parasites form a hybrid ER- Golgi compartment (65) that accumulates proteins utilizing the canonical secretory pathway. We interpret the similarity of BFA- and Torin2-treated EEF phenotypes as highly suggestive that Torin2, like BFA, causes a failure in anterograde protein trafficking. The compartment in which UIS4 is retained appears qualitatively different, however, with Torin2 treatment leading to the appearance of small puncta of UIS4 and BFA treatment leading to a more continuous distribution of UIS4 inside the parasite soma. Future characterization of the intracellular location in which PVM-resident proteins accumulate after Torin2 treatment may help shed light on which trafficking step is inhibited by Torin2.

Localization of a membrane protein to a specific compartment can be achieved by either its retention at, or continuous transport to, the compartment. Most intriguingly, our data illustrate that UIS4 and EXP1 must be continuously transported to the PVM throughout at least the first 30 h of liver stage development. Several fascinating questions arise from this: Are UIS4 and EXP1 "lost" to the host cell during EEF development? Are UIS4 and EXP1 subject to retrograde trafficking back into the PV or parasite soma? Are these dynamics generalizable to all liver stage PVM-resident proteins, or do they reflect the specific functions of EXP1 and UIS4? Whether or not torin treatment alters protein trafficking in *Plasmodium* asexual and sexual blood stages also remains to be established.

Proteins that are known to populate the nascent PVM of the invading *P. falciparum* merozoite are synthesized during the preceding schizont stage and stored in the apical organelles of the merozoite before release in the invasion process (66). The translocon components HSP101, PTEX150, and EXP2 are examples of this; they are found in the dense granules of merozoites, but will be associated with the PVM throughout the subsequent cycle post-invasion (67). The sporozoite invasion process is assumed to be analogous to that of the merozoite. During the transit of the *Plasmodium* sporozoite from the bite site to the hepatocytes, UIS4 is stored inside the sporozoite where it colocalizes with TRAP (40), apparently in the micronemes, and is discharged only once the sporozoite is in the process of hepatocyte invasion. We clearly demonstrate that the pool of UIS4 that initially populates the young EEF PVM is gone after 6 h of either Torin2 or BFA treatment. As BFA is not thought to affect retrograde trafficking, it is very unlikely that this indicates a block in UIS4 recycling from the parasite soma to the PVM, suggesting that this pool of UIS4 has been degraded either by the host cell or the parasite itself. However, this is not the case with the translocon components in the iRBC, in which the initial pool of proteins released from the dense granules appears to be stably retained at the PVM throughout blood stage development, with further synthesis and trafficking not required (67).

Although it is clear that the blood stage parasite is actively secreting proteins, such as the stage-specific ETRAMPS (24), to the PVM throughout development, more investigation will be required to determine if some blood PVM proteins show dynamics like those of UIS4, and indeed whether EXP1 itself is similarly dynamically localized to the blood stage PVM. The hypothesis that PVM protein turnover would be related to protein function is attractive, but as the liver stage PVM also must contend with extensive interactions with hepatocyte components (22, 68), it remains possible that the host cell itself dictates the turnover of the liver stage PVM-resident proteins that we have examined.

Regardless of whether host or parasite ultimately drives the turnover of the liver stage PVM-resident proteins that we have studied, their replenishment at the PVM via continued expression and secretion through the early schizont stage, at the least, is crucial for parasite viability. Clearly, the trafficking route to the liver stage PVM and the molecular players that mediate it, as well as the protective role of the PVM, constitute fascinating avenues for future research into *Plasmodium* biology, as well as antimalarial drug development.

Experimental Procedures

See detailed version in *SI Experimental Procedures*.

***Plasmodium* Liver Stage Assays.** GFP-expressing *P. berghei* sporozoites were added to HepG2 or Huh7 cells cultured in 24-well plates. Infected cells were processed and analyzed by flow cytometry as described in ref. 31.

A total of 10,000 *P. berghei*-GFP sporozoites were injected i.v. into C57BL6 mice; 2 h later, a 10-mg/kg dose of Torin2 was given orally as a sunflower oil slurry. Control animals received an equal dose of oil. Livers were harvested 44 h after infection, mRNA was extracted, and liver parasite load was determined by quantitative RT-PCR of *P. berghei* 18s rRNA.

***Plasmodium* Blood Stage Assays.** *P. falciparum* strains were cultured in vitro, and parasite proliferation was determined by flow cytometry.

To test the antimalarial properties of Torin2 in vivo, 1×10^6 *P. berghei*-GFP iRBCs were injected intraperitoneally into C57BL/6 mice, and parasitaemia was monitored by flow cytometry. Torin2 (10 mM) in DMSO was diluted in PBS, and 10 mg/kg was given orally on day 4 postinfection when parasitaemia was above 3%. Control animals received equal doses of DMSO in PBS.

For resistance selection, $\sim 10^9$ parasites were subject to a stepwise intermittent selection protocol beginning with $10\times$ EC_{50} for various exposure-time windows. Optimal resistance-selection conditions were obtained that selected against the majority of parasites, but allowed recrudescence of resistant parasites within 60 d. Upon recrudescence, additional selection rounds were conducted to optimally obtain clones uninhibited by Torin2.

Immunofluorescence and Microscopy. Infected cells were fixed in 4% paraformaldehyde (wt/vol) for 10 min at room temperature, permeabilized, blocked in 2% BSA (wt/vol), and incubated with 1° antibodies. After washing, appropriate 2° antibodies were added, and coverslips were mounted in Fluoromount. All images were acquired on Zeiss confocal microscopes.

ACKNOWLEDGMENTS. We thank Ana Parreira for mosquito production and infection; Fernanda Baptista for laboratory support; and Liliana Mancio, Vanessa Luis, and Ghislain Cabal for advice and reagents. Additionally, we are grateful to Volker Heussler, Stefan Kappe, and Miguel Seabra for providing antisera, and to David Sabatini for providing Torin1. This work was supported by Fundação para a Ciência e Tecnologia (FCT, Portugal) Grants PTDC/SAU-GMG/100313/2008 and EXCL/IMI-MIC/0056/2012, and European Research Council funding (to M.M.M.). K.K.H. was supported by funds from the European Community's Seventh Framework Programme (FP7/2007-2013) Marie Curie IntraEuropean Fellowship Grant PIEF-GA-2008-221854 and FCT Grant SFRH/BPD/40989/2007.

1. Murray CJL, et al. (2012) Global malaria mortality between 1980 and 2010: A systematic analysis. *Lancet* 379(9814):413–431.
2. O'Brien C, Henrich PP, Passi N, Fidock DA (2011) Recent clinical and molecular insights into emerging artemisinin resistance in Plasmodium falciparum. *Curr Opin Infect Dis* 24(6):570–577.
3. Prudêncio M, Rodriguez A, Mota MM (2006) The silent path to thousands of merozoites: The Plasmodium liver stage. *Nat Rev Microbiol* 4(11):849–856.
4. Moradin N, Descoteaux A (2012) Leishmania promastigotes: Building a safe niche within macrophages. *Front Cell Infect Microbiol* 2:121.
5. Kumar Y, Valdivia RH (2009) Leading a sheltered life: Intracellular pathogens and maintenance of vacuolar compartments. *Cell Host Microbe* 5(6):593–601.
6. Lingelbach K, Joiner KA (1998) The parasitophorous vacuole membrane surrounding Plasmodium and Toxoplasma: An unusual compartment in infected cells. *J Cell Sci* 111 (Pt 11):1467–1475.

7. Wang L, Boyer JL (2004) The maintenance and generation of membrane polarity in hepatocytes. *Hepatology* 39(4):892–899.
8. Bast A, et al. (2011) Defense mechanisms of hepatocytes against Burkholderia pseudomallei. *Front Microbiol* 2:277.
9. de Koning-Ward TF, et al. (2009) A newly discovered protein export machine in malaria parasites. *Nature* 459(7249):945–949.
10. Maier AG, et al. (2008) Exported proteins required for virulence and rigidity of Plasmodium falciparum-infected human erythrocytes. *Cell* 134(1):48–61.
11. Mueller AK, et al. (2005) Plasmodium liver stage developmental arrest by depletion of a protein at the parasite-host interface. *Proc Natl Acad Sci USA* 102(8):3022–3027.
12. Mueller AK, Labaied M, Kappe SH, Matuschewski K (2005) Genetically modified Plasmodium parasites as a protective experimental malaria vaccine. *Nature* 433(7022):164–167.
13. Maier AG, Cooke BM, Cowman AF, Tilley L (2009) Malaria parasite proteins that remodel the host erythrocyte. *Nat Rev Microbiol* 7(5):341–354.
14. Singh AP, et al. (2007) Plasmodium circumsporozoite protein promotes the development of the liver stages of the parasite. *Cell* 131(3):492–504.
15. Vaughan AM, et al. (2012) Complete Plasmodium falciparum liver-stage development in liver-chimeric mice. *J Clin Invest* 122(10):3618–3628.
16. Hunn JP, Feng CG, Sher A, Howard JC (2011) The immunity-related GTPases in mammals: A fast-evolving cell-autonomous resistance system against intracellular pathogens. *Mamm Genome* 22(1–2):43–54.
17. Labaied M, et al. (2007) Plasmodium yoelii sporozoites with simultaneous deletion of P52 and P36 are completely attenuated and confer sterile immunity against infection. *Infect Immun* 75(8):3758–3768.
18. van Dijk MR, et al. (2005) Genetically attenuated, P36p-deficient malarial sporozoites induce protective immunity and apoptosis of infected liver cells. *Proc Natl Acad Sci USA* 102(34):12194–12199.
19. Silvie O, Goetz K, Matuschewski K (2008) A sporozoite asparagine-rich protein controls initiation of Plasmodium liver stage development. *PLoS Pathog* 4(6): e1000086.
20. Aly AS, et al. (2008) Targeted deletion of SAP1 abolishes the expression of infectivity factors necessary for successful malaria parasite liver infection. *Mol Microbiol* 69(1): 152–163.
21. Desai SA, Rosenberg RL (1997) Pore size of the malaria parasite's nutrient channel. *Proc Natl Acad Sci USA* 94(5):2045–2049.
22. Bano N, Romano JD, Jayabalasingham B, Coppens I (2007) Cellular interactions of Plasmodium liver stage with its host mammalian cell. *Int J Parasitol* 37(12):1329–1341.
23. MacKellar DC, Vaughan AM, Aly AS, DeLeon S, Kappe SH (2011) A systematic analysis of the early transcribed membrane protein family throughout the life cycle of Plasmodium yoelii. *Cell Microbiol* 13(11):1755–1767.
24. Spielmann T, Fergusen DJ, Beck HP (2003) etramps, a new Plasmodium falciparum gene family coding for developmentally regulated and highly charged membrane proteins located at the parasite-host cell interface. *Mol Biol Cell* 14(4):1529–1544.
25. Mikolajczak SA, Jacobs-Lorena V, MacKellar DC, Camargo N, Kappe SH (2007) L-FABP is a critical host factor for successful malaria liver stage development. *Int J Parasitol* 37 (5):483–489.
26. Albuquerque SS, et al. (2009) Host cell transcriptional profiling during malaria liver stage infection reveals a coordinated and sequential set of biological events. *BMC Genomics* 10:270.
27. Chattopadhyay R, et al. (2011) Early transcriptional responses of HepG2-A16 liver cells to infection by Plasmodium falciparum sporozoites. *J Biol Chem* 286(30):26396–26405.
28. Laplante M, Sabatini DM (2012) mTOR signaling in growth control and disease. *Cell* 149(2):274–293.
29. Guertin DA, Sabatini DM (2009) The pharmacology of mTOR inhibition. *Sci Signal* 2 (67):pe24.
30. Thoreen CC, et al. (2009) An ATP-competitive mammalian target of rapamycin inhibitor reveals rapamycin-resistant functions of mTORC1. *J Biol Chem* 284(12): 8023–8032.
31. Prudêncio M, Rodrigues CD, Ataíde R, Mota MM (2008) Dissecting in vitro host cell infection by Plasmodium sporozoites using flow cytometry. *Cell Microbiol* 10(1): 218–224.
32. Liu Q, et al. (2011) Discovery of 9-(6-aminopyridin-3-yl)-1-(3-(trifluoromethyl)phenyl) benzo[h][1,6]naphthyridin-2(1H)-one (Torin2) as a potent, selective, and orally available mammalian target of rapamycin (mTOR) inhibitor for treatment of cancer. *J Med Chem* 54(5):1473–1480.
33. Buchholz K, et al. (2011) A high-throughput screen targeting malaria transmission stages opens new avenues for drug development. *J Infect Dis* 203(10):1445–1453.
34. Feldman ME, et al. (2009) Active-site inhibitors of mTOR target rapamycin-resistant outputs of mTORC1 and mTORC2. *PLoS Biol* 7(2):e38.
35. Van Tyne D, et al. (2011) Identification and functional validation of the novel antimalarial resistance locus PF10_0355 in Plasmodium falciparum. *PLoS Genet* 7(4): e1001383.
36. Dharia NV, et al. (2009) Use of high-density tiling microarrays to identify mutations globally and elucidate mechanisms of drug resistance in Plasmodium falciparum. *Genome Biol* 10(2):R21.
37. Rottmann M, et al. (2010) Spiroindolones, a potent compound class for the treatment of malaria. *Science* 329(5996):1175–1180.
38. Vera IM, Beatty WL, Sinnis P, Kim K (2011) Plasmodium protease ROM1 is important for proper formation of the parasitophorous vacuole. *PLoS Pathog* 7(9):e1002197.
39. Sturm A, et al. (2009) Alteration of the parasite plasma membrane and the parasitophorous vacuole membrane during exo-erythrocytic development of malaria parasites. *Protist* 160(1):51–63.
40. Kaiser K, Matuschewski K, Camargo N, Ross J, Kappe SH (2004) Differential transcriptome profiling identifies Plasmodium genes encoding pre-erythrocytic stage-specific proteins. *Mol Microbiol* 51(5):1221–1232.
41. Doolan DL, et al. (1996) Identification and characterization of the protective hepatocyte erythrocyte protein 17 kDa gene of Plasmodium yoelii, homolog of Plasmodium falciparum exported protein 1. *J Biol Chem* 271(30):17861–17868.
42. Delves M, et al. (2012) The activities of current antimalarial drugs on the life cycle stages of Plasmodium: A comparative study with human and rodent parasites. *PLoS Med* 9(2):e1001169.
43. Nam TG, et al. (2011) A chemical genomic analysis of decoquinate, a Plasmodium falciparum cytochrome b inhibitor. *ACS Chem Biol* 6(11):1214–1222.
44. da Cruz FP, et al. (2012) Drug screen targeted at Plasmodium liver stages identifies a potent multistage antimalarial drug. *J Infect Dis* 205(8):1278–1286.
45. Cunha-Rodrigues M, et al. (2008) Genistein-supplemented diet decreases malaria liver infection in mice and constitutes a potential prophylactic strategy. *PLoS ONE* 3(7): e2732.
46. Hobbs CV, et al. (2009) HIV protease inhibitors inhibit the development of preerythrocytic-stage plasmodium parasites. *J Infect Dis* 199(1):134–141.
47. Meister S, et al. (2011) Imaging of Plasmodium liver stages to drive next-generation antimalarial drug discovery. *Science* 334(6061):1372–1377.
48. Gershon PD, Howells RE (1986) Mitochondrial protein synthesis in Plasmodium falciparum. *Mol Biochem Parasitol* 18(1):37–43.
49. Deponte M, et al. (2012) Wherever I may roam: Protein and membrane trafficking in P. falciparum-infected red blood cells. *Mol Biochem Parasitol* 186(2):95–116.
50. Crary JL, Haldar K (1992) Brefeldin A inhibits protein secretion and parasite maturation in the ring stage of Plasmodium falciparum. *Mol Biochem Parasitol* 53(1–2):185–192.
51. Wickham ME, et al. (2001) Trafficking and assembly of the cytoadherence complex in Plasmodium falciparum-infected human erythrocytes. *EMBO J* 20(20):5636–5649.
52. Nacer A, Berry L, Slomianny C, Mattei D (2001) Plasmodium falciparum signal sequences: Simply sequences or special signals? *Int J Parasitol* 31(12):1371–1379.
53. Jayabalasingham B, Bano N, Coppens I (2010) Metamorphosis of the malaria parasite in the liver is associated with organelle clearance. *Cell Res* 20(9):1043–1059.
54. D'Alessandro A, Righetti PG, Zolla L (2010) The red blood cell proteome and interactome: An update. *J Proteome Res* 9(1):144–163.
55. Brown JR, Auger KR (2011) Phylogenomics of phosphoinositide lipid kinases: Perspectives on the evolution of second messenger signaling and drug discovery. *BMC Evol Biol* 11:4.
56. Ward P, Equinet L, Packer J, Doerig C (2004) Protein kinases of the human malaria parasite Plasmodium falciparum: The kinome of a divergent eukaryote. *BMC Genomics* 5:79.
57. Tawk L, et al. (2010) Phosphatidylinositol 3-phosphate, an essential lipid in Plasmodium, localizes to the food vacuole membrane and the apicoplast. *Eukaryot Cell* 9(10):1519–1530.
58. Vaid A, Ranjan R, Smythe WA, Hoppe HC, Sharma P (2010) PfPI3K, a phosphatidylinositol-3 kinase from Plasmodium falciparum, is exported to the host erythrocyte and is involved in hemoglobin trafficking. *Blood* 115(12):2500–2507.
59. Oduola AM, Milhous WK, Weatherly NF, Bowdre JH, Desjardins RE (1988) Plasmodium falciparum: Induction of resistance to mefloquine in cloned strains by continuous drug exposure in vitro. *Exp Parasitol* 67(2):354–360.
60. Ritchie GY, et al. (1996) In vitro selection of halofantrine resistance in Plasmodium falciparum is not associated with increased expression of Pgh1. *Mol Biochem Parasitol* 83(1):35–46.
61. Eastman RT, Dharia NV, Winzeler EA, Fidock DA (2011) Piperaquine resistance is associated with a copy number variation on chromosome 5 in drug-pressured Plasmodium falciparum parasites. *Antimicrob Agents Chemother* 55(8):3908–3916.
62. Korsinczky M, et al. (2000) Mutations in Plasmodium falciparum cytochrome b that are associated with atovaquone resistance are located at a putative drug-binding site. *Antimicrob Agents Chemother* 44(8):2100–2108.
63. Barnes DA, Foote SJ, Galatis D, Kemp DJ, Cowman AF (1992) Selection for high-level chloroquine resistance results in deamplification of the pfmdr1 gene and increased sensitivity to mefloquine in Plasmodium falciparum. *EMBO J* 11(8):3067–3075.
64. Baumgartner F, Wiek S, Paprotka K, Zauner S, Lingelbach K (2001) A point mutation in an unusual Sec7 domain is linked to brefeldin A resistance in a Plasmodium falciparum line generated by drug selection. *Mol Microbiol* 41(5):1151–1158.
65. Elmendorf HG, Haldar K (1993) Identification and localization of ERD2 in the malaria parasite Plasmodium falciparum: Separation from sites of sphingomyelin synthesis and implications for organization of the Golgi. *EMBO J* 12(12):4763–4773.
66. Cowman AF, Berry D, Baum J (2012) The cellular and molecular basis for malaria parasite invasion of the human red blood cell. *J Cell Biol* 198(6):961–971.
67. Bullen HE, et al. (2012) Biosynthesis, localization, and macromolecular arrangement of the Plasmodium falciparum translocon of exported proteins (PTEX). *J Biol Chem* 287(11):7871–7884.
68. Gomes-Santos CS, et al. (2012) Highly dynamic host actin reorganization around developing Plasmodium inside hepatocytes. *PLoS ONE* 7(1):e29408.

REFERENCES:

1. Suh, K. N., Kain, K. C. & Keystone, J. S. Malaria. *CMAJ* **170,** 1693–1702 (2004).
2. Breman, J. G. Clinical manifestations of malaria. *UptoDate* 1–14 at <http://www.uptodate.com/contents/clinical-manifestations-of-malaria?source=search_result&search=malaria&selectedTitle=1~150>
3. World Health Organization. Guidelines for the treatment of malaria. (2010).
4. Hay, S. I. & Snow, R. W. The malaria Atlas Project: developing global maps of malaria risk. *Plos Med* **3,** e473 (2006).
5. Project, M. A. *The clinical burden of Plasmodium falciparum map in 2007 globally*. at <http://www.map.ox.ac.uk/browse-resources/clinical-burden/Pf_burden/world/ >
6. Murray, C. J. L. *et al.* Global malaria mortality between 1980 and 2010: a systematic analysis. *Lancet* **379,** 413–431 (2012).
7. Kiszewski, A. *et al.* A global index representing the stability of malaria transmission. *American Journal of Tropical Medicine and Hygiene* **70,** 486–498 (2004).
8. Gwatkin, D. R., Guillot, M. & Heuveline, P. The burden of disease among the global poor. *The Lancet* **354,** 586–589 (1999).
9. Sachs, J. & Malaney, P. The economic and social burden of malaria. *Nature* **415,** 680–685 (2002).
10. Ettling, M., McFarland, D. A., Schultz, L. J. & Chitsulo, L. Economic impact of malaria in Malawian households. *Trop. Med. Parasitol.* **45,** 74–79 (1994).
11. Worrall, E., Basu, S. & Hanson, K. Is malaria a disease of poverty? A review of the literature. *Trop. Med. Int. Health* **10,** 1047–1059 (2005).
12. Teklehaimanot and Paola Mejia, A. Malaria and Poverty. *Annals of the New York Academy of Sciences* **1136,** 32–37 (2008).
13. Yeh, E. & DeRisi, J. L. Chemical rescue of malaria parasites lacking an apicoplast defines organelle function in blood-stage Plasmodium falciparum. *PLoS Biol* **9,** e1001138–e1001138 (2011).
14. Graczyk, T. K., Cranfield, M. R., McCutchan, T. F. & Bicknese, E. J. Characteristics of naturally acquired avian malaria infections in naive juvenile African black-footed penguins (Spheniscus demersus). *Parasitology research* **80,** 634–637 (1994).
15. Gardner, M. J. *et al.* Genome sequence of the human malaria parasite Plasmodium falciparum. *Nature* **419,** 498–511 (2002).
16. Hayashi, T. *et al.* Complete Genome Sequence of Enterohemorrhagic Eschelichia coli O157:H7 and Genomic Comparison with a Laboratory Strain K-12. (2001).
17. Venter, J. C., Adams, M. D., Myers, E. W., Li, P. W. & Mural, R. J. The Sequence of the Human Genome. *Science* (2001).
18. Lander, E. S. *et al.* Initial sequencing and analysis of the human genome. *Nature* **409,** 860–921 (2001).
19. Prudêncio, M., Rodriguez, A. & Mota, M. M. The silent path to thousands of merozoites: the Plasmodium liver stage. *Nature Reviews Microbiology* **4,** 849–856 (2006).
20. Nguitragool, W. *et al.* Malaria Parasite clag3 Genes Determine Channel-Mediated Nutrient Uptake by Infected Red Blood Cells. *Cell* **145,** 665–677 (2011).
21. Dvorin, J. D. *et al.* A plant-like kinase in Plasmodium falciparum regulates parasite egress from erythrocytes. *Science* **328,** 910–912 (2010).
22. Franke-Fayard, B., Fonager, J., Braks, A., Khan, S. M. & Janse, C. J. Sequestration and tissue accumulation of human malaria parasites: can we learn anything from rodent models of malaria? *PLoS Pathog* **6,** e1001032 (2010).
23. Babiker, H., Schneider, P. & Reece, S. Gametocytes: insights gained during a decade of molecular monitoring. *Trends Parasitol* **24,** 525–530 (2008).
24. Dowdle, W. R. & Cochi, S. L. The principles and feasibility of disease eradication. *Vaccine* **29 Suppl 4,** D70–3 (2011).
25. Dowdle, W. R. The principles of disease elimination and eradication. *Bulletin of the World Health Organization* **76 Suppl 2,** 22–25 (1998).
26. Heppner, D. G. The malaria vaccine--status quo 2013. *Travel Med Infect Dis* **11,** 2–7 (2013).
27. Daily, J. P. Malaria vaccine trials--beyond efficacy end points. *N Engl J Med* **367,** 2349–2351 (2012).
28. BABIKER, H. A. *et al.* Population dynamics of Plasmodium falciparum in an unstable malaria area of eastern Sudan. *Parasitology* **120,** 105–111 (2000).
29. Babiker, H. Unstable malaria in Sudan: the influence of the dry season. Plasmodium falciparum population in the unstable malaria area of eastern Sudan is stable and genetically complex. *Transactions of the Royal Society of Tropical Medicine and Hygiene* **92,** 585

30. Theander, T. Malaria in areas of unstable and seasonal transmission. Lessons from Daraweesh. *Transactions of the Royal Society of Tropical Medicine and Hygiene* **92,** 589–592 (1998).
31. Okell, L. C. *et al.* Factors determining the occurrence of submicroscopic malaria infections and their relevance for control. *Nat Commun* **3,** 1237 (2012).
32. Krotoski, W. A. *et al.* Demonstration of hypnozoites in sporozoite-transmitted Plasmodium vivax infection. *American Journal of Tropical Medicine and Hygiene* **31,** 1291–1293 (1982).
33. Markus, M. B. The hypnozoite concept, with particular reference to malaria. *Parasitology research* **108,** 247–252 (2010).
34. Jones, M. K. & Good, M. F. Malaria parasites up close. *Nature Medicine* **12,** 170–171 (2006).
35. Nájera, J. A., González-Silva, M. & Alonso, P. L. Some lessons for the future from the Global Malaria Eradication Programme (1955-1969). *Plos Med* **8,** e1000412 (2011).
36. Wongsrichanalai, C., Pickard, A. L., Wernsdorfer, W. H. & Meshnick, S. R. Epidemiology of drug-resistant malaria. *The Lancet Infectious Diseases* **2,** 209–218 (2002).
37. Noedl, H. *et al.* Evidence of artemisinin-resistant malaria in western Cambodia. *N Engl J Med* **359,** 2619–2620 (2008).
38. Wellems, T. E. & Plowe, C. V. Chloroquine-resistant malaria. *J Infect Dis* **184,** 770–776 (2001).
39. O'Brien, C., Henrich, P. P., Passi, N. & Fidock, D. A. Recent clinical and molecular insights into emerging artemisinin resistance in Plasmodium falciparum. *Current Opinion in Infectious Diseases* **24,** 570–577 (2011).
40. Chiodini, P. L. *et al.* Evaluation of atovaquone in the treatment of patients with uncomplicated Plasmodium falciparum malaria. *Journal of Antimicrobial Chemotherapy* **36,** 1073–1078 (1995).
41. Osman, M. E., Mockenhaupt, F. P., Bienzle, U., Elbashir, M. I. & Giha, H. A. Field-based evidence for linkage of mutations associated with chloroquine (pfcrt/pfmdr1) and sulfadoxine-pyrimethamine (pfdhfr/pfdhps) resistance and for the fitness cost of multiple mutations in P. falciparum. *Infect. Genet. Evol.* **7,** 52–59 (2007).
42. Björkman, J., Nagaev, I., Berg, O. G., Hughes, D. & Andersson, D. I. Effects of environment on compensatory mutations to ameliorate costs of antibiotic resistance. *Science* **287,** 1479–1482 (2000).
43. Levin, B. R., Perrot, V. & Walker, N. Compensatory Mutations, Antibiotic Resistance and the Population Genetics of Adaptive Evolution in Bacteria. *Genetics* 985–997 (2000).
44. Mharakurwa, S. *et al.* Malaria antifolate resistance with contrasting Plasmodium falciparum dihydrofolate reductase (DHFR) polymorphisms in humans and Anopheles mosquitoes. *Proc Natl Acad Sci USA* **108,** 18796–18801 (2011).
45. Felger, I. & Beck, H. P. Fitness costs of resistance to antimalarial drugs. *Trends Parasitol* **24,** 331–333 (2008).
46. Korsinczky, M. *et al.* Mutations in Plasmodium falciparum cytochrome b that are associated with atovaquone resistance are located at a putative drug-binding site. *Antimicrobial Agents and Chemotherapy* **44,** 2100–2108 (2000).
47. Fisher, N. *et al.* Cytochrome b mutation Y268S conferring atovaquone resistance phenotype in malaria parasite results in reduced parasite bc1 catalytic turnover and protein expression. *Journal of Biological Chemistry* **287,** 9731–9741 (2012).
48. Rosenthal, P. J. The interplay between drug resistance and fitness in malaria parasites. *Molecular Microbiology* (2013). doi:10.1111/mmi.12349
49. Walliker, D., Hunt, P. & Babiker, H. Fitness of drug-resistant malaria parasites. *Acta Trop* **94,** 251–259 (2005).
50. de Vries, P. J. & Dien, T. K. Clinical pharmacology and therapeutic potential of artemisinin and its derivatives in the treatment of malaria. **52,** 818–836 (1996).
51. Burrows, J. N., Chibale, K. & Wells, T. N. C. The state of the art in anti-malarial drug discovery and development. *Curr Top Med Chem* **11,** 1226–1254 (2011).
52. Burns, W. R. East meets West: how China almost cured malaria. *Endeavour* **32,** 101–106 (2008).
53. Tu, Y. The discovery of artemisinin (qinghaosu) and gifts from Chinese medicine. *Nature Medicine* **17,** 1217–1220 (2011).
54. Tonkin, I. A new antimalarial drug. *Nature* (1945).
55. Sundrud, M. S. *et al.* Halofuginone Inhibits TH17 Cell Differentiation by Activating the Amino Acid Starvation Response. *Science* **324,** 1334–1338 (2009).
56. Keller, T. L. *et al.* Halofuginone and other febrifugine derivatives inhibit prolyl-tRNA synthetase. *Nature chemical biology* (2012). doi:10.1038/nchembio.790
57. Holcik, M. Translational control in stress and apoptosis. *Nat Rev Mol Cell Biol* (2005).
58. Istvan, E. S. *et al.* Validation of isoleucine utilization targets in Plasmodium falciparum. *Proc Natl Acad Sci USA* **108,** 1627–1632 (2011).
59. Fennell, C. *et al.* PfeIK1, a eukaryotic initiation factor 2alpha kinase of the human malaria parasite Plasmodium falciparum, regulates stress-response to amino-acid starvation. *Malar J* **8,** 99 (2009).
60. Divo, A., Geary, T., Davis, N. & Jensen, J. Nutritional requirements of Plasmodium falciparum in culture. I. Exogenously supplied dialyzable components necessary for continuous growth. *Journal of Eukaryotic*

Microbiology **32,** 59–64 (1985).
61. Ginsburg, H., Kutner, S., Krugliak, M. & Ioav Cabantchik, Z. Characterization of permeation pathways appearing in the host membrane of plasmodium falciparum infected red blood cells. *Molecular and Biochemical Parasitology* 313–322 (1984).
62. McCormick, G. J. Amino acid transport and incorporation in red blood cells of normal and Plasmodium knowlesi-infected rhesus monkeys. *Experimental Parasitology* **27,** 143–149 (1970).
63. Sharma, P. *et al.* An Epigenetic Antimalarial Resistance Mechanism Involving Parasite Genes Linked to Nutrient Uptake. *Journal of Biological Chemistry* **288,** 19429–19440 (2013).
64. Mira-Martínez, S. *et al.* Epigenetic switches in clag3 genes mediate blasticidin S resistance in malaria parasites. *Cell Microbiol* **15,** 1913–1923 (2013).
65. SeveraliMedPub. *World Health Statistics 2012*. (World Health Organization, 2012).
66. Lozano, R. *et al.* Global and regional mortality from 235 causes of death for 20 age groups in 1990 and 2010: a systematic analysis for the Global Burden of Disease Study 2010. *Lancet* **380,** 2095–2128 (2012).
67. Rodrigues, T., Prudêncio, M. & Moreira, R. Targeting the liver stage of malaria parasites: a yet unmet goal. *Journal of medicinal …* (2011).
68. Derbyshire, E. R., Prudêncio, M., Mota, M. M. & Clardy, J. Liver-stage malaria parasites vulnerable to diverse chemical scaffolds. *Proc Natl Acad Sci USA* **109,** 8511–8516 (2012).
69. Control, T. M. C. G. O. V. A Research Agenda for Malaria Eradication: Vector Control. *Plos Med* **8,** e1000401 (2011).
70. Ariey, F. *et al.* A molecular marker of artemisinin-resistant Plasmodium falciparum malaria. *Nature* **505,** 50–55 (2014).
71. Wongsrichanalai, C. & Meshnick, S. R. Declining artesunate-mefloquine efficacy against falciparum malaria on the Cambodia-Thailand border. *Emerging Infect Dis* **14,** 716–719 (2008).
72. Fidock, D. A., Rosenthal, P. J., Croft, S. L., Brun, R. & Nwaka, S. Antimalarial drug discovery: efficacy models for compound screening. *Nature Reviews Drug Discovery* **3,** 509–520 (2004).
73. Nilsen, A. *et al.* Quinolone-3-diarylethers: a new class of antimalarial drug. *Sci Transl Med* **5,** 177ra37 (2013).
74. Lowes, D. J. *et al.* Optimization of propafenone analogues as antimalarial leads. *Journal of medicinal chemistry* **54,** 7477–7485 (2011).
75. Jackson, K. E. *et al.* Protein translation in Plasmodium parasites. *Trends Parasitol* **27,** 467–476 (2011).
76. Zhang, Y.-K. *et al.* Benzoxaborole antimalarial agents. Part 2: Discovery of fluoro-substituted 7-(2-carboxyethyl)-1,3-dihydro-1-hydroxy-2,1-benzoxaboroles. *Bioorganic & medicinal chemistry letters* **22,** 1299–1307 (2012).
77. Jackson, K. E. *et al.* Dual targeting of aminoacyl-tRNA synthetases to the apicoplast and cytosol in Plasmodium falciparum. *International Journal for Parasitology* **42,** 177–186 (2012).
78. Wells, T. N. C., Alonso, P. L. & Gutteridge, W. E. New medicines to improve control and contribute to the eradication of malaria. *Nature Reviews Drug Discovery* **8,** 879–891 (2009).
79. Pines, M., Vlodavsky, I. & Nagler, A. Halofuginone: From veterinary use to human therapy. *Drug Dev. Res.* **50,** 371–378 (2000).
80. McGaha, T. L., Phelps, R. G., Spiera, H. & Bona, C. Halofuginone, an Inhibitor of Type-I Collagen Synthesis and Skin Sclerosis, Blocks Transforming-Growth-Factor-β-Mediated Smad3 Activation in Fibroblasts. *J Investig Dermatol* **118,** 461–470 (2002).
81. Trager, W. & Jensen, J. Human malaria parasites in continuous culture. *Science* **193,** 673–675 (1976).
82. Johnson, J. D. *et al.* Assessment and continued validation of the malaria SYBR green I-based fluorescence assay for use in malaria drug screening. *Antimicrobial Agents and Chemotherapy* **51,** 1926–1933 (2007).
83. Dong, C. K. *et al.* Identification and validation of tetracyclic benzothiazepines as Plasmodium falciparum cytochrome bc1 inhibitors. *Chemistry & Biology* **18,** 1602–1610 (2011).
84. Rosario, V. Cloning of naturally occurring mixed infections of malaria parasites. *Science* **212,** 1037–1038 (1981).
85. Li, H. *et al.* The Sequence Alignment/Map format and SAMtools. *Bioinformatics* **25,** 2078–2079 (2009).
86. McKenna, A. *et al.* The Genome Analysis Toolkit: a MapReduce framework for analyzing next-generation DNA sequencing data. *Genome Research* **20,** 1297–1303 (2010).
87. Hu, Y. *et al.* Approaching a complete repository of sequence-verified protein-encoding clones for Saccharomyces cerevisiae. *Genome Research* **17,** 536–543 (2007).
88. Alberti, S., Gitler, A. D. & Lindquist, S. A suite of Gateway cloning vectors for high-throughput genetic analysis in Saccharomyces cerevisiae. *Yeast* **24,** 913–919 (2007).
89. Daniel Gietz, R. & Woods, R. A. in *Methods in enzymology* **350,** 87–96 (Elsevier, 2002).
90. *Current Protocols in Molecular Biology*. (John Wiley & Sons, Inc., 2004). doi:10.1002/0471142727
91. Gueldener, U., Heinisch, J., Koehler, G. J., Voss, D. & Hegemann, J. H. A second set of loxP marker cassettes for Cre-mediated multiple gene knockouts in budding yeast. *Nucleic Acids Research* **30,** e23 (2002).

92. Goldstein, A. L. & McCusker, J. H. Three new dominant drug resistance cassettes for gene disruption in Saccharomyces cerevisiae. *Yeast* **15,** 1541–1553 (1999).
93. Friesner, R. A. *et al.* Extra precision glide: docking and scoring incorporating a model of hydrophobic enclosure for protein-ligand complexes. *Journal of medicinal chemistry* **49,** 6177–6196 (2006).
94. Friesner, R. A. *et al.* Glide: a new approach for rapid, accurate docking and scoring. 1. Method and assessment of docking accuracy. *Journal of medicinal chemistry* **47,** 1739–1749 (2004).
95. Case, D. A., Darden, T. A., Iii, T. C. & Simmerling, C. L. AMBER 10. *University of California* (2008).
96. Jorgensen, W. L. & Chandrasekhar, J. Comparison of simple potential functions for simulating liquid water. *The Journal of …* (1983).
97. Schafmeister, C., Ross, W. & Romanovski, V. The leap module of AMBER. *University of California* (1995).
98. Wang, J., Wolf, R. M., Caldwell, J. W., Kollman, P. A. & Case, D. A. Development and testing of a general amber force field. *J Comput Chem* **25,** 1157–1174 (2004).
99. Wang, J., Wang, W., Kollman, P. A. & Case, D. A. Automatic atom type and bond type perception in molecular mechanical calculations. *J. Mol. Graph. Model.* **25,** 247–260 (2006).
100. Fox, T. & Kollman, P. A. Application of the RESP Methodology in the Parametrization of Organic Solvents. *J. Phys. Chem. B* **102,** 8070–8079 (1998).
101. Yarkony, D. *Modern Electronic Structure Theory*. (1995).
102. Ryckaert, J.-P., Ciccotti, G. & Berendsen, H. J. C. Numerical integration of the cartesian equations of motion of a system with constraints: molecular dynamics of n-alkanes. *Journal of Computational Physics* **23,** 327–341 (1977).
103. Pastor, R. W., Brooks, B. R. & Szabo, A. An analysis of the accuracy of Langevin and molecular dynamics algorithms. *Molecular Physics* **65,** 1409–1419 (1988).
104. Essmann, U. *et al.* A smooth particle mesh Ewald method. *The Journal of Chemical Physics* **103,** 8577–8593 (1995).
105. Petersen, H. G. Accuracy and efficiency of the particle mesh Ewald method. *The Journal of Chemical Physics* **103,** 3668–3679 (1995).
106. Marchler-Bauer, A. *et al.* CDD: a Conserved Domain Database for the functional annotation of proteins. *Nucleic Acids Research* **39,** D225–9 (2011).
107. Linder, M. R. *et al.* (2R,3S)-(+)- and (2S,3R)-(-)-Halofuginone lactate: synthesis, absolute configuration, and activity against Cryptosporidium parvum. *Bioorganic & medicinal chemistry letters* **17,** 4140–4143 (2007).
108. Kikuchi, H. *et al.* Potent antimalarial febrifugine analogues against the plasmodium malaria parasite. *Journal of medicinal chemistry* **45,** 2563–2570 (2002).
109. Takeuchi, Y., Oshige, M., Azuma, K. & Abe, H. Concise synthesis of dl-febrifugine. *CHEMICAL AND …* (2005).
110. Peters, W. The chemotherapy of rodent malaria, XXII. The value of drug-resistant strains of P. berghei in screening for blood schizontocidal activity. *Ann Trop Med Parasitol* **69,** 155–171 (1975).
111. Hanson, K. K. *et al.* Torins are potent antimalarials that block replenishment of Plasmodium liver stage parasitophorous vacuole membrane proteins. *Proc Natl Acad Sci USA* (2013). doi:10.1073/pnas.1306097110
112. Derbyshire, E. R., Mazitschek, R. & Clardy, J. Characterization of Plasmodium liver stage inhibition by halofuginone. *ChemMedChem* **7,** 844–849 (2012).
113. Jiang, S. *et al.* Antimalarial activities and therapeutic properties of febrifugine analogs. *Antimicrobial Agents and Chemotherapy* **49,** 1169–1176 (2005).
114. de Jonge, M. J. A. *et al.* Phase I and pharmacokinetic study of halofuginone, an oral quinazolinone derivative in patients with advanced solid tumours. *Eur. J. Cancer* **42,** 1768–1774 (2006).
115. Paul, M. & Schimmel, P. Essential nontranslational functions of tRNA synthetases. *Nature chemical biology* **9,** 145–153 (2013).
116. Bhatt, T. *et al.* A genomic glimpse of aminoacyl-tRNA synthetases in malaria parasite Plasmodium falciparum. *BMC Genomics* **10,** 644 (2009).
117. Zhou, H., Sun, L., Yang, X.-L. & Schimmel, P. ATP-directed capture of bioactive herbal-based medicine on human tRNA synthetase. *Nature* (2012). doi:10.1038/nature11774
118. Hinnebusch, A. G. Translational regulation of GCN4 and the general amino acid control of yeast. *Annu. Rev. Microbiol.* **59,** 407–450 (2005).
119. McNamara, C. W. *et al.* Targeting Plasmodium PI(4)K to eliminate malaria. *Nature* (2013). doi:10.1038/nature12782
120. Flannery, E. L., Fidock, D. A. & Winzeler, E. A. Using genetic methods to define the targets of compounds with antimalarial activity. *Journal of medicinal chemistry* 130808161720006 (2013). doi:10.1021/jm400325j
121. Valbuena, N., Rozalén, A. E. & Moreno, S. Fission yeast TORC1 prevents eIF2α phosphorylation in response to nitrogen and amino acids via Gcn2 kinase. *Journal of Cell Science* **125,** 5955–5959 (2012).
122. Trotz-Williams, L. A., Jarvie, B. D., Peregrine, A. S., Duffield, T. F. & Leslie, K. E. Efficacy of halofuginone

lactate in the prevention of cryptosporidiosis in dairy calves. *Vet. Rec.* **168,** 509 (2011).
123. Naciri, M., Mancassola, R., Yvoré, P. & Peeters, J. E. The effect of halofuginone lactate on experimental Cryptosporidium parvum infections in calves. *Vet. Parasitol.* **45,** 199–207 (1993).
124. Zhang, D.-F. *et al.* Anticoccidial effect of halofuginone hydrobromide against Eimeria tenella with associated histology. *Parasitology research* **111,** 695–701 (2012).
125. Desjardins, R. E., Canfield, C. J., Haynes, J. D. & Chulay, J. D. Quantitative assessment of antimalarial activity in vitro by a semiautomated microdilution technique. *Antimicrobial Agents and Chemotherapy* **16,** 710–718 (1979).
126. Bei, A. K. *et al.* A flow cytometry-based assay for measuring invasion of red blood cells by Plasmodium falciparum. *Am. J. Hematol.* **85,** 234–237 (2010).
127. Townsend, M. K. *et al.* Reproducibility of metabolomic profiles among men and women in 2 large cohort studies. *Clin. Chem.* **59,** 1657–1667 (2013).
128. Pham, J. S. *et al.* Aminoacyl-tRNA synthetases as drug targets in eukaryotic parasites. *International Journal for Parasitology: Drugs and Drug Resistance* (2013). doi:10.1016/j.ijpddr.2013.10.001
129. Hoepfner, D. *et al.* An integrated approach for the identification and target validation of anti-fungal compounds active against Erg11p. *Antimicrobial Agents and Chemotherapy* (2012). doi:10.1128/AAC.06332-11
130. Hoepfner, D. *et al.* Selective and Specific Inhibition of the Plasmodium falciparum Lysyl-tRNA Synthetase by the Fungal Secondary Metabolite Cladosporin. *Cell Host & Microbe* **11,** 654–663 (2012).
131. Habibi, D. *et al.* Borrelidin, a small molecule nitrile-containing macrolide inhibitor of threonyl-tRNA synthetase, is a potent inducer of apoptosis in acute lymphoblastic leukemia. *Invest New Drugs* (2011). doi:10.1007/s10637-011-9700-y
132. Eggeling, L. & Sahm, H. New ubiquitous translocators: amino acid export by Corynebacterium glutamicum and Escherichia coli. *Arch. Microbiol.* **180,** 155–160 (2003).
133. Pillai, A. D. *et al.* Solute restriction reveals an essential role for clag3-associated channels in malaria parasite nutrient acquisition. *Molecular Pharmacology* **82,** 1104–1114 (2012).
134. Milton H Saier, J. Families of transmembrane transporters selective for amino acids and their derivatives. *Microbiology* (2000).
135. Lukens, A. K. *et al.* Harnessing evolutionary fitness in Plasmodium falciparum for drug discovery and suppressing resistance. *Proc Natl Acad Sci USA* (2013). doi:10.1073/pnas.1320886110
136. Weisberg, E., Manley, P. W., Cowan-Jacob, S. W., Hochhaus, A. & Griffin, J. D. Second generation inhibitors of BCR-ABL for the treatment of imatinib-resistant chronic myeloid leukaemia. *Nature Reviews Cancer* **7,** 345–356 (2007).